博士論文

Development and characterization of carbon-based nano-fillers/polyaniline hybrids reinforced polymer composites

（炭素系ナノフィラーとポリアニリン複合体を用いた樹脂系複合材料の開発と評価）

成　秀燕（Cheng Xiuyan）

Department of Aeronautics and Astronautics, School of Engineering

The University of Tokyo, Tokyo, Japan

2017

TABLE OF CONTENTS

Chapter 1 4
General Introduction 4
1.1 Nanofiller Reinforced Polymer Conductive Composites 7
1.2 Conductive Polymer 9
1.3 Conductive Mechanism 12
1.4 Object of this research 16
Chapter 2 20
GO/PANI hybrid reinforced polymer nanocomposites 20
2.1 Introduction 21
2.2 Experimental details 22
2.3 Results and discussion 31
2.4 Conclusion 46
Chapter 3 48
MWCNT/GO hybrid reinforced polymer composites 48
3.1 Introduction 48
3.2 Experimental details 50
3.3 Results and discussion 52
3.4 Conclusion 68
Chapter 4 69
C_{60}/PANI hybrid reinforced polymer composites 69
4.1 Introduction 70
4.2 Experimental details 71
4.3 Results and discussion 75
4.4 Conclusion 85
Chapter 5 86
Comparative study of the carbon/PANI hybrid system 86
5.1 General Introduction 87
5.2 Study of the hybrid system 87
5.3 Conclusion 101
Chapter 6 103
Summary and Perspective 103
Attachment: DPD Simulation 106
List of Publications 110
Acknowledgements 112
Reference 114

Abbreviations

GO – Graphene Oxide

MWCNT – Multiwalled carbon nanotube

C60 – Fullerene

PANI - polyaniline

DBSA - dodecylbenzenesulfonic acid

DVB – divinylbenzene

TGA – thermogravimetric analysis

SEM – Scanning Electron Microscopy

Xrd- X-ray powder diffraction

TEM - Transmission Electron Microscopy

DPD – Dissipative particle dynamic

Chapter 1

General Introduction

Carbon fiber composite material has been widely used in aerospace, clean energy vehicles, civil engineering, wind turbine blades, sports equipment due to their high-strength, high modulus, corrosion resistance, high temperature resistance, fatigue resistance, conductive, heat transfer and other excellent features[1-3]. In recent years, carbon fiber composites with the functional properties like stealth, electrostatic protection, electromagnetic shielding and other unique features get more and more attention. However, since the carbon fiber composite material usually contains about 30% of the insulating polymer matrix as showed in Fig. 1.1, resulting in the through thickness conductivity of the traditional carbon fiber composite material is very poor, which has become a fatal defects of composites as shown in Fig 1.2. Therefore, the research and development of functional polymer composite material system has turned into an important branch in the field of materials.

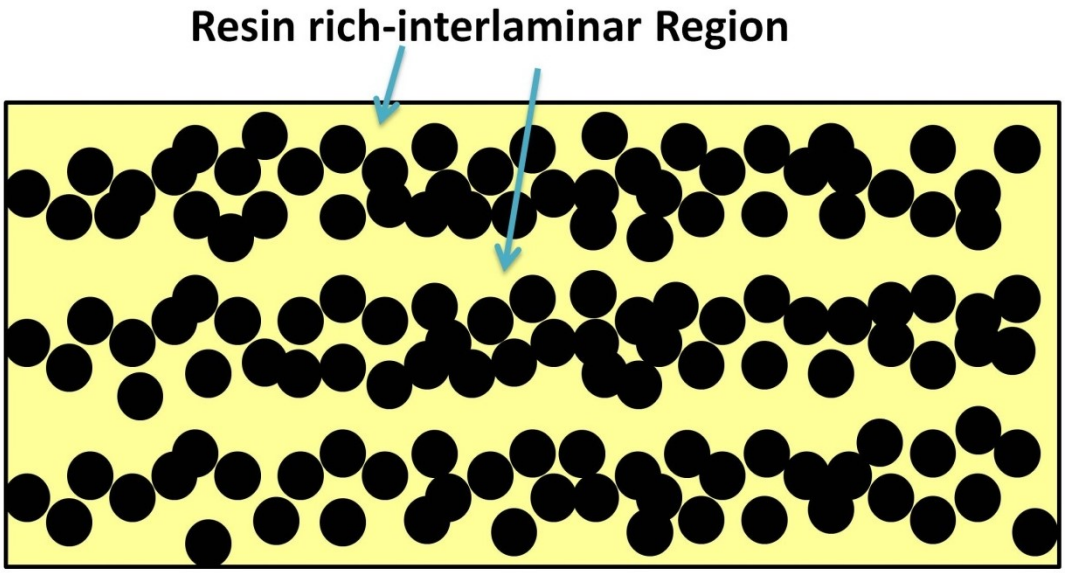

Fig. 1.1 The sandwich structure of carbon fiber composites

Fig 1.2 The defects of carbon fiber reinforced composites
[Source: https://image.baidu.com]

Several techniques have been devised to improve the through-thickness electrical conductivity, e.g. using conducting polymers (as indicated in Fig 1.3), conductive fillers [4-8], and carbon nanofillers into polymer for electrical functional applications develop[9, 10]. For example, Weikang Li et al [11] added 0.5 wt.% CNT–Al_2O_3 into the glass fabric/epoxy composites, increased AC conductivity 4–5 orders of magnitude for both in-plane and through-thickness directions at 10^3 Hz. Growing CNTS on the carbon fiber can enhance the in-plane electrical conductivity of the CF/epoxy composites by 170% [12]. The throughthickness electrical conductivities of the CFRP were improved by two orders of magnitude to 1S m^{-1} through the addition of CNTs [13]. However, this still cannot meet requirements of some unique applications. For example, the electrical conductivity of electromagnetic shielding material claims higher than 10 S/m [14]. No investigations have been reported on the enhanced effect of carbon-based nano-fillers/polyaniline hybrids on the through-thickness electric conductivity of carbon fiber reinforced polymer, to the best of our knowledge.

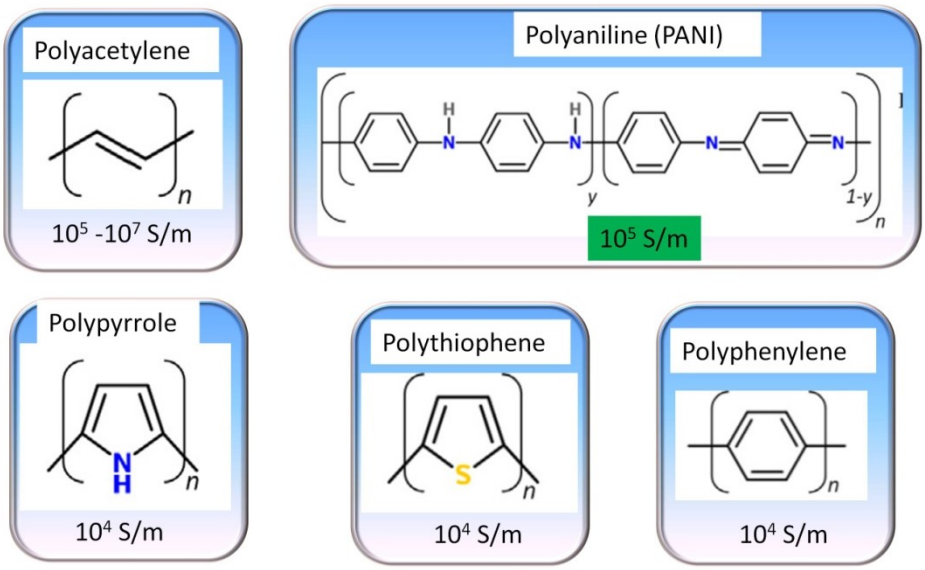

Fig. 1.3 The commonly used conduct polymer

In this work, GO/PANI, MWCNT/PANI and C60/PANI hybrids were employed into polymers by dispersing them into the divinylbenzene (DVB) solution. The conductivity tests were conducted to investigate the difference of three carbon/PANI hybrids. It is observed that the max AC conductivity of CFRP made of MWCNT/PANI was measured to be 22.4 S/m, which has been improved by more than 3 orders of magnitude compared to CF/DVB, and more than 2 orders of magnitude compared to CF/epoxy. GO/PANI hybrids show a cooperative improvement of through-thickness electrical conductivity and interlaminar shear strength (ILSS). For the C60/PANI hybrids reinforced polymer composites, the AC electrical conductivity increased from 9×10^{-10} S/m to 63.7 S/m at the frequency of 1Hz, more than 10 orders of magnitude. On the contrary, the thermal conductivity was reduced to extremely low of only 0.164W/m. K from 0.579 W/m. K. This decoupling of electrical and thermal conductivity of polymer bulk composites opens diverse opportunities for new materials and systems.

These outstanding results make the carbon/PANI hybrids reinforced composites become a competitive material for EMI shielding material, light strike protection material and thermal electrical materials. This work provides us with a novel vision to design functional materials by utilizing synergetic effects of different

ingredients.

1.1 Nanofiller Reinforced Polymer Conductive Composites

At present, the main way to improve the interlayer conductivity of carbon fiber reinforced composites are to add nanocomposites with excellent electrical properties, such as carbon nanotubes, graphene and metal nanowires, to the polymer matrix. Among them, the carbon nanotubes reinforced insulating polymer system conductivity is more typical. Such as A.H.Windle, Liu, Lei, Gojny[15-17] added carbon nanotubes to the epoxy resin system to increase the conductivity of the epoxy to 10^{-2} S / m; Sundararaj [18] studied the electrical properties and electromagnetic shielding properties of multi-walled carbon nanotubes/polycarbonate composites. It was found that the electromagnetic reflectance and absorption of the composites increased with the increase of the addition of carbon nanotubes. Jihua Gou of the University of Central Florida Task group [19] made nanofibers paper with carbon nanofibers and nickel nanowires. Carbon nanofibers paper was attached to the surface of CFRP laminates under the resin transfer molding process, replacing the existing lightning protection surface and significantly.

The carbon fiber composite material surface conductivity, and thus effectively reduce the material lightning damage;; Jinbo Bai et al. [11] added 0.5 wt% CNT-Al_2O_3 mixed nanofillers to the fiber composites, increasing the conductivity of the fiber composites by 4-5 orders of magnitude. In addition, graphite reinforced conductive composites seem to have a lot of research, the conductivity of polymer materials after adding graphite to show a few orders of magnitude to improve. For example, Novak et al. [20] studied the effect of graphite powder on the electrical properties of epoxy resin and polyurethane composites. It was found that the limit concentration of the packing was 22 vol% and the maximum conductivity was close to 10^{-2} S / m. Recently, with the extensive application of graphene materials, graphene nanosheets enhance the polymer conductivity research has also made progress. Yousefi [21] introduced graphene into the epoxy resin system to obtain a new composite material with anisotropic conductivity; Macosko, Christopher W [22] prepared a conductive polyurethane by adding 0.5 wt% thermal reduction of

graphene oxide to a polyurethane material system; Seung Hyun Hur [23] designed a graphene/silver nanowire reinforced epoxy composite, which has greatly improved the conductivity of the composites because the silver nanowires reduce the tunneling resistance between graphene; Chandrasekaran [24] investigated the conductivity of graphene nanosheets/epoxy composites, and the conductivity reached a maximum of 1.8 * 10^{-3} S / m when the addition was 1 wt%.

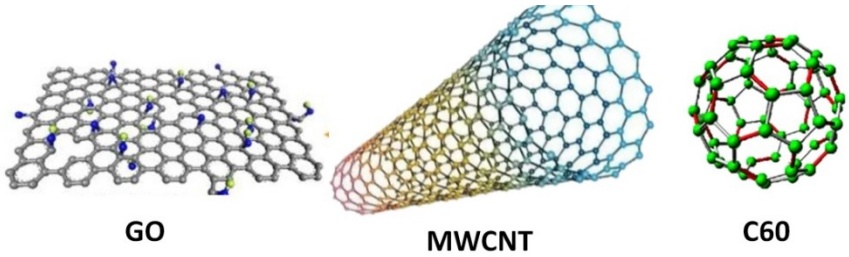

Fig. 1.4 The commonly used carbon-based nanofillers

https://image.baidu.com

In general, we can discover that material scientists have more interest in designing polymer-based conductive composites by adding carbon-based nanofillers (in Fig. 1.4). However, it is noted that the research of polymer-based conductive composites reported is usually simple to add conductive filling measures, the mechanism of the conductivity of the composite material is relative lack of research. The strategy by addingnano-filler to improve the polymer conductivity still has the following questions:

(1) The addition of nanofillerscannot infinitely increase the conductivity of the composites due to the presence of percolation thresholds. For example, when the carbon nanotubes is added 1 wt%, the conductivity in the thickness direction of the carbon fiber / epoxy composite material achieves a maximum of 1 S/m, and the increase in the conductivity of the carbon nanotubes is not significant. The presence of this bottleneck makes it easier add conductive nanofillers that cannot meet the needs of highly conductive applications. For example, electromagnetic shielding materials require conductivity to be greater than 10 S/m.

(2) Simple physical addition of nano-material dispersion is hard to control.

(3) Although the carbon nanotubes have a large gap between them and cannot effectively form a conductive network.

1.2 Conductive Polymer

Conductive polymer, refers to the doping or other means can make the conductivity between the conductor and the insulator inside the polymer [25]. Usually refers to the intrinsic conductive polymer, this type of polymer main chain contains alternating single and double bonds, thus forming a large conjugated π electronic system. Flow of π electrons creates the possibility of conduction. The first conductive polymer was discovered in 1977, when American Scientist Alan J. Heeger, Alan G. MacDiarmid and Japanese scientist Hideki Shirakawa found that the polyacetylene film after iodine doping had a room temperature conductivity of 10^5S/m, and compared with the conductivity before the increase compared to nearly 10^{10} times [26]. This discovery completely broke the "polymer is the insulator," the inherent concept. Since then, a new field - conductive polymer was born. As a result of the discovery and development of conductive polymer field has made outstanding contributions, Three Scientists Professor Heeger, Professor MacDiarmid and Professor Shirakawa jointly earned the 2000 Nobel Prize in Chemistry [27]. Conductive polymer combines the performance of traditional polymer materials and semiconductor materials, have received rapid development. After more than 30 years'research and development, conductive polymer has become a set of chemical, solid physics and materials science in one of the latest interdisciplinary.

Conductive polymer materials can usually be divided into composite and structural.

(1) composite conductive polymer material refers to the ordinary polymer materials, a variety of conductive substances through the filling compound, surface composite, and other ways to produce conductive composite materials [25, 28, 29]. The principal varieties are conductive rubber [30-32], conductive plastic [33, 34], conductive fiber fabrics [35, 36], conductive coatings, conductive adhesives and conductive film. Its performance is closely related to the type, particle size, dosage, state and the dispersion state of the conductive filler. Commonly used conductive fillers are carbon black, metal powder, metal fiber, metal foils, metal oxides, carbon

fibers, carbon nanotubes, and the like [37, 38].

(2) Structural conductive polymer material [39] refers to the intrinsic conductive polymer, chemical or electrochemical doping through the conjugated π electronic structure [25]. Doping of conductive macromolecules refers to the oxidation or reduction of polymers, which correspond to migration of π electrons in the conjugated chains. Therefore, the doping of conductive polymers is divided into p (positive) and n(negative) type doping, also known as oxidative doping and reduction doping. The departure or entry of π electrons in the conjugated structure results in free radical ions in the conjugated chains. In order to keep electrical neutrality of the polymer, it is necessary to confine ions with oppositely charged ions around the conjugate chain, which is called the ion. Under the action of an applied electric field, these charged carriers move along the conjugate π bond, thereby achieving electron transfer, making the polymer conductive. Self-conductive polyacetylene (PA) [40] has been discovered since conductive polymers have attracted much attention due to their unique physical and chemical properties. Compared with ordinary polymers, conductive polymers have the following salient features[25, 41-43]: 1) large π electron conjugate structure; 2) the conductivity is strongly dependent on the main chain structure of the polymer, the nature of the dopant and the doping rate and other factors; 3) doping and de-doping process are reversible; 4) The conduct polymer has excellent physical and chemical properties, such as higher conductivity, reversible redox properties, doping or de-doping. Based on the above distinctive performance, conductive polymer in the forefront of electronic technology has a considerable application value.

Conductive polymer materials play an important part in the field of materials science. At present, conductive polymers have been widely used in electronic devices [44, 45], such as field-effect transistors, light-emitting diodes and solar cells, etc. However, compared with ordinary polymers, the conductive polymer has poor environmental stability, poor machinability and poor mechanical properties. At present, there are more mature, more sensitive intrinsic conductive polymers [46-50] such as polyacetylene, polythiophene, polypyrrole, polyaniline and their derivatives(in Fig. 1.5).

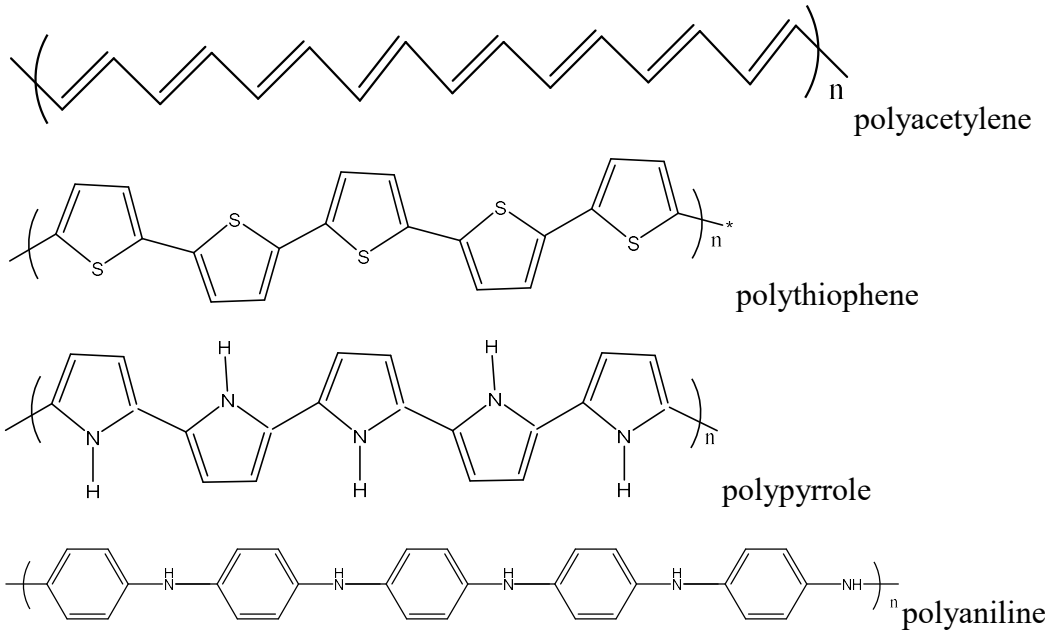

Fig. 1.5 Chemical structures of conductive polymer

Primary studies on conductive polymers focused on the conductivity of their doped states. Then, after nearly three decades of progress, the study of conductive polymer performance is in the ascendant. The conductive polymer has turned out to be the hotspots of materials science because of its unique structure and excellent physical and chemical properties. Conductive polymer materials in the thermoelectric materials, optoelectronic devices, conductive materials, sensors, and other fields get a wide range of application prospects [51-57].

(1) The conductive polymer has excellent conductivity between the insulator and the metal conductor, low thermal conductivity, easy to improve and modify the structure, light weight, low cost and other excellent performance, and thus in the field of organic thermoelectric materials has great application prospects [56, 57]. Thermoelectric materials are an environmentally friendly "green" energy conversion materials, can directly achieve the thermal energy and energy conversion. Inorganic semiconductor, as a traditional thermoelectric material, is at a bottleneck. The emergence of conductive polymer materials for thermoelectric materials research has opened up a fresh space. Compared with inorganic thermoelectric materials, conductive polymer as a new type of thermoelectric materials has the following

advantages: low thermal conductivity, easy synthesis and processing molding, lightweight, rich raw materials are simple to obtain, no poison. In addition, the conductive polymer material also has a unique chemical inert, conductive, rich electronic energy band structure, and its structure and performance can be introduced through the various functional groups to modify. Therefore, it is extremely important to study the thermoelectric properties of conductive polymer materials.

(2) Conductive polymers also can be used in electromagnetic shielding [58-61], printed circuit boards [62], microwave absorbing materials [63, 64], antistatic materials [50, 65], anticorrosive materials [66, 67] etc. However, the simple structure of the conductive polymer material make it has poor stability and poor processing formability, poor mechanical properties, has not yet entered the practical stage. For example, iodine-doped polyacetylene has a comparable conductivity to that of a metal conductor, but becomes less stable and cannot replace copper, aluminum, silver and other metals in applications.

(3) The conductive polymer has reversible dedoping-doping property, and there are a few reversible changes in the performance of the conductive polymer accompanying the reversible process. So it can apply to secondary batteries [68-70], electrochromic devices [71-73] and the like.

(4) Conductive polymer materials have similar properties with semiconductor materials [74, 75]. Therefore, the conductive polymer material in the electronic components has got rapid development. After the first conductive polymer was discovered, A. J. Heeger invented an ultra-thin and flexible electronic device, a light-emitting diode, using a conductive polymer to achieve the first application of conductive polymers.

1.3 Conductive Mechanism

1.3.1 Electrical conductive mechanism

The conductive mechanism of filled composite conductive polymer materials is very complex. There are many factors influencing the formation of conductive

pathways, such as the size and shape of the conductive filler's particles, the distribution of fillers in the resin, the kind of the matrix resin, the interfacial effect of the conductive filler particles and the matrix resin, and the composite material processing technology, curing conditions.The experimental results demonstrate that when the content of conductive filler in the composite system increases to a certain critical content [76], the resistivity of the system decreases abruptly, and the change range is about 10 orders of magnitude. In order to clarify this phenomenon of conductive properties of the mutation, people put forward a lot of theory [77-80], including the percolation theory, tunneling theory and field emission theory.

At present, the percolation theory, known as the conductive channel theory has been proposed, which supposes that the system of conductive particles are connected to each other into a chain, electrons go through the chain to produce the conductivity. It is primarily used to explain the relationship between resistivity and filler concentration. For example, the percolation theory can explain the abrupt change of resistivity at the critical concentration of conductive filler [81]. At present, all kinds of percolation models can only describe the laws of some targeted systems. Theoretical research and practical results are still large deviation [82-84], so the research in this area needs to be further refined.

The tunneling theory [85]introduce the quantum mechanics into the study of the relationship between the resistivity and the gap. The tunneling theory considers that conduction is not decided by direct contact of conductive particles, but by the vibration of electron [86]. The tunneling effect theory can reasonably explain the conduct behavior of the polymer matrix and the conductive filler. This theory can be consistent with the experimental data of various conductive composite systems. However, the tunneling mechanism can only analyze and discuss the conductive behavior of the composites in a certain concentration range of the conductive filler.

The conventional conductive mechanism of filled polymer composites is combing the three mechanisms of percolation theory, tunneling and field emission. When the content of conductive filler and the applied voltage are small, the distance between the conductive particles is larger. The probability of forming the chained conductive

channel is smaller. In this situation, the tunneling mechanism plays a dominant role. When the content of the conductive filler is low and the applied voltage is high, the field-emission mechanism can explain. While the content of conductive filler is high, the distance between conductive particles is small, the probability of forming chain-like conductive channel is large, and the mechanism of percolation theory becomes remarkable.

1.3.2 Thermal conductive mechanism

Heat is transferred from a higher temperature to a lower contact object, or a portion of a high temperature to a lower temperature part in an object called heat conduction. The simple thermal process is due to the movement of microscopic particles such as molecules, atoms and electrons in the object, transferring energy from the high temperature region to the low temperature region.The basic law of heat conduction was proposed by the French mathematician Fourier in 1822. On the basis of experiment, Fourier made a scientific summary of the steady-state thermal phenomena in the same homogeneous objects, and established the connection between the temperature field and the heat flux density inside the object, which is called the elementary law of thermal conductivity. The mathematical expression of Fourier's law is showed in formula.1-1.

$$q = -K\frac{\partial y}{\partial x} = -Kgradt \qquad (1\text{-}1)$$

Where q is the heat flux, in units of W/m^2; *grad t* is the temperature gradient; *K* is the thermal conductivity, with the unit of *W/m.K*.

The response of the polymer material always lags behind the stimulus because of the viscoelasticity of the polymer, so the thermal conductivity of polymers is more complex than metal. There are numerous factors that affect the thermal conductivity of polymer materials, such as the temperature, pressure, crystallinity, orientation, and degree of crosslinking. All the atoms in the system are assumed to vibrate at the same frequency, and these vibrations have a fixed phase relationship with each other, so

there is a plane wave in the lattice. These waves are called lattice waves [78]. And the energy of the grid wave is quantified, and we call it the phonon.

The thermal conductivity of the phonon can be expressed as Formula.1-2:

$$K_t^h = \frac{1}{3} C_V^h \upsilon_s \overline{\lambda_s} \qquad (1\text{-}2)$$

C_V^h is phonon heat capacity; υ_s is the speed of the phonon in the material; $\overline{\lambda_s}$ is the phonon average free path.

The thermal conductivity of photons can be expressed as Formula.1-3:

$$K_t^r = \frac{1}{3} C_V^r \upsilon_r \overline{\lambda_r} \qquad (1\text{-}3)$$

C_V^r is radiant heat capacity; υ_r is the speed of the photon in the material; $\overline{\lambda_r}$ is the photon average free path.

The thermal conductivity of electronics can be expressed as Formula.1-13:

$$K_t^e = \frac{1}{3} C_V^e \upsilon_e \overline{\lambda_e} \qquad (1\text{-}4)$$

C_V^e is electronic heat capacity; υ_r is the speed of the electronics in the material; $\overline{\lambda_r}$ is the average free electronic path.

In order to predict thermal conductivity of filled thermal polymer composites, many scholars have proposed various theoretical models: Maxwell-Eucken model [87], Bruggeman model [88], Russell model [89], Jefferson model [90], and Peterson model [91] are used to predict the thermal conductivity of composite materials. Agari [92] proposed a new mathematical model (1-5) by studying the thermal conductivity of high-filled and ultra-high-filled polymer composites. In his model, it is assumed that the particles are uniformly dispersed

$$lg\kappa = V_f C_2 lg\kappa_2 + \left(1 - V_f\right) l\, g(C_1 \kappa_1) \qquad (1\text{-}5)$$

C_1 is the factors affecting the matrix crystallinity and crystal size, C_2 is the free factors; κ is the thermal conductivity of the composites, κ_1 is the thermal conductivity of polymer; κ_2 is the thermal conductivity of the filler; V_f is the volume fraction of the filler.

1.4 Object of this research

Enhanced electrical conductivities also can be achieved in polymer composites by integrating carbon nanofillers and conduct polymers (CPs) [93, 94]. Besides this, CPs like polyaniline (PANI) addition is also reported increasing the CFRP's conductivity [6, 95]. However, no investigations have been reported on the design of multifunctional material based on the hybrids of carbon-based nano-fillers/polyaniline hybrids, to the best of our knowledge.

In this work, MWCNT/PANI, GO/PANI and C_{60}/PANI hybrids were employed into the polymer matrix to improve the different functional polymer composites by dispersing them into the divinylbenzene (DVB) solution. As far as we are concerned, this is the first attempt to study the difference of the functional materials obtained by carbon-based nano-fillers/polyaniline hybrids.

The present research focus on the development of the functional polymer composites by adding carbon-based nano-fillers/polyaniline hybrids into the polymer. The objectives of this research are (1) to develop an conductive polymer system; (2) to gain a better understanding of the conductive mechanism of the polymer composites; (3) to provide a feasible and economical method for the design of polymer nanocomposites.

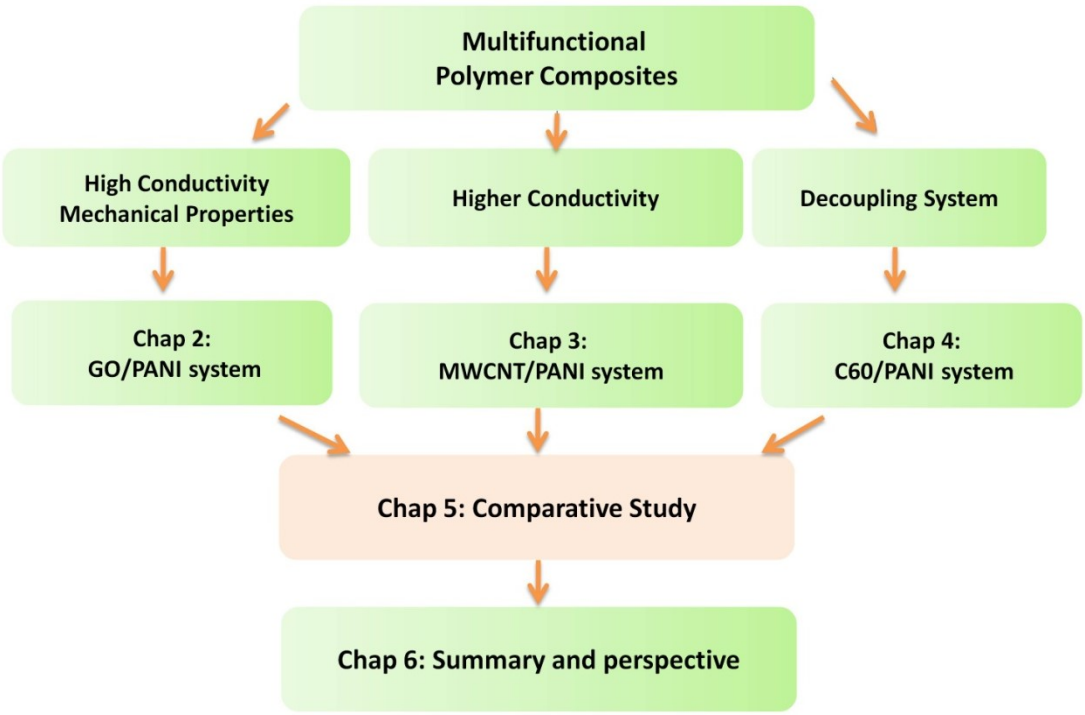

Fig. 1.6 The flowing chart of the Ph.D thesis

There are in total 4 main chapters in this thesis not including the introduction and summary as showed in Fig. 1.6. Chapter 2: graphene oxide (GO) was added to a polymer composites system consisting of surfactant-wrapped/doped polyaniline (PANI) and divinylbenzene (DVB). The nanocomposites were fabricated by a simple blending, ultrasonicdispersion and curing process. New composites show higher conductivity (0.02–9.8 S/cm) than the other reported polymer system filled with PANI (10^{-9}–10^{-1}S/cm). With as low as 0.45 wt% loading of GO, at least 29% enhancements in electric conductivity and 29.8% increase in bending modulus were measured. Besides, thermal stability of the composites was also improved. UV–Vis spectroscopy, X-Ray diffraction analysis (XRD) and scanning electron microscopy (SEM) revealed that the addition of GO improves the dispersion of PANI in the polymer composite, which is the key to realizing high conductivity.

Chapter 3 targets the conductivity enhancement effect and its mechanism for different types of carbon-based nano-fillers/conduct polymer hybrids in carbon fiber reinforced polymer (CFRP). Multi-walled carbon nanotubes (MWCNT) /polyaniline (PANI) and graphene oxide (GO) /PANI hybrids were separately dispersed into

divinylbenzene (DVB) to make the CFRP composites. The alternating current (AC) electrical conductivity results show that both the binary MWCNT/PANI and GO/PANI hybrids have significant enhancement on AC conductivity of the CFRP composites, while MWCNT/PANI gives better improvement over GO/PANI hybrids. The mechanism for the conductivity enhancement was studied in details by SEM, XRD, UV-Vis and nanoindenter. From the experimental results, circuit models of the CF/DVB, CF/DVB-MWCNT-PANI and CF/DVB-GO-PANI systems were proposed for the first time. An "interfacial excess energy" and quantum tunneling effect were supposed to account for the enhance conductivity. The max AC conductivity of CFRP made of MWCNT/PANI was measured to be 22.4 S/m, which has been improved by more than 3 orders of magnitude compared to CF/DVB, and more than 2 orders of magnitude compared to CF/epoxy. Thus, CF/MWCNT-PANI composites can be considered as promising candidates for multifunctional material where high conductivity is demanded.

Chapter 4 targets hybrid nanoparticles, fullerene (C_{60}) and polyaniline (PANI), were incorporated into the polydivinylbenzene (PDVB), and their decoupling effect of electrical and thermal conductivity was investigated. The hybrid particles were fabricated through a simple one-step process in the solution of divinylbenzene (DVB) monomer. The morphology and structure were characterized by TEM, SEM and FTIR. After the incorporation of C_{60}/PANI hybrids into DVB monomer, the electrical conductivity was improved significantly while the thermal conductivity was reduced simultaneously, resulting in effectively decoupling thermal/electrical conductivity. The AC electrical conductivity increased from 9×10^{-10} S/m to 63.7 S/m at the frequency of 1Hz, more than 10 orders of magnitude. On the contrary, the thermal conductivity was reduced to extremely low of only 0.164W/m. K from 0.579 W/m. K. Dissipative particle dynamics (DPD) simulations were also conducted to gain further understanding about the decoupling effect and mechanisms related to dispersibility of C_{60} in the polymer system. The DPD results exhibited better agreement with the experiment results of electrical and thermal conductivity. These results suggest that DPD can be a versatile method for designing functional polymer composites.

Simultaneously, the decoupling of electrical and thermal conductivity of polymer bulk composites opens diverse opportunities for new materials and systems.

Chapter 5 targets the comparative study of 3 different carbon/PANI hybrid systems will be discussed in this part. The doping action in three systems is different and the system of PANI/Carbon hybrid system appears as a uniform network structure. GO has a smaller χ parameter than MWCNT and C60. GO/PANI and C_{60}/PANI samples have higher decomposition temperature and lower thermal loss, while the MWCNT/PANI hybrids reinforced composites have lower decomposite temperature and thermal loss, that mean MWCNT cannot improve the thermal stability of the composites. The electrical conductivity of MWCNT-PANI/PDVB can fit the law of LANDAUER model. However, the electrical conductivities of GO-PANI/PDVB and C60-PANI/PDVB systems cannot fit the law at all. The calculated results of PANI/DVB have the perfectly consistent with the experiment results. After addition of GO and MWCNT, the calculated results also have perfect consistence with the experiment results. But for the calculated result, after the addition of C60, it introduces a huge difference with the experiment results. Voigt-Reuss model was chosen to explain the modulus's change. For GO-PANI/PDVB, there are hardly differences between Voigt-Reuss model and experimental values. However, in systems of MWCNT-PANI/PDVB and C60-PANI/PDVB, great divergence exists between the theoretical model and the experimental data.

Chapter 2

GO/PANI hybrid reinforced polymer nanocomposites

Abstract:

Graphene oxide (GO) was added to a polymer composites system consisting of surfactant-wrapped/doped polyaniline (PANI) and divinylbenzene (DVB). The nanocomposites was fabricated by a simple blending, ultrasonic dispersion and curing process. New composites show higher conductivity (0.02–9.8 S/cm) than the other reported polymer system filled with PANI (10^{-9}–10^{-1}S/cm). With as low as 0.45 wt% loading of GO, at least 29% enhancements in electric conductivity and 29.8% increase in bending modulus were measured. Besides, thermal stability of the composites was also improved. UV–Vis spectroscopy, X-Ray diffraction analysis (XRD) and scanning electron microscopy (SEM) revealed that the addition of GO improves the dispersion of PANI in the polymer composite, which is the key to realizing high conductivity. Utilizing synergetic effects of different ingredients is an important strategy to design new multi-functional composites. In this work, high-strength graphene oxide (GO) and conductive polyaniline (PANI) were selected to introduce into divinylbenzene (DVB) to fabricate a new type carbon fiber reinforced polymer (CFRP) laminates, where a cooperative improvement of through-thickness electrical conductivity and interlaminar shear strength (ILSS) was observed. With addition of 15wt% of PANI-GO at the optimized weight ratio of 60:1 to the hybrid CF/DVB-PANI-GO, a 150% enhancement of the electrical conductivity

(from 2.5×10^{-2} S/cm to 6.36×10^{-2} S/cm at the frequency of 10^2 Hz) compared to the CF/DVB-PANI, and a 76% enhancement of the ILSS (from 15.3 to 27.0 MPa) compared to the CF/DVB-GO were realized. The mechanism for such a synergic enhancement for both electrical and mechanical performance was investigated by rheology measurement and scanning electron microscopy (SEM), where uniform 3-D network formed by PANI/GO has been clearly observed.

2.1 Introduction

Conductive polymer composites are at the forward position of materials science research owing to the large number of applications that have been developed utilizing their interesting and unique features integrating the good mechanical, electrical [6], and thermal properties [96]. Polyaniline (PANI) is one of the most promising conducting polymers for industrial application mainly for its easy preparation, low cost, excellent electrical, optical, magnetic properties and environmental stability [97-102]. However, due to poor mechanical properties and processiblities, blending PANI with another polymer matrix has been shown to be a good strategy to develop conducting structural composites [103-105]. For example, epoxy resin/PANI-DBSA(Dodecylbenzenesulphonic acid) composite with the electrical conductivity in the range for electrostatic discharge (ESD) applications (10^{-9} to 10^{-2} S/cm) have been reported by Tsotra [106], Jia [107] and Massoumi [108] et al. Afzal [109] used a solution blending technique to synthesize poly-vinyl chloride/PANI-DBSA blends with the highest tensile strength of 37.7 MPa. Our group has also reported a simplified one-step method to prepare PANI/DVB conductive composites, where doping of PANI and curing of the composite take place simultaneously [105].

Graphene oxide (GO) is an attractive nanomaterial because of its low cost, mass production and solution processability. One the one hand, GO can help to get a better dispersion of other additives in the polymer matrix by synergetic effects due to its extremely high aspect ratio and surface area [110, 111]. Good dispersion of the

components leads to the formation of efficient networks for strain, electrical and thermal transfer in composite materials [110, 112-114]. On the other hand, as an oxidized derivative of graphene, GO has diverse chemical functional groups: carbonyl, epoxide, carboxylate and alcohols [115], which can reduce restacking, enhance interfacial interactions between the dispersed GO and the polymer matrix. At the same time, the templating effect of the GO can also improve the electrical conductivity, which is reported by Tkalya, E. As a result, GO has been used as multiscale reinforcement fillers to fabricate polymer composites. For example, Hussain reported multiscale polymer composites by using aramid fibers and GO nano-sheets, where the tensile strength of the material improved significantly [116].

In this chapter, we investigated the effect of GO added to a polymer composites system consisting of surfactant-wrapped/doped polyaniline (PANI) and divinylbenzene (DVB), where simultaneous improved conductivity and mechanical properties were obtained in the new nanocomposites. The nanocomposites are prepared by using DVB as solution-phase premixed with GO for different concentrations, which were then mixed with the part-doping PANI to form an all-organic composite and then followed by curing at higher temperature. The morphology of nanocomposites, dispersity and doping process was studied by SEM, UV-Vis and XRD. We report a new type of CFRP laminates utilizing our original thermosetting polymer system. The synergistic effects combining the high-strength of GO and the conductivity of PANI were confirmed by rheology measurement and scanning electron microscopy (SEM). Cooperative improvement of through-thickness electrical conductivity and interlaminar shear strength (ILSS) was realized by the addition of 15 wt% of PANI-GO at the optimized weight ratio of 60:1.

2.2 Experimental details

2.2.1 Materials

PANI Powder in Fig. 2.1a, supplied by Regulus Co. Ltd., Tokyo, Japan; DBSAin

Fig. 2.1c, Kanto Chemical Co. Inc., Tokyo, Japan; DVB in Fig. 2.1b, supplied by Sigma-Aldrich Co., St. Louis, USA. GO was synthesized based on Hummers method [23] The detailed process was reported elsewhere [24].

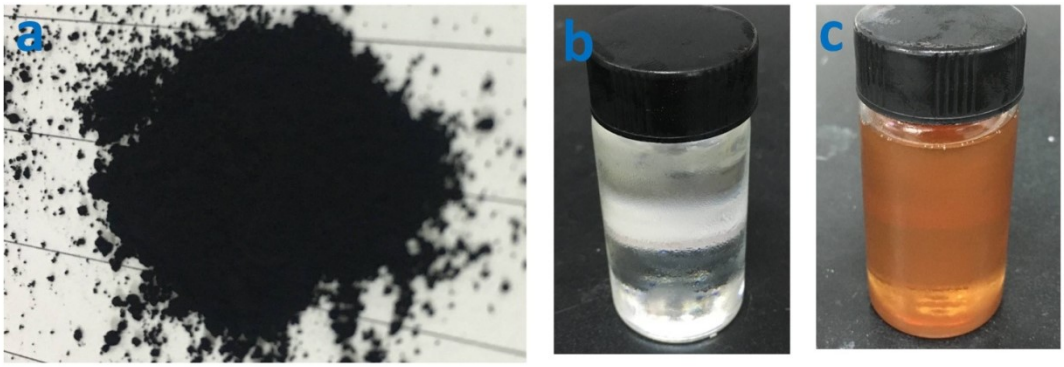

Fig. 2.1 The material used in the design of the material system

2.2.2 Processing of composites

The process for preparing DVB nanocomposites is shown in scheme 1. The composites were prepared by the following 3 main steps. Firstly, fine-grinded GO was dispersed into a DVB solution using a centrifugal mixer Fig. 2.2a and a sonicator in Fig.2-2 b (scheme 1:a-c_1). In parallel, PANI and DBSA were mixed thoroughly in a centrifugal mixer to obtain a homogeneous paste (scheme 1: c_2), which was then added to the GO/DVB solution. The suspension was again mixed thoroughly (scheme 1: d) and then poured into the mould for curing in a hot-press machine (scheme 1: e).

Fig. 2.2The centrifugal mixer and sonicator used in this system

Scheme 1. Schematic illustration of the preparation process for DVB composites with PANI and GO

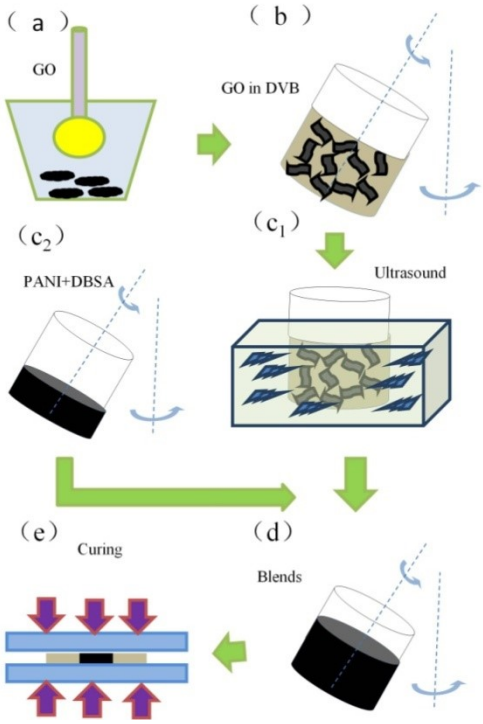

(a) Grinding GO into small particles; (b) Centrifugal mixing GO in DVB; (c_1) Dispersing GO in DVB by sonication; (c_2) Centrifugal mixing of PANI with DBSA; (d) Final centrifugal mixing; (e) Curing under hot-press machine.[94]

Preparation of PANI-DBSA doping paste

PANI was kept in an oven(Fig. 2.3a) for 2 h at 40℃ to eliminate moisture content. Dried PANI and DBSA were mixed to form the PANI-DBSA paste by physical mixing(Fig. 2.3b) in the ratio of 30:70 by weight percentage which is equivalent to the molar ratio of 1:0.69 of PANI:DBSA [105]. The mixed paste (Fig. 2.3c) of PANI-DBSA was made by a centrifugal mixer with speed of 2000 rpm for 5 minutes 3 times.

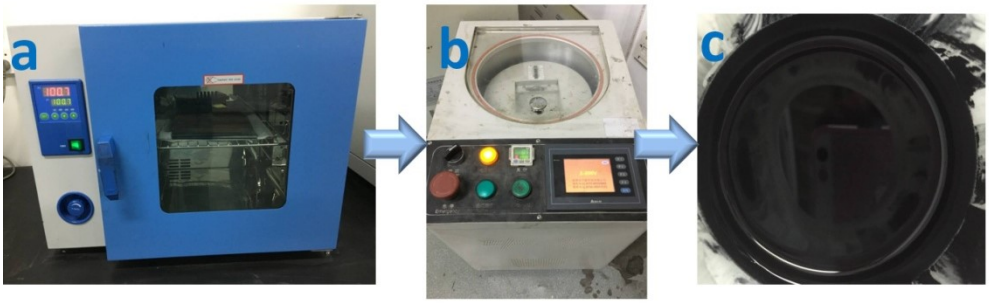

Fig. 2.3 The process for making PANI paste

Preparation of DVB-GO solution

GO was dispersed in by sonication for inconsecutive 10 h in the ice bath to get good disperse suspension. The content of the suspension is 0.15%, 0.3%, 0.45%, 0.6%. Dispersion stability against Vander Waals aggregation of GO in DVB was monitored at 10 min, 12 h and 24 h in Fig. 2.4. We can find that GO stayed homogenous in the DVB suspension at least for 24 h during which no obvious settlement was observed.

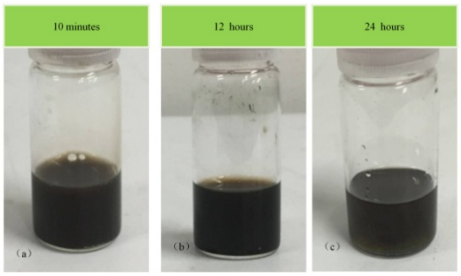

Fig.2.4 Stability monitoring of the GO dispersions in DVB(A) After 10 min, (B) after 12 h and (C) after 24 h[94].

Preparation of PANI-DBSA/DVB-GO

Paste of PANI–DBSA and DVB-GO was then mixed by a centrifugal mixer (Fig.2-5a) and poured into a mold (Fig.2-5b), cured using a Hot-press machine (Toyoseiki Minitest press.10, Fig. 2.5c). Samples were put into the Hot-press machine at 120℃ for 2 h [105]. Samples (Fig. 2.5d) of different dimensions were obtained for various measurements.

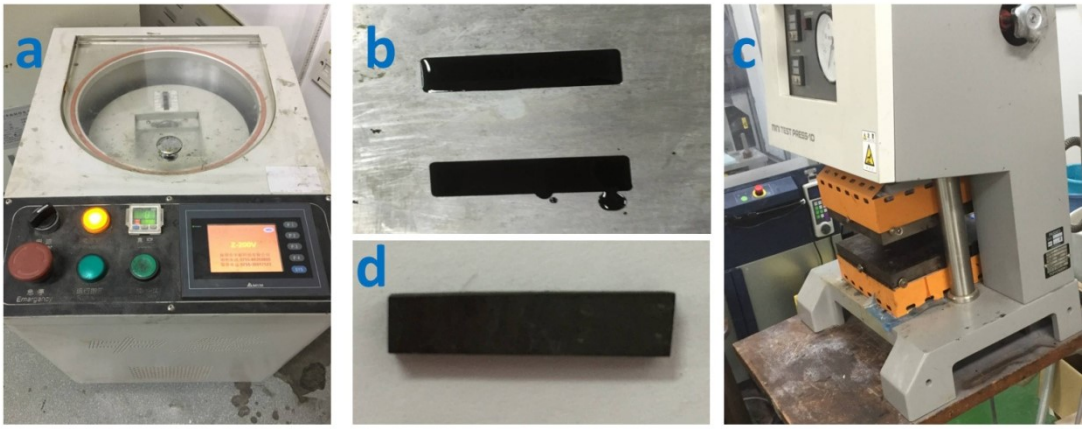

Fig. 2.5The process of the fabrication of the polymer composites

Processing of the composites

CF/DVB-PANI-GO laminates were prepared by applying the polymer matrix to the carbon fabric(Fig.2-6a). The fabrication process included two steps: (1) Preparation of DVB-PANI-GO hybrid polymer matrix; (2) Impregnation of the suspension into the carbon fabric to get the carbon fiber laminates. CF/DVB-PANI and CF/DVB-GO laminate as reference samples (Fig. 2.6c) were also fabricated by a cutting machine(Fig. 2.6b) according to the same procedure as above.

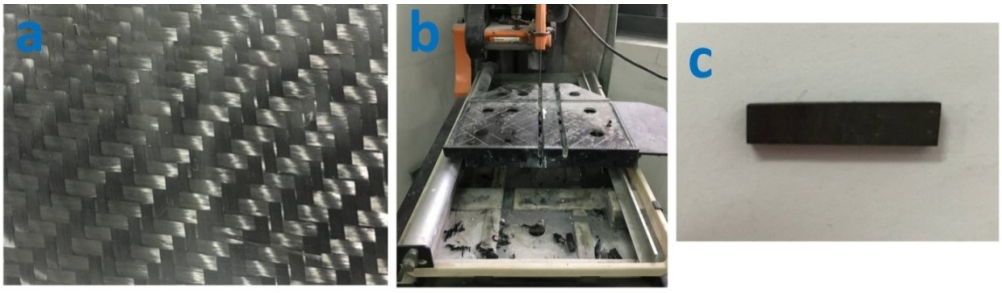

Fig. 2.6 The fabrication process of CFRP

PANI-DBSA doping paste and DVB-GO solution was firstly prepared according to our reported procedures [117]. Then paste of PANI–DBSA and DVB-GO was mixed by a 3-roller mill. The contents of each component are as follows: DVB 50 wt%, DBSA 35 wt%, PANI-GO 15 wt%. The mass ratio between PANI and GO varied from 300:1, 100:1, 60:1, to 45:1 for comparison.

The polymer suspension was spread uniformly on each fabric layer by using hand lay-up technique. The fabric layers were properly stacked into 12 plies and the fibers were aligned by $(0/90)_6$. Then, the laminates were cured in a hot-press machine under 4 MPa following the curing route as showed in Scheme 2a. Finally, cured laminates was taken out and cut into the required testing samples as showed in Scheme 2b. The volume fraction of carbon fiber is 60 vol%. For comparison, a conventional CF/epoxy laminate was also fabricated using the identical carbon fiber fabric accordingly. The fabricated baseline CF/DVB, CF/Epoxy samples and CF/DVB-PANI-GO samples are depicted in Scheme 2c and Scheme 2d.

Scheme 2. Preparation of carbon fiber reinforced polymer: (a) Curing process for the CFRP, (b) Picture of the CF/DVB-PANI-GO laminates; Micro-schematic representation of CF/DVB (c) and CF/DVB-PANI-GO (d).

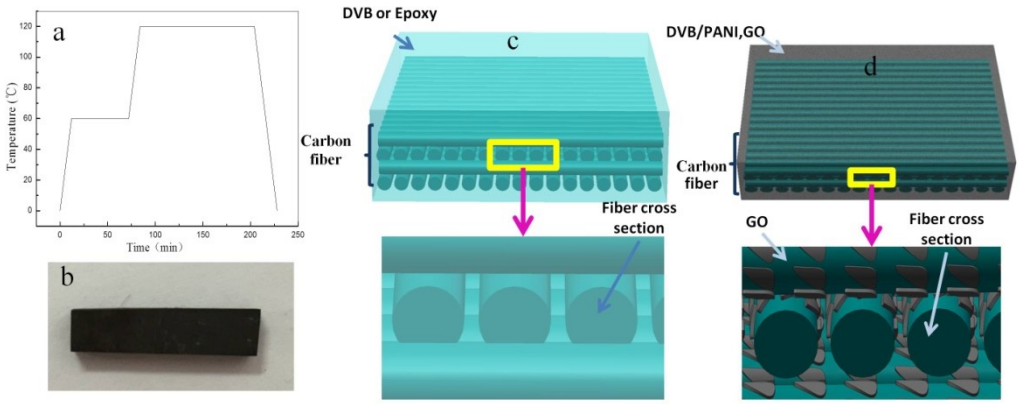

2.2.3 Characterizations

UV-Vis absorption spectra (Fig. 2.7a) of PANI-DBSA, PANI-DBSA/DVB, PANI-DBSA/DVB-GO films were obtained using a U-4100 spectrophotometer. Spectra were recorded from 250-1100nm. Wide-angle X-ray, scattering (WAXS, Fig. 2.7b) measurements were performed on a MicroMax007, RAXIS-IV + with a copper X-ray tube (CuK, wavelength λ=0.15418nm). The data were collected in the

step-by-step mode of 0.038 from 5°to 45°in 2θ. Thermogravimetric analysis was performed with a SDT Q600 V20.9 Build 20 instruments (Fig. 2.7c) under a 100 mL min^{-1} N_2 at the heating rate of 10 ℃.min^{-1}. The electrical conductivity (DC measurement) of the polymer composites was measured using LCR meter (3522-50LCR HiTESTER, Hioki E.E. Corporation, Ueda, Japan) by a four-probe method. DOTITE conductive adhesive paste (supplied by Fujikura Kasei Co. Ltd. Tokyo, Japan) and aluminum tape have been used to measure the conductivity. The flexural properties of Polymer composites were investigated according to ASTM D790, using Universal Testing Machine (Instron-5582, Fig. 2.7d) by three-point bending method. Scanning electron microscopy (SEM, Fig. 2.7e) images were acquired using a JSM-6700F cold field-emission gun scanning electron microscope using a SEI detector at 15 kV.

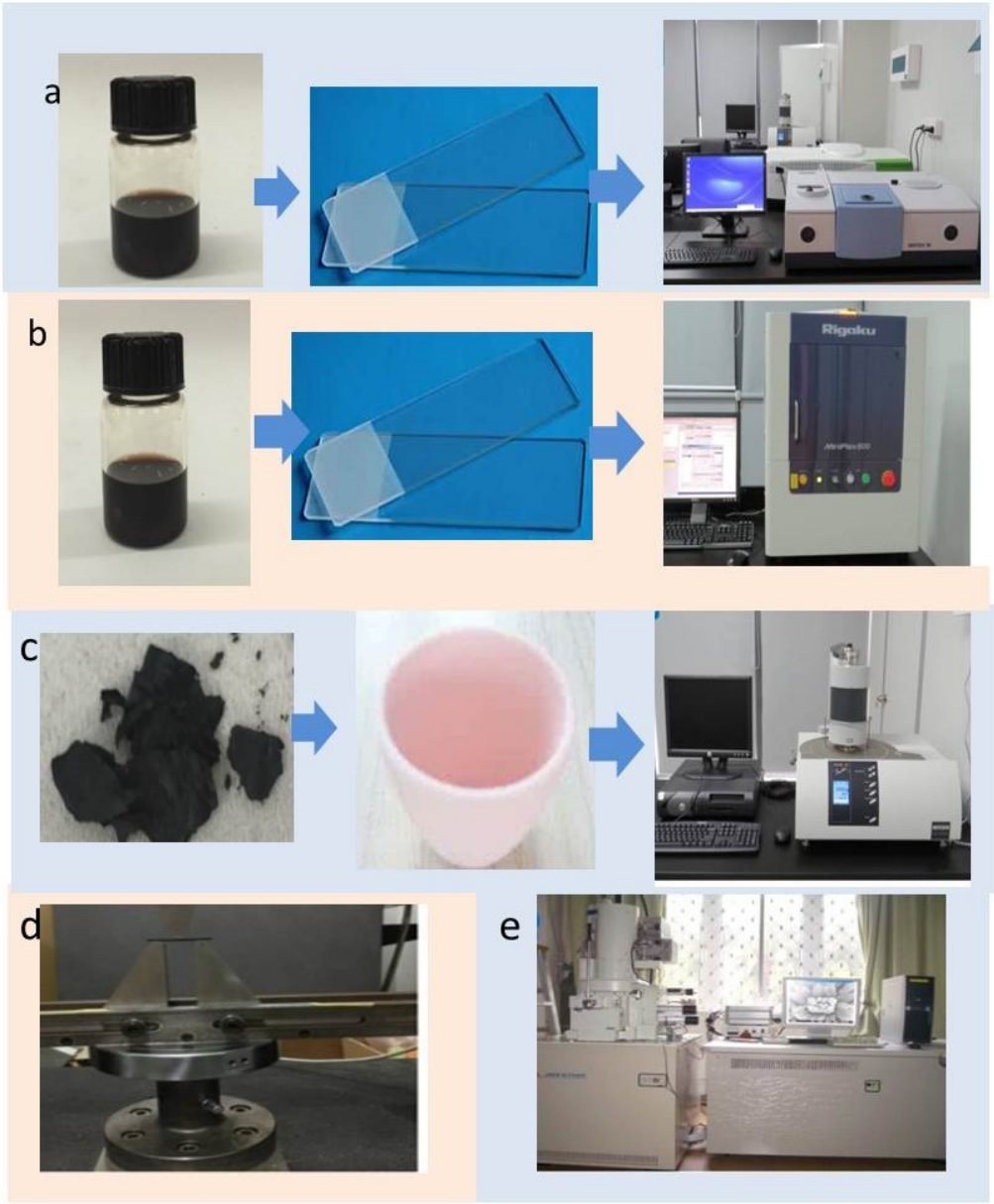

Fig. 2.7 Devices used in the research

The nanocomposite bulk of 10×20×2mm^3 in the plane perpendicular to the thickness were glued onto the stage of a nanomechanical testing instrument (Hysitron Inc., TriboIndenter 950. Fig. 2.8a). The samples (Fig. 2.8b) were mechanically ground and polished with 4000 grit silicon carbide papers and 1 μm diamond suspension. Subsequently, the samples were brought into contact with the diamond tip (Berkovich probe of 50nm radii) at a basic QS trapezoid with a max force of 3000 μN.

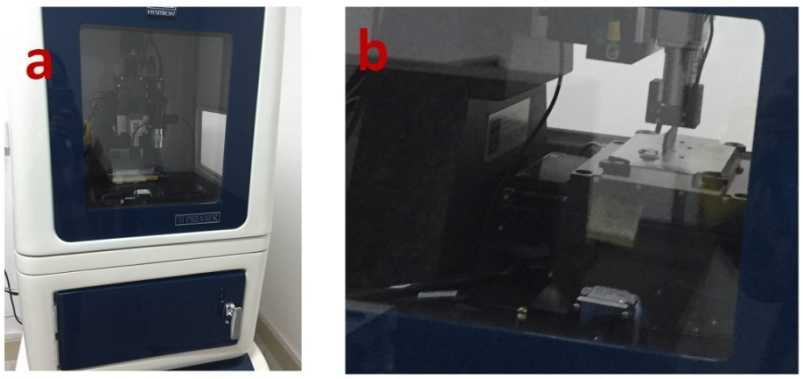

Fig. 2.8 The measure of nanoindentation

The alternating current (AC) electrical conductivity of the CFRP specimens (2×20×20.0 mm) were tested on a CHI660D electrochemical workstation (CHI660D, Shanghai Chenhua instrument Co., Ltd) in the out-of-plane (perpendicular to the fiber-plane) directions by applying an AC voltage of 5 mV in the frequency range from 10^2 to 10^5 Hz at room temperature.

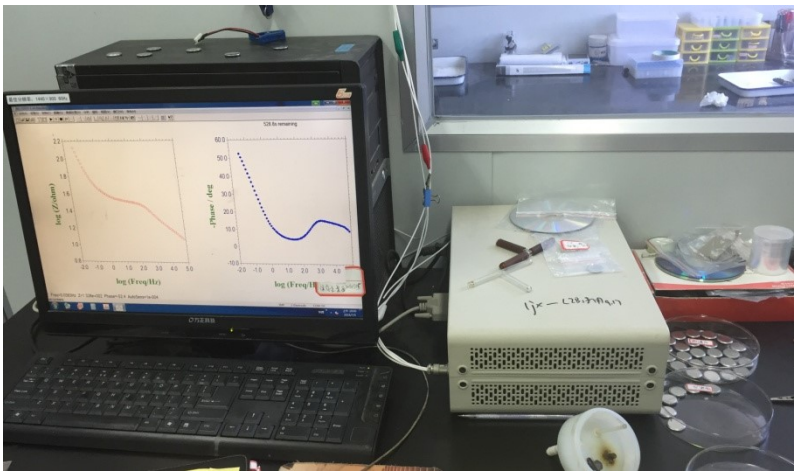

Fig. 2.9 The CHI660D electrochemical workstation used in this paper

ILSS were tested according to the ASTM D2344. CFRP specimens were cut from the composite panel using garnet-abrasive-assisted water-jet and their surface was polished prior to measurement. At least three specimens were tested.

High quality SEM pictures were obtained on a SU8010/EDX using a SEI detector at 5 kV.

Dynamic rheological measurements of the DVB-PANI-GO nanocomposites were

performed using a rheometer (Fig.2-10, Discovery Hybrid Reometer-2, DHR-2, TA, USA) with parallel plate–plate geometry with a diameter of 40mm, a gap of 500 μm. Rheological experiments were performed in the angular frequency range [10^{-1}–10^{2}] rad/s at 25°C. The shear modulus (G' for storage modulus and G'' for loss modulus) and the viscosity were measured as a function of angular frequency. Samples were stirred by ultrasound and then allowed to equilibrate for 5 min before each frequency sweep performed.

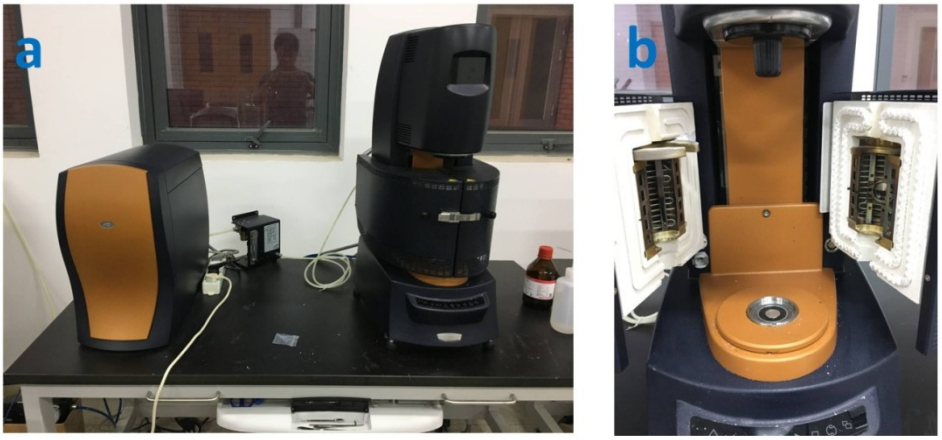

Fig. 2.10The measurement of dynamic rheological properties

2.3 Results and discussion

2.3.1 Properties of the polymer composites

The doping process analysis

The UV-Vis spectroscopy has been successfully employed to investigate the dispersion behavior of carbon nanomaterials [118, 119]. Solid-state UV–Vis samples were prepared by heating the blends films in between two layers of glass plates over 2 h at 120℃. The spectra for PANI in DVB, PANI-DBSA/DVB and PANI-DBSA/DVB-GO are shown in Fig. 2.11. The two absorption peaks at below 350 and 630nm are attributed to the characteristic peaks of undoped PANI [120]. For the PANI-DBSA/DVB and PANI-DBSA/DVB-GO, the peak 630nm disappears. This indicates that PANI is in a fully protonated state. The position of the peak at below 350nm still exists, whereas two new peaks at 450 and 810nm occur, which can be

attributed to delocalized polarons, relating to the doping process and conductivity of PANI [121, 122]. The peaks lying in these regions are found in all the films of the blends.

UV-Vis spectra of PANI-DBSA/DVB composite and PANI-DBSA/DVB-GO with different GO content in DVB are plotted in Fig. 2.12. It can be observed that peaks are shifted to longer wavelength after addition of GO from 0.15% to 0.6%, which might be due to the change of polarons' state from localization to delocalization, proving that the PANI molecular chains changed from compact to extend conformation [123]. In addition, the red-shift of the PANI-DBSA/DVB-GO composites was more obvious when added more GO, indicating that more extended PANI molecular chains were achieved in the PANI-DBSA/DVB-GO composite.

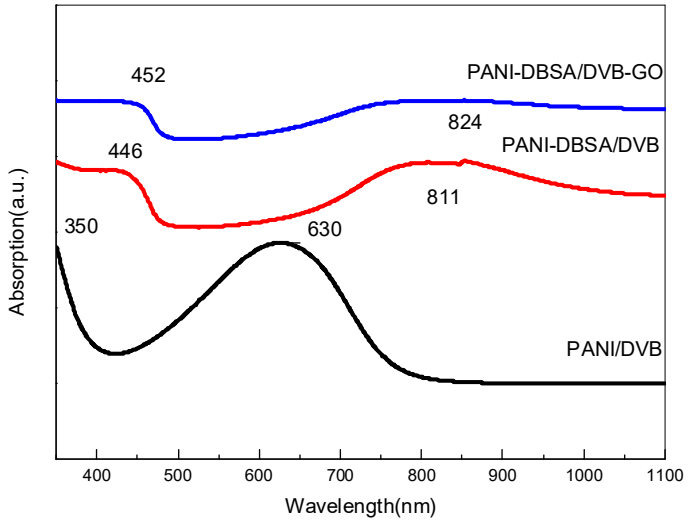

Fig. 2.11. UV-Vis spectra of PANI, PANI-DBSA/DVB and PANI-DBSA/DVB-GO[94]

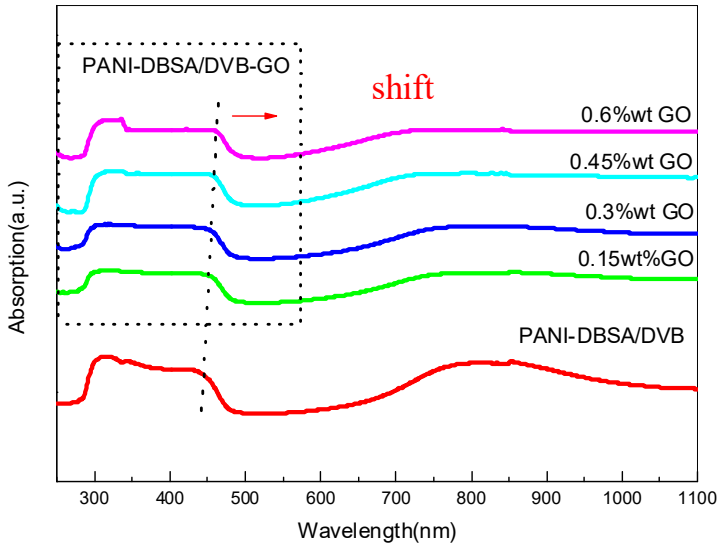

Fig. 2.12 UV-Vis spectra of PANI-DBSA/DVB composite and PANI-DBSA/DVB-GO with different GO content in **DVB**[94]**.**

Characterization of fillers and composites

The structures of various fillers and the process products in each stage were also investigated by XRD measurements. Fig. 2.13 shows the XRD patterns of GO, PANI, PANI-DBSA and PANI-DBSA/DVB-GO. The XRD pattern of GO exhibits a sharp reflection peak (002) at 2θ = 7.714°, corresponding to an layer to layer distance of 1.15 nm, indicating that the interlayer distance increases obviously because of the intercalation of oxide functional groups compared to pristine graphite (only has a d-spacing of 0.34 nm). In contrast to the XRD patterns of GO, the peaks corresponding to GO were not observed in PANI-DBSA/DVB-GO composites. The PANI is a lack of obvious crystalline character which shows a very broad reflection peak with the 2θ from about 16° to 26°. After doping with DBSA, the reflection peaks of PANI-DBSA become a little sharper, indicating an increase of crystallinity that means doping between PANI and DBSA formed salt. After addition of GO, The conduct element PANI-DBSA salt can keep its form and its conductivity.

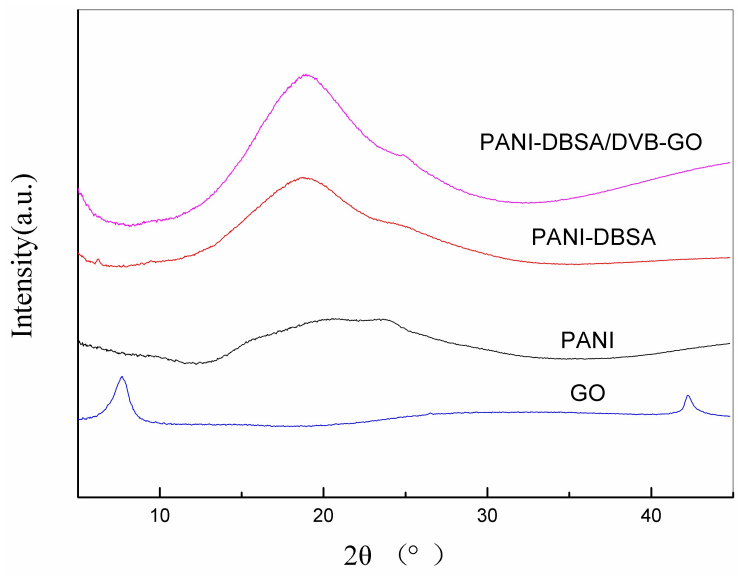

Fig. 2.13 X-ray diffraction patterns of GO, PANI,PANI-DBSA and PANI-DBSA/DVB-GO[94]

Thermal properties

TGA is one of the thermal analysis techniques used to quantify the weight change and thermal decomposition of the sample. Thermal stability analysis was further used to study the composition and structure of various materials. Fig. 2.14 shows the TGA curves of PANI, PANI-DBSA, PANI-DBSA/DVB, PANI-DBSA/DVB-GO. The composition of PANI-DBSA is 30% of PANI and 70% of DBSA. The PANI-DBSA/DVB composite is made of 15% PANI, 35% DBSA and 50% DVB. The content of GO is set at 0.45%. All the weight loss below 100 ℃ can be attributed to the deintercalation of water [124]. The weight loss of PANI-DBSA/DVB is about 70% after heating up to 600℃, but after the addition of GO, the weight loss of PANI-DBSA/DVB-GO is about 63%. A shift of 20℃ (from 310℃ to 330℃) in the decomposition temperature is observed in Fig. 2.14, suggesting an improvement in thermal stability. The enhancement in thermal stability is observed because RGO/PANI acts as ordered barrier [125] to minimize the permeability of volatile degradation products from the DVB composites. The TGA results demonstrated that a small quantity of GO can apparently improve the thermal stability of the composites. Mobility of PANI and poly DVB was restricted by the

good-disperse GO which may act as “efficient heat sinks” [126].

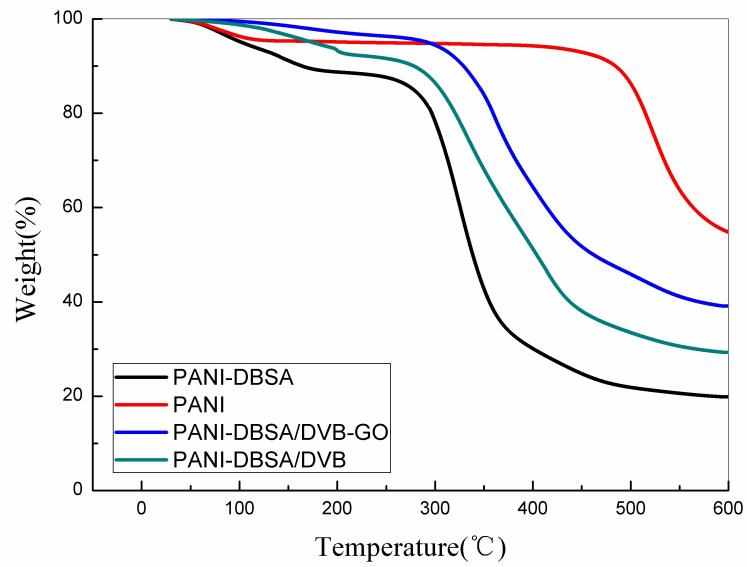

Fig. 2.14TGA curves of PANI, PANI-DBSA, PANI-DBSA/DVB and PANI-DBSA/DVB-GO [94]

Fig. 2.15 shows that when the content of GO increase from 0.15% to 0.6%, the initial decomposition temperature increase from 250℃ to 270℃. The end decomposition temperature and the weight-loss have no big difference when the content of GO increases. From 0.15% to 0.3%, the end decomposition temperature has an increase of 10 ℃ from 520℃ to 530℃ and a 5% reduction of weight-loss showed from 60% to 55%.

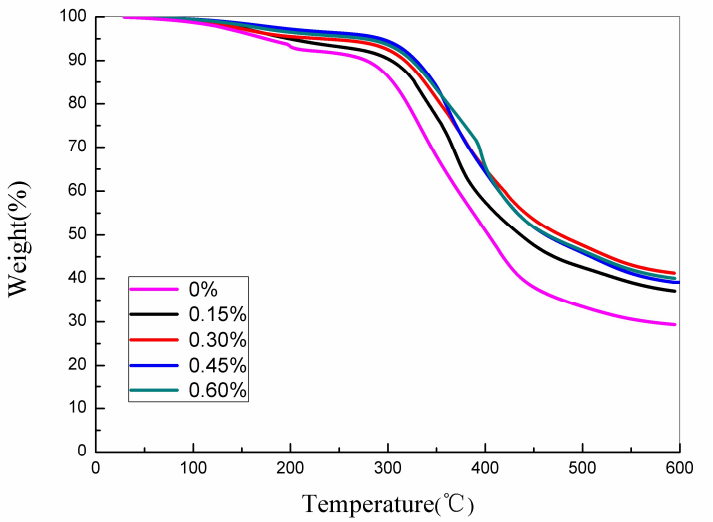

Fig. 2.15TGA curves of PANI-DBSA/DVB-GO with different GO contents [94]

Morphology

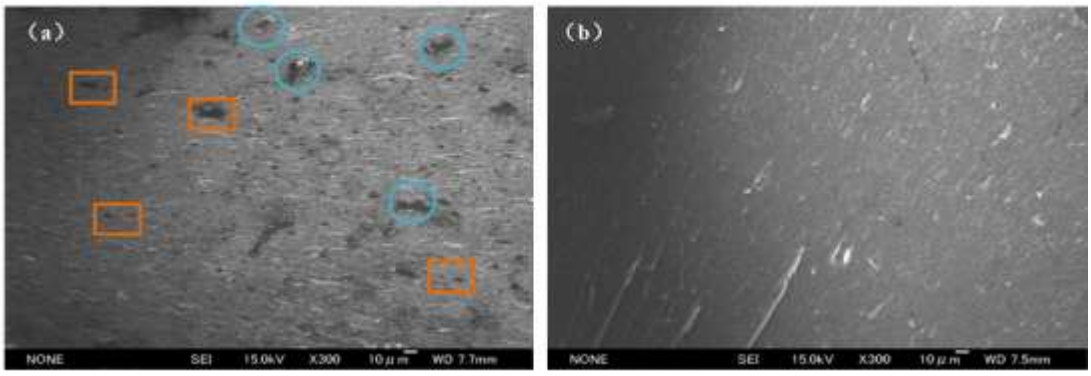

Fig. 2.16**.** TheSEM-image of the (a) PANI-DBSA/DVB composites and (b) PANI-DBSA/DVB-GO composites [94]

In order to observe the dispersion change, after the addition of GO, the cross-sections of PANI-DBSA/DVB and PANI-DBSA/DVB-GO were characterized by SEM. As showed in Fig. 2.16 (a), a lot of PANI–DBSA particles (blue circle) with an average size of 20 μm and 10 μm DVB holes (orange square) were observed in PANI-DBSA/DVB composites. In contrast, the PANI-DBSA/DVB-GO composites appear a uniform network structure as showed in Fig. 2.16(b), indicated that the GO layers can improve the dispersity of doped PANI particles. It is suggested that the good dispersion of the GO/PANI particles in DVB matrix could enhance the

surface-to-volume ratio and interfacial factors, which could on the whole contribute to potent electrical and mechanical properties of polymer composites. Because of this especial structure, the interfacial affinity of the GO/PANI with the DVB matrix increased and led to an ensured thermal stability too.

Electrical properties

The electrical conductivity (DC measurement) of the polymer composites was measured using LCR meter by the four-probe method, where very high conductivity (0.02-9.8 S/cm) were measured for all the PANI-DBSA/DVB-GO nanocomposites. To the best of our knowledge, this stands for the highest values reported so far for conducting polymer composites, which usually fall in the range of 10^{-9} to 10^{-1} S/cm [108, 127, 128].

Fig. 2.17 shows that the electrical conductivities of the blend composites ranged from 0.21 to 0.4 S/cm with the same PANI-DBSA content of 50%. In the same content of DBSA acid-doped PANI–DVB polymer, the conductivity improved at least 29% from 0.21 to 0.27 S/cm when the content of GO in DVB is only 0.15%. The highest conductivity is up to 0.4S/cm for DBSA-doped PANI composite when the content of GO in DVB is 0.3%. However, the electrical conductivity declined when the GO is 0.45% that maybe because of the aggregation of GO can lead to bad dispersity and destroyed the uniform network.

Fig. 2.17 is the comparison of the electrical conductivity between different composites prepared with GO and without GO. The content of GO is set at 0.45%. The content of PANI-DBSA in the composite is 30%, 50%, 70% and 90%. It is obvious to notice that the electrical conductivity go up with the increase of PANI-DBSA content. The electrical conductivity was improved by the addition of GO in all the composite with different PANI-DBSA content. The highest conductivity is up to 9.8 S/cm when the content of PANI-DBSA is 90%.

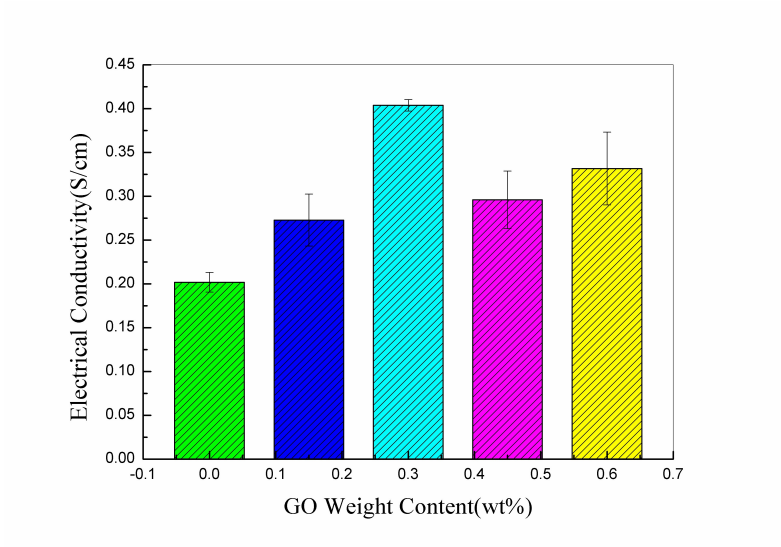

Fig. 2.17The nanocomposites'electrical conductivitywith different GO contents [94].

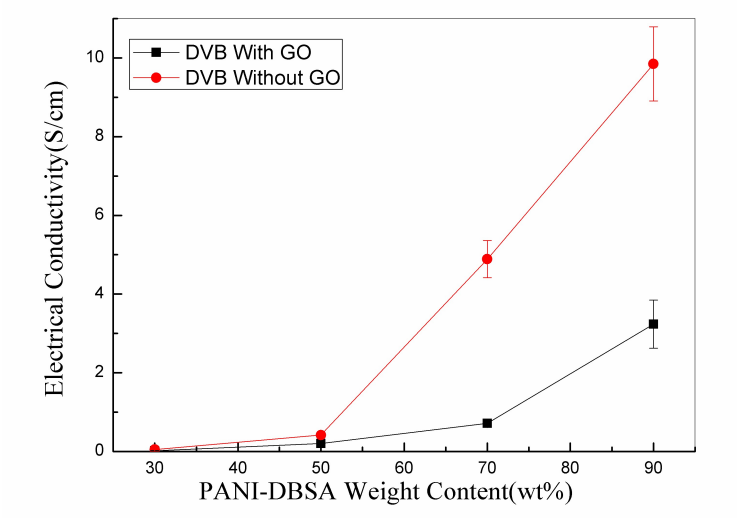

Fig. 2.18 The composite conductivity before and after GO addition with different PANI-DBSA contents [94].

Mechanical Properties

Three-point bending tests were performed to investigate the effect of GO on the mechanical properties. The results are presented in Fig. 2.19. In Fig. 2.19 all the content of PANI-DBSA is set at 50%, and DVB is 50%. Content of GO in DVB is from 0.15%, 0.3%, 0.45% and 0.6%. From the Fig. 2.19, we can see that the flexural modulus increase with the increase of GO's content. When the GO's content is 0.45%, the bending modulus reach to the highest 1.42GPa, respectively, which are increased by 29.8% compared with those of the neat PANI-DBSA/DVB composites when the

PANI-DBSA is 50% and DVB is 50%. The bending strength also shows an overall increasing trend as the content of the GO increases. The bending strength reaches to the highest 46.6 MPa when the GO's content is 0.6%.

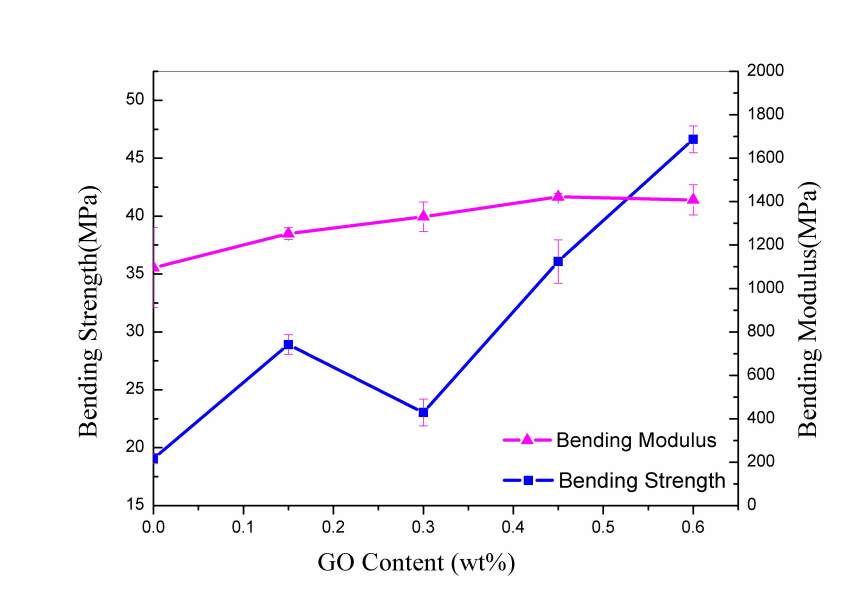

Fig. 2.19 Bending strengths and modulus of the PANI-DVB nanocomposites with different GO content [94].

In Fig. 2.20 and Fig. 2.21, content of GO in DVB was set at 0.45%. The flexural modulus and strength were compared with and without GO in different PANI-DBSA content, which respectively is 30%, 50%,70% and 90%. The flexural modulus and strength were improved after the addition of GO in all different content of PANI-DBSA. The highest flexural modulus and strength were 2.01GPa and 39.2MPa, respectively, which are increased by 12.5% and 2% compared with those of the neat PANI DVB composites, when the PANI-DBSA is 30% and DVB is 70%.

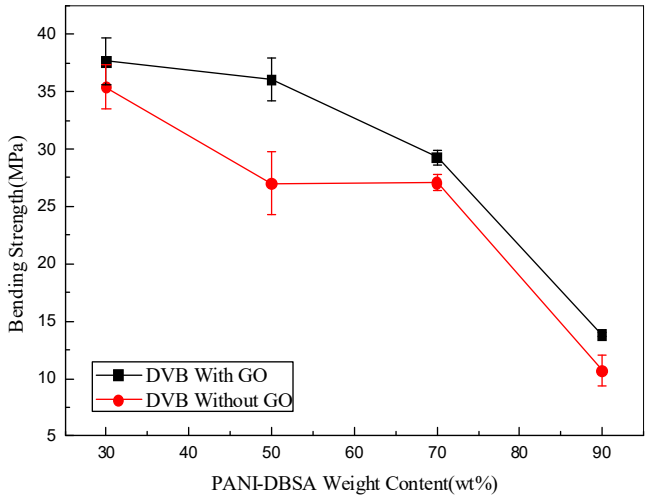

Fig. 2.20The bending strength of the PANI-DVB nanocomposites with different content of PANI-DBSA [94].

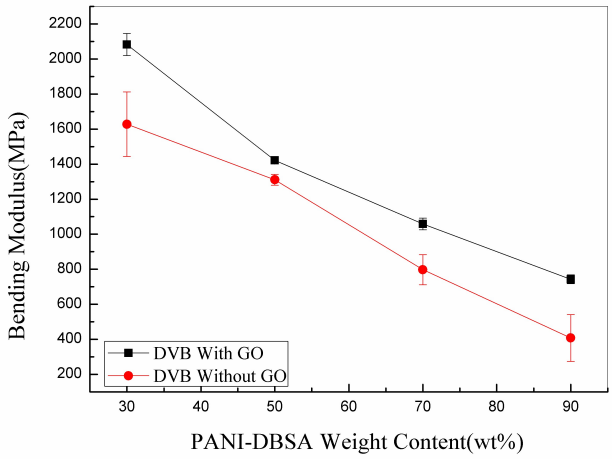

Fig. 2.21. The bending modulus of the PANI-DVB nanocomposites with different content of PANI-DBSA [94]

2.3.2 Properties of CFRP

Nano indentation surface mapping

An array of 10 by 10 indentations separated by 2 μm, covering an area of 20×20 μm^2, was mapped for the composites. Fig. 2.22(a-c) illustrates the results of the modulus map obtained three composites for DVB-PANI, DVB-PANI-GO and DVB-GO, correspondingly. The modulus values for the DVB-PANI composites lie in

a large range from 0.3 to 2.06 GPa, with large blue areas with low modulus observed (Fig. 2.22a), which means PANI agglomerates or low degree of polymerization of DVB happened [129]. While the DVB-GO composites modulus map (Fig. 2.22c) also shows a lager modulus range from 0.3 to 3.4 GPa, and a clearly high modulus region of enhanced mechanical properties was observed, the modulus values within this region approach 3.4 GPa, which is almost 70% higher than the highest values in Fig. 13a and Fig. 2.22b, which usually can attribute to the aggregation of GO. In spite of this, 3.4 GPa is a significantly low value compared to that usually attributed to pure GO (E = 32 GPa [130]. GO agglomerates result in a multi-layers GO platelet may be a reason. Secondly, DVB chains attached to the GO sheets as part of the strategy adopted to enhance their dispersion are also expected to decrease the modulus. The sample of DVB-PANI-GO (Fig. 2.22b) shows a relatively small modulus range from 1.1 to 2.2 GPa, indicating fairly homogenous distribution of mechanical properties at the submicron scale along the sample surface.

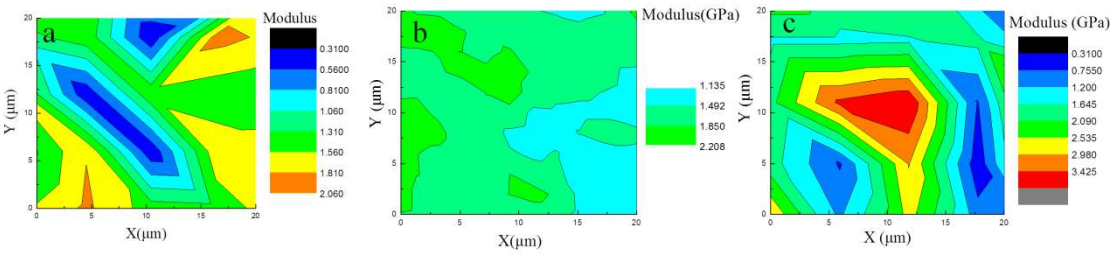

Fig. 2.22 Modulus contour plots constructed by the indentation data for DVB-PANI (a), DVB-PANI-GO (b) and DVB-GO (c) composites [131].

Through-thickness AC electrical conductivity properties

The through-thickness AC conductivity of the multiscale CF/DVB-PANI-GO laminates with the same fraction (50 wt%) of PANI-DBSA mixture but different GO: PANI ratio were measured in the frequency range from 10^2 to 10^5 Hz. CF/Epoxy was measured as contrast sample. The conductivities of the laminates as a function of frequency in the through thickness were measured.

As showed in Fig. 2.23, the through-thickness conductivity of CF/DVB-GO is only 7.37×10^{-4} S/cm, while the conductivity of CF/DVB-PANI is much higher

(2.5×10^{-2}S/cm). This is expected as GO is known to be poorly conductive but PANI is a highly conductive polymer. Surprisingly, the fabrication of CFRPs combined with hybrid PANI-GO fillers all showed much higher conductivities than the CFRP with either GO or PANI only in the frequency range from 10^2 to 10^5 Hz. As showed in Fig. 14b, the conductivities at the frequency of 10^2 Hz for the CF/DVB-PANI-GO hybrid increased from 3.5×10^{-2} to 6.36×10^{-2} S/cm while at ratio of PANI and GO varied from 300:1 to 60:1, which is about 86 times higher than the CF/DVB-GO laminates, 103 times higher than CF/Epoxy and 2.5 times higher than CF/DVB-PANI laminates. Such observations clearly confirmed the synergetic enhancement of electrical properties for the hybrid CFRP laminates. Further addition of GO to a ratio of 45:1 resulted in a drop in conductivity, indicating the aggregation of the redundant GO which will breakdown the uniform 3-D networks.

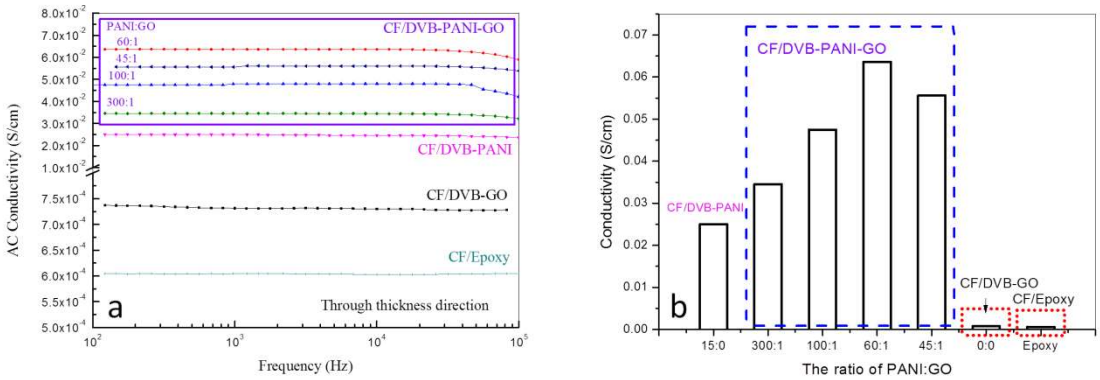

Fig. 2.23 The through-thickness AC electrical conductivity of CFRP with different ratio of PANI: GO plotted to frequency (a) and plotted to the ratio of PANI: GO at the frequency of 10^{-2} Hz (b) [131].

Interlaminar shear properties

ILSS tests were also measured to quantify the synergistic effects of GO and PANI on the interlaminar properties. Fig. 2.24 shows the relationship between ILSS of the laminate and the PANI-GO ratio. With addition of 15 wt% of PANI-GO at the optimized weight ratio of 60:1 to the hybrid CFRP, a 76% enhancement of the ILSS (from 15.3 to 27.0 MPa) compared to the CF/DVB-GO laminates and 73% increase (from 15.6 to 27 MPa) compared to the CF/DVB-PANI laminates were observed.

When the ration of GO increased to 45:1, the ILSS fells to 20.98 MPa, in consistent with the AC conductivity drop observed above.

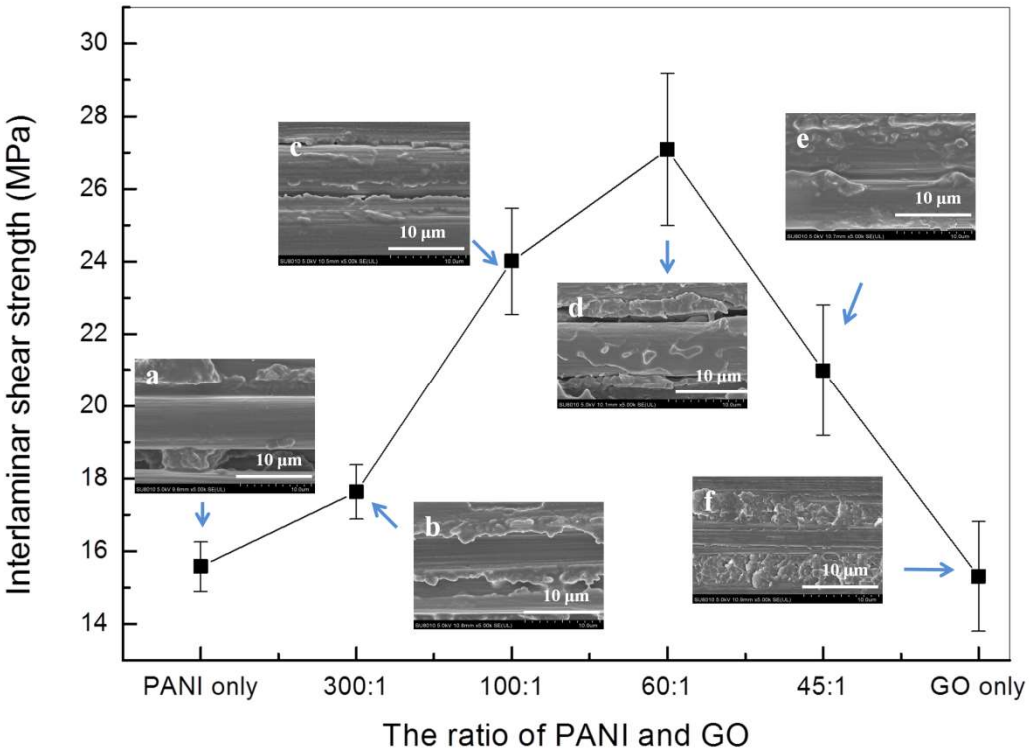

Fig. 2.24 The ILSS strength the CF/PANI-DVB laminates with different ratio of PANI/GO and the corresponding SEM images for the fracture surfaces of the laminates after short beam shear tests [131].

In order to understand the interface behavior and the mechanism responsible for the enhanced ILSS, the fracture surfaces of the laminates after short beam shear tests were examined by scanning electron microscopy (SEM). The SEM image for the CF/DVB-PANI laminates shown in Fig. 2.24a reveals that carbon fiber is completely detached from the matrix due to a weak adhesion interaction without GO. Meanwhile, the DVB matrix between the fibers is uniform, with a lot of PANI particles observed. It means that the fiber/matrix debonding is the dominant mechanism for the shear failure. In contrast, Fig. 2.24(b-e) show that the carbon fibers do not display a complete matrix debonding at the fiber surface. Especially in the Fig. 2.24d, a lot of GO sheets can be found on the surface of carbon fibers, probably because GO sheets

can cause the increasing strength and toughness of the interfacial region surrounding the carbon fiber [132].

Insight into the influence of hybrid PANI-GO on the electrical conductivity and the ILSS of the CFRP laminates

Rheology properties

Rheology were used to offer insight into the micro structural changes occurring within composite systems, depending on the filler–matrix interactions and the method of preparation [133]. Rheological properties of the DVB-PANI-GO hybrid composites with varying ratio of PANI: GO were investigated. Fig. 2.25(a-c) show the dynamic shear behavior, the storage modulus G', loss modulus G" (Fig. 2.25b) and viscosity (Fig. 2.25c) at 25℃ as a function of shear frequency (x) plotted to the different PANI-GO ratio. Both G' and G" increased for the DVB-PNAI-GO composites over the whole frequency range, without following a typical newtonian fluid behavior with scaling properties of approximately $G' \sim \omega^2$ and $G'' \sim \omega$. The DVB-PANI-GO behaves like solid by the formation of a mechanically stable network structure [134, 135]. Thus, the combination of PANI and GO can form a stronger and stable network in DVB matrix [135], which provides a precondition for the enhanced electrical conductivity and ILSS of composites.

Suspensions all show an apparent shear thickening, which may be attributed to an increase in geometric confinement of the GO with increasing concentration. Additions of GO caused a higher viscosity over the entire range of shear rate. Unlike in the epoxy matrix [136], the viscosity of the composite only shows a maximum viscosity of 2.82 Pa·S, which can provide a better infiltration of the polymer matrix to carbon fiber. Usually, mixing nanofillers into the poly matrix will result in a significant increase in the viscosity of the resin [137]. For example, the incorporation of CNTs into the resin will increase the viscosity of matrix. The viscosity of E20 is as high as 4000Pa·S [138], five orders of magnitude higher than that of the matrix, 1400 times of our system. Such high viscosity will introduce very high make the infiltration of carbon fiber fabrics become much more difficult in the resin infusion process. On the other hand, in our system, resin viscosity does not increase compare to the high

viscosity of epoxy after dispersing the nanofillers. The processing for fabricating composites, like resin infusion molding, can be performed with the traditional procedure. The infiltration of carbon fiber fabrics will become much easier in resin infusion process and obtain high quality CFRP laminate with low porosity finally.

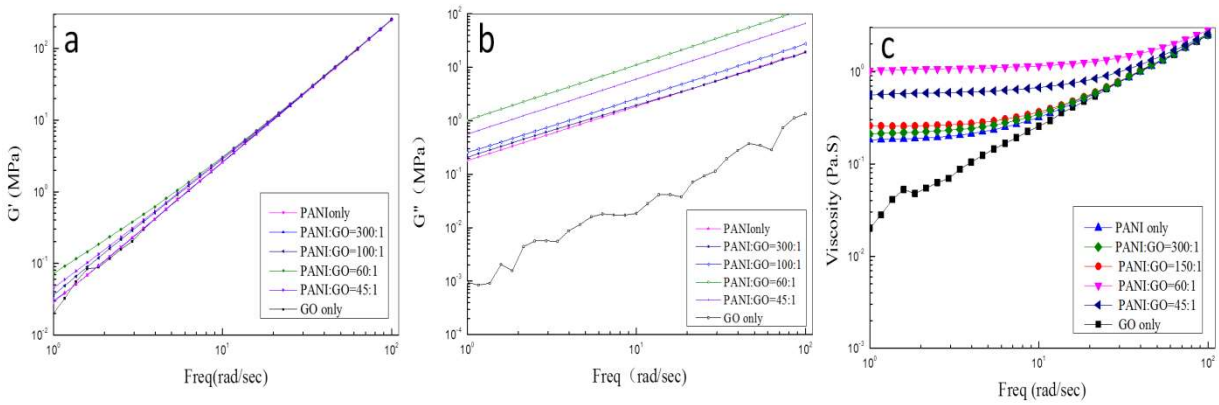

Fig. 2.25 Effects of GO and PANI fillers in DVB on storage modulus (a), loss modulus (b), and complex viscosity (c), at the frequency of [10^{-1}–10^{2}] rad/s[131].

Microstructure comparison of DVB-PANI and DVB-PANI-GO

Thin films made by DVB-PANI and DVB-PANI-GO solutions were characterized by SEM in order to confirm that 3-D network structures are formed by the hybrid PANI-GO fillers. As showed in Fig. 2.26a, a lot of PANI particles are observed in DVB-PANI composites. In contrast, in the DVB-PANI-GO composites appear as a uniform 3-D network structure as showed in Fig. 2.26b, indicating that the GO layers can form a 3-D frame with the inserted PANI particles.

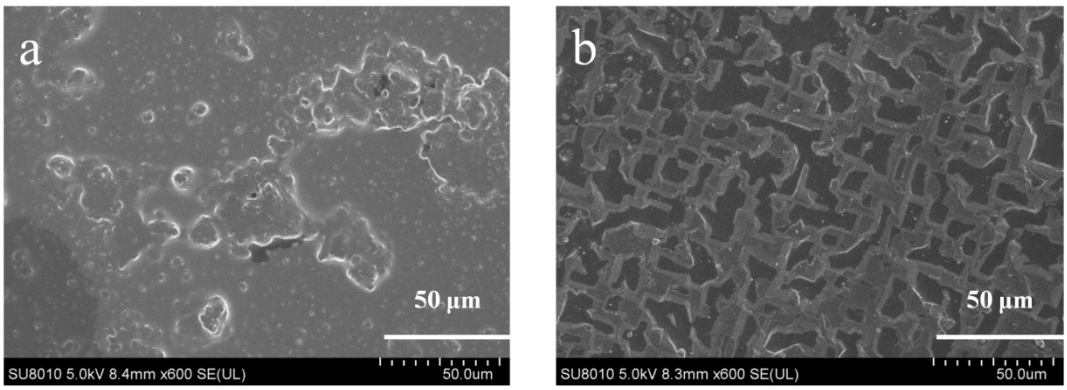

Fig. 2.26 The SEM-images for (a) DVB-PANI composites and (b) the DVB-PANI-GO

composites [131].

Hypothesis for the dispersion status

In summary, a synergetic effect between PANI and GO is proposed to count for the cooperative enhancement of ILSS and AC conductivity. To the randomly distributed PANI (Fig. 2.27a) and GO (Fig. 2.27c), they tend to form big particles and agglomerations that leads to poor dispersity of the matrix. However, with an appropriate mixture of PANI and GO hybrid, the self-aggregation are hindered possibly due to multi-point electrostatic interactions between the carboxylate groups on GO and the ammonium groups on PANI, which is responsible for the good dispersity of the hybrid fillers (Fig. 2.27b).

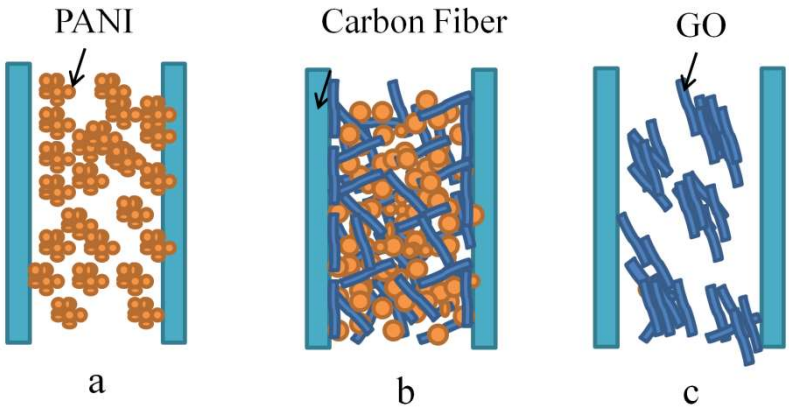

Fig. 2.27 Schematic representations for the dispersion status of (a) randomly distributed PANI, (b) PANI-GO hybrids, (c) GO only in the CFRP laminates [131].

2.4 Conclusion

In conclusion, a high conductive PANI/GO hybrid polymer nanocomposite system was obtained with a maximum electrical conductivity of 9.8 S/cm in a very low GO content of 0.45% at 90wt % of the PANI-DBSA with the corresponding bending strength is 14 MPa and the bending modulus is 0.72 GPa. The highest flexural modulus and strength were 2.01 GPa and 39.2 MPa with 0.45% of GO, 30% of PANI-DBSA. The polymer nanocomposites showed 29% improvement of electric

conductivity after the addition of GO. Also a significant enhancement in the mechanical properties of PANI-DBSA/DVB polymer composites was obtained. The characterizations reveals that the GO disperses well in the DVB polymer matrix, and a 3D conductive network composed of GO sheet and PANI chains was also formed. On the other hand, thermal stability of the GO/PANI/DVB nanocomposites is also improved. The present research introduces a novel conductive composites material with potential applications in electromagnetic shielding, lightning protection materials et al.

A synergistic enhancement of both ILSS and AC conductivity has been realized in the hybrid CFRP laminates system incorporating PANI and GO nanofillers, which can form a homogeneous 3-D network as confirmed by rheology measurements and SEM observations. A multi-point electrostatic interactions between the carboxylate groups on GO and the ammonium groups on PANI are proposed to account for the good dispersity of the hybrid fillers. Electrical conductivity and interlaminar shear strength enhancement of CF/DVB-PANI-GO show dramatically improved through this synergetic effect compared with CF/DVB and a conventional CF/epoxy composite.

Further study along this line is currently underway. We also envision that many other types of specific functional CFRP materials can be created by taking advantage of such a positive cooperative effect.

Chapter 3

MWCNT/GO hybrid reinforced polymer composites

Abstract:

Overall goal of this research is to study the conductivity enhancement effect and its mechanism for different types of carbon-based nano-fillers/conducting polymer hybrids in carbon fiber reinforced polymer (CFRP). Multi-walled carbon nanotubes (MWCNT) /polyaniline (PANI) and graphene oxide (GO) /PANI hybrids were separately dispersed into divinylbenzene (DVB) to make the CFRP composites. The alternating current (AC) electrical conductivity results show that both the binary MWCNT/PANI and GO/PANI hybrids have significant enhancement on AC conductivity of the CFRP composites, while MWCNT/PANI gives better improvement over GO/PANI hybrids. The mechanism for the conductivity enhancement was studied in detail by SEM, XRD, UV-Vis and nanoindenter. From the experimental results, circuit models of the CF/DVB, CF/DVB-MWCNT-PANI and CF/DVB-GO-PANI systems were proposed for the first time. An "interfacial excess energy" and "quantum tunneling effect" were assumed to account for the enhancement of conductivity. The maximum AC conductivity of CFRP made up of MWCNT/PANI was measured to be 22.4 S/m, which has been enhanced by more than 3 orders of magnitude compared to CF/DVB, and more than 2 orders of magnitude compared to CF/epoxy. Thus, CF/MWCNT-PANI composites can be considered as promising candidates for multifunctional materials where high conductivity is in demand.

3.1 Introduction

Carbon fiber reinforced polymer composites (CFRP) have been widely used in

the aerospace, military, automotive and sporting goods industries in recent decades owing to their high specific strength and stiffness [139-141]. However, one of the main drawbacks is their low through thickness electrical conductivity, which has limited their applications, especially in aircraft, wind turbine blade, strain/stress sensing, health monitoring, damage detecting, chemical and thermal sensing and the electromagnetic shielding material fields [6, 142-144].

Several techniques have been devised to improve the through thickness electrical conductivity, e.g. by using conducting polymers (CPs) or designing 3-d network with conductive fillers [4-8]. Carbon nanotubes (CNT) possess exceptionally high electrical and thermal conductivity [9, 10], making them ideal fillers for polymer matrix composites for electrical functional applications [145]. For example, Weikang Li *et al* [11] added 0.5 wt.% CNT–Al_2O_3 into the glass fabric/epoxy composites, increased AC conductivity 4–5 orders of magnitude for both in-plane and through-thickness directions at 10^3 Hz. Growing CNTS on the carbon fiber can increase the in-plane electrical conductivity of the CF/epoxy composites by 170% [12]. The through-thickness electrical conductivities of the CFRP were improved by two orders of magnitude to 1S m^{-1} through the addition of CNTs [13]. However, this still cannot meet requirements of some special applications. For example, the electrical conductivity of electromagnetic shielding material claims higher than 10 S/m [14].

Enhanced electrical conductivities also can be achieved in polymer composites by integrating them with CPs and graphene oxide (GO) [93, 94]. Besides this, CPs like polyaniline (PANI) addition is also reported increasing the CFRP's conductivity [6, 95]. However, no investigations have been reported on the enhanced effect of carbon-based nano-fillers/polyaniline hybrids on the through-thickness electric conductivity of carbon fiber reinforced polymer, to the best of our knowledge.

In this work, both MWCNT/PANI and GO/PANI hybrids were employed into CFRP by dispersing them into the divinylbenzene (DVB) solution. AC conductivity tests were performed to investigate the difference of the enhancement effect between MWCNT/PANI and GO/PANI hybrids. Moreover, thermal stability was also studied.

The enhancement mechanism of MWCNT/PANI and GO/PANI hybrids was also studied in detail by SEM, XRD, UV-Vis and a nanoindenter. As far as we are concerned, this is the first attempt to study their different enhancement effect for the carbon-based nano-fillers/polyaniline hybrids on the electric conductivity of CFRP.

3.2 Experimental details

Materials

PANI powder, DBSA and DVB used same one with 2.2.The conductivity of the prepared emeraldine salt was in the range of 10^3-2*10^3S/m; GO was synthesized based on the hummers method [146], and the detailed process was reported elsewhere [147]; MWCNT with 10–30 um in length and 10-20 nm in diameter are obtained from Chengdu Organic Chemistry Co., Ltd.

Processing of the composites

CF/DVB-PANI(DBSA), CF/DVB-MWCNT-PANI(DBSA) and CF/DVB-GO-PANI(DBSA) laminates were prepared by applying the polymer matrix to the carbon fabric. The process for preparing CFRP composites is shown in Fig. 3.1, which includes two main steps: (1) Preparation of DVB-PANI(DBSA), DVB-MWCNT-PANI(DBSA) and DVB-GO-PANI(DBSA) hybrid polymer matrix(Fig. 3.1: a-i); (2) Impregnation of the suspension into the carbon fabric to get the CF laminates(Fig. 3.1j).

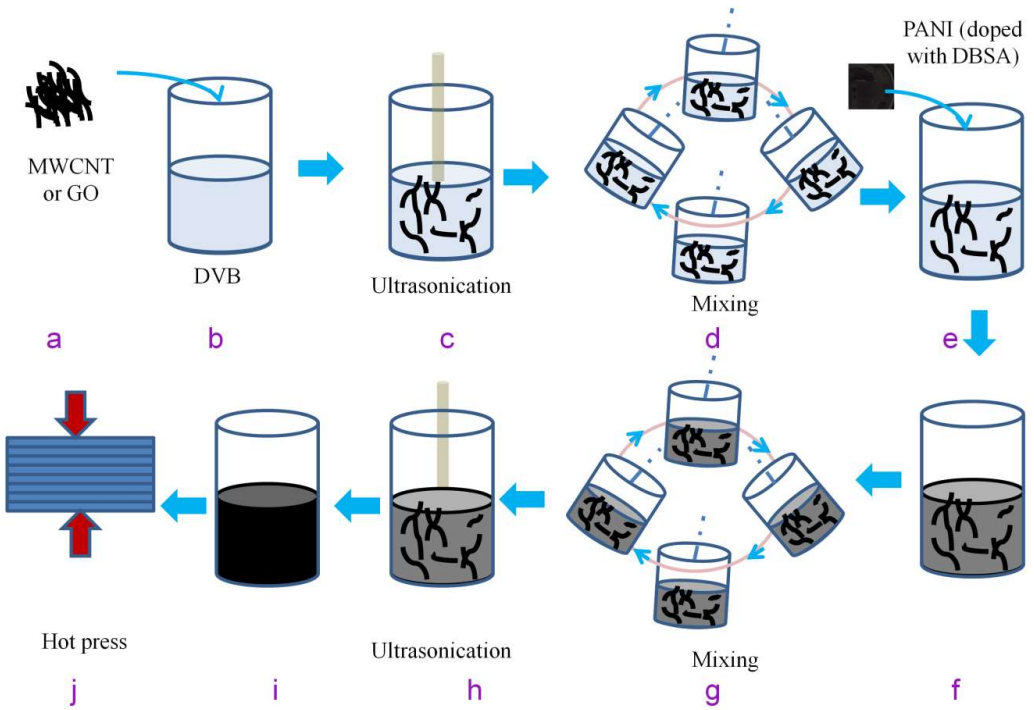

Fig. 3.1 Preparation of carbon fiber reinforced DVB-MWCNT-PANI(DBSA) and DVB-GO-PANI(DBSA) system

Firstly, MWCNT or GO was dispersed into DVB solution by a centrifugal mixer and a sonicator (Fig. 3.1: a-d). In parallel, PANI was kept in a vacuum oven for 2 h at 40℃to eliminate the moisture content. Dried PANI and DBSA were mixed to form the PANI(DBSA) paste by a 3-rolled machine in the ratio of 30:70 by weight percentage which is equivalent to the molar ratio of 1:0.69 of PANI: DBSA [105]. PANI(DBSA) paste was made thoroughly in a 3-rolled machine [129], which was then added to the GO/DVB solution (Fig. 3.1e). Contents of PANI(DBSA) are set at 50%, and DVB(Carbon Nanofillers) is 50%. Secondly, the suspension was again mixed thoroughly (Fig. 3.1: f-i) and applied to the carbon fiber fabric by using hand lay-up technique. Then, the fabric layers were properly stacked into 8 plies and the fibers were aligned by $(0/90)_4$. The laminates were cured in a 120 ℃ hot-press machine for 2 h under 4 MPa. Finally, cured laminates were taken out and cut into the required testing samples, where the volume fraction of carbon fiber is 60 vol% by density measurement.

Characterizations

UV-Vis absorption spectra of DVB-PANI, DVB-PANI(DBSA), DVB-MWCNT-PANI(DBSA) and DVB-GO-PANI(DBSA) films were obtained using a U-4100 spectrophotometer. Spectra were recorded from 250-1100 nm; Wide-angle X-ray scattering (WAXS) measurements were performed on a MicroMax007, RAXIS-IV++ with copper X-ray tube (CuK, wavelength λ=0.15418 nm), the data were collected in the step-by-step mode of 0.038° from 5° to 45° in 2θ; Thermogravimetric analysis (TGA) was performed with a SDT Q600 V20.9 Build 20 instrument under a 100 mL min^{-1} N_2 at the heating rate of 10 ℃ min^{-1}; High quality of scanning electron microscopy (SEM) pictures were obtained on a scanning electron microscope machine (SU8010/EDX), using a SEI detector at 5 kV; The nanocomposite bulks of 10×20×2 mm^3 in the plane perpendicular to the thickness were glued onto the stage of a nanomechanical testing instrument (Hysitron Inc., TriboIndenter 950), the samples were mechanically ground and polished with 4000 grit silicon carbide paper and 1 μm diamond suspension. Subsequently, the samples were brought into contact with the diamond tip (Berkovich probe of 50 nm radius) at a basic QS trapezoid with a max force of 1000 μN; The alternating current (AC) electrical conductivity of the CFRP was tested on a CHI660D electrochemical workstation (Shanghai Chenhua instrument Co. Ltd.) in the out-of-plane (perpendicular to the fiber-plane) directions, by applying an AC voltage of 5 mV in the frequency range of 10^2-10^5 Hz at room temperature. CFRP laminates were measured based on ASTM D150.

3.3 Results and discussion

AC electrical conductivity

AC impedances

Measurement results of AC impedances are shown in Fig. 3.2, where Z is expressed as a Nyquist plot, Z' and Z" are real and imaginary part of the complex impedance (Z). Z' represents the resistive part of the system and Z" represents the reactance arising due to the capacitive or inductive nature of the system.

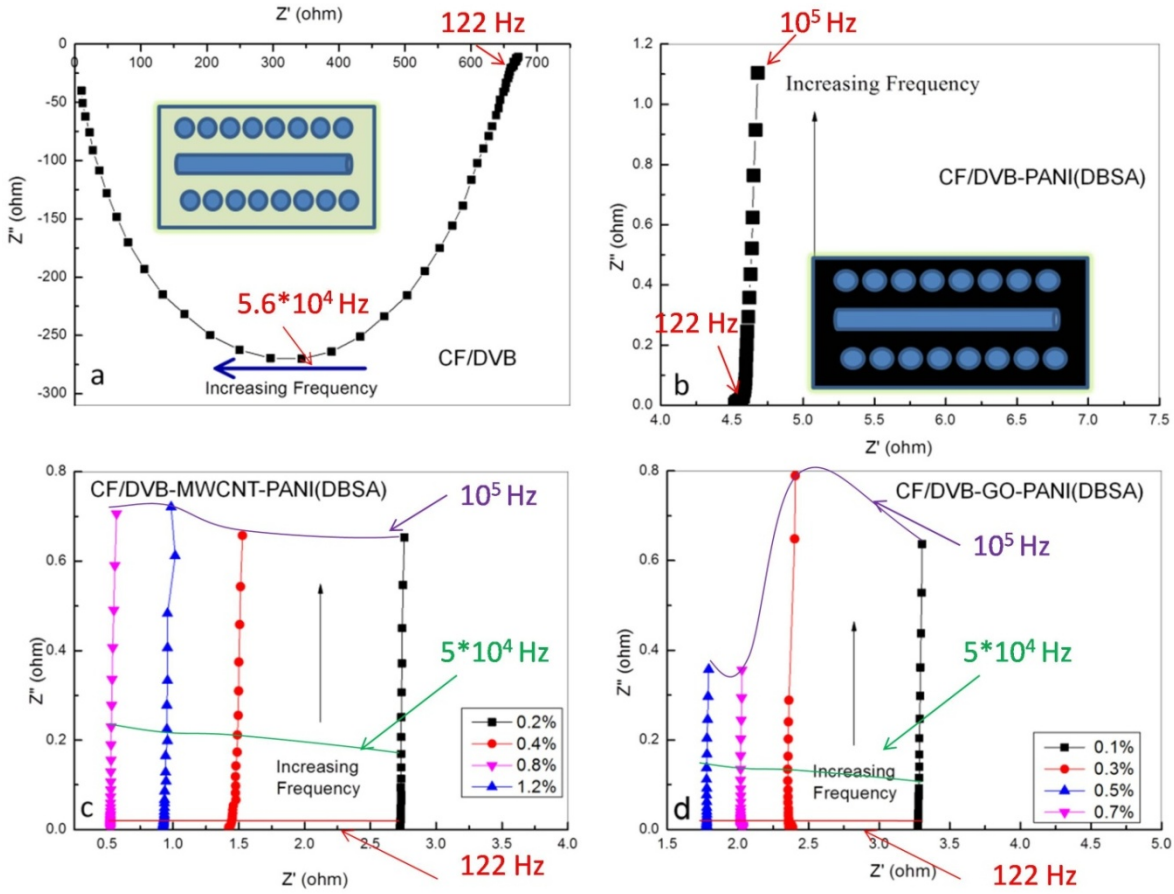

Fig. 3.2. Measured through-thickness impedance: (a) CF/DVB, (b) CF/DVB-PANI(DBSA), (c) CF/DVB-MWCNT-PANI(DBSA) with different MWCNT content and (d) CF/DVB-GO-PANI(DBSA) samples with different GO content.

Baseline samples of CF/DVB (Fig. 3.2a) show an insulating capacitive behavior as expected. Z" is negative, and |Z"|reaches the highest value when the frequency is $5.62*10^4$ Hz, decreases rapidly as the frequency increases; Z' decreases in the full scale as the frequency increases. This behavior can be attributed to the CFRP of

insulating DVB matrix sandwiched by conductive carbon fibers. As showed in Fig. 3.2b, when 50 wt% of PANI(DBSA) is introduced, the capacitive behavior disappeared and a smaller resistance (4.6 Ω at 100 Hz) in sharp comparison to that of the baseline sample (680 Ω at 100 Hz) was observed. These results illustrate that the CFRP laminates transformed from insulating to conductive by the introduction of PANI.

In Fig. 3.2c-d, the AC impedances of CF/DVB-PANI(DBSA) with different MWCNT or GO content are plotted. In both cases, the Z' stays at a very low constant, indicating that the resistance portion further decreased. However, the Z" increase with frequency, suggesting that and the capacitance effects diminish and the inductance effects become the main contribution. This can be explained on the basis of electron hopping mode of conduction [148]. Introducing nanofillers like MWCNT and GO results not only in hydrodynamic interactions but also leads to complex physical–chemical interactions between the polymer matrix and the filler surface; Because of the high surface area of the MWCNT and GO, the polymer-filler interaction is very high, which leads to the formation of a strong interphase. Such interphase leads to higher stiffness of the bound polymer matrix layer than that of the bulk polymer and hinders molecular mobility [149]. As a result, a stable real impedance is obtained in both CF/DVB-MWCNT-PANI(DBSA) and CF/DVB-GO-PANI(DBSA) composites.

In Fig. 3.2c, it can be observed that AC impedances further decrease as the content of MWCNT increase from 0.2% to 0.8%, which might be due to the conductivity of MWCNT. The smallest AC impedance is only 0.57 Ω when the content of MWCNT is 0.8%. In Fig. 3.2d, the content of GO in DVB is from 0.1%, 0.3%, 0.5% and 0.7%. We can see that the AC impedance increase with the increase of GO's content. When the GO's content is 0.5%, the AC impedance reaches to the lowest 1.79 Ω, which is decreased by 61% compared with those of the neat CF/DVB-PANI(DBSA) composites (4.6 Ω). This decrease in resistance can be attributed to the increased charge transport capability enabled by the π–π stacking interaction between the carbon nanofillers and the PANI chains. The smallest AC

impedance of CF/DVB-GO-PANI(DBSA) is still 3.1 times higher than the CF/DVB-MWCNT-PANI(DBSA) composites (only 0.57 Ω).

Circuit models

Two combining models are proposed to account for the different AC impedance between CFRPs with and without carbon nanofillers/PANI hybrids. The CF/DVB system can be presented as a model shown in Fig. 3.3a, where the total AC impedance is composed of a parallel combination of a resistance R_r and capacitance C_d, which is then in a series combination with resistance R_1. This is consistent with the sandwich structure of CFRP laminate, where the conductive carbon fibers are embedded in an insulating matrix [150]. The carbon fiber can be responsible for the resistance. The impedance spectra show a semi-circle which may be due to the contribution of the insulating PDVB, behaving a capacitor action.

The resistance element R1 corresponds to the resistance of carbon fiber itself. On the other hand, the resistance elementR0 means contact area of carbon fiber Fig. 3.3(c). The places where carbon fibers are not in contact with each other can be represented as captors. However, the matrix with monohybridbecomes conductive by the 3D conductive networks, which bridge the carbon fibers, so that the current can transfer easily in between carbon fibers as shown in Fig. 3.3(d). In this situation, the resistance becomes smaller than the tunneling resistance. So, in the hybrid system, R2 represents the combined resistance of carbon fiber, contact resistance and the conductive matrix. The reactance, L, corresponds to the obvious inductive behavior of the network formed by PANI, which has been reported [151].

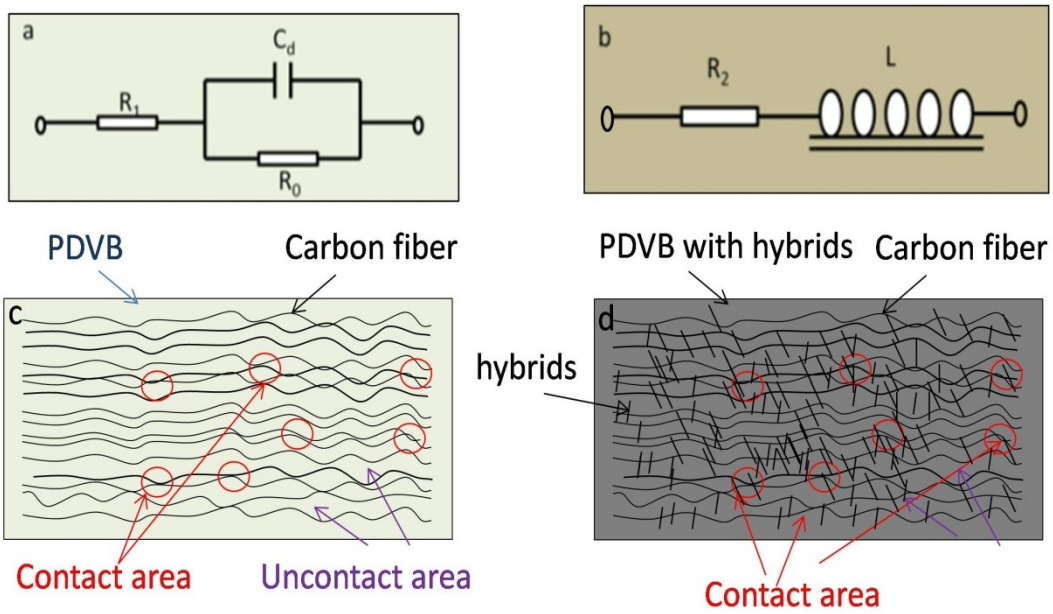

Fig. 3.3 Circuit models of (a) CF/DVB; (b) CF/DVB-MWCNT-PANI or CF/DVB-GO-PANI.

According to the model in Fig. 3.3a, the overall impedance of the circuit can be described by Equation (3 −1). The definition of $Z'$and Z'' by Equation (3 −4) and (3 −5) fits very well with the characteristics observed for $Z'$and Z'' in Fig. 3.2a. On the other hand, the CF/DVB-MWCNT-PANI and CF/DVB-GO-PANI systems can be modeled as Fig. 3.3b, where the total AC impedance, as described by Equation (3 −6), can be regarded as a series combination of a resistance R2 and a reactance of L. The disappearance of capacitance can be due to the formation of conductive networks after the addition of hybrids, while the inductive behavior of PANI [151] make the CFRP exhibit a inductive reactance L. In this case, the definition of $Z'$and Z'' by Equation (3 −7) and (3 −8) can explain the experimental plots shown in Fig3-2: (c-d).

For model (a):

$$Z = R_1 + \frac{1}{\frac{1}{R_0} + i\omega C_d} = R_1 + \frac{R_0}{1 + (\omega R_0 C_d)^2} - \frac{\omega {R_0}^2 C_d}{1 + (\omega R_0 C_d)^2} i \qquad (3-1)$$

$$Z = Z' + iZ'' \qquad (3-2)$$

$$\omega = 2\pi f \qquad (3-3)$$

$$Z' = R_1 + \frac{R_0}{1 + (\omega R_0 C_d)^2} = R_1 + \frac{R_0}{1 + (2\pi R_0 C_d)^2 f^2} \qquad (3-4)$$

$$Z'' = -\frac{\omega {R_0}^2 C_d}{1 + (\omega R_0 C_d)^2} = -\frac{{R_0}^2 C_d}{\frac{1}{2\pi f} + (2\pi R_0 C_d)^2 f} \qquad (3-5)$$

For model (b):

$$Z = R_2 + i\omega L \qquad (3-6)$$

$$Z' = R_2 \qquad (3-7)$$

$$Z'' = 2\pi f L \qquad (3-8)$$

Where: Z' is the real part, Z'' is the imaginary part, i is the imaginary unit, R_1 and R_0 is the resistance, C_d is the capacitance and L is the reactance, ω is the angular frequency, f is frequency.

Table 1 gives the values for the model parameters that are generated by the AC impedance results in Fig. 3.2. According to table 3-1, we can see that the smallest resistancebelongs to the CF/DVB-MWCNT(0.8%) -PANI sample, which is less than one-third of CF/DVB-GO(0.8%) PANI.

Table 3-1 - Parameters evaluated from the results of AC impedance

Parameters	Value			
	CF/DVB			
R_1	10.2 Ω			
R_0	662 Ω			
C_d	5.2 nF			
	CF/DVB-MWCNT/PANI			
MWCNT%	0.2	0.4	0.8	1.2
R_2	2.76 Ω	1.53 Ω	0.57 Ω	0.98 Ω
L	1.04 μH	1.69 μH	2.08 μH	1.22 μH

CF/DVB-GO/PANI				
GO%	0.1	0.3	0.5	0.7
R_2	3.3 Ω	2.41 Ω	1.79 Ω	2.02 Ω
L	1.01 μH	1.46 μH	2.08 μH	1.80 μH

According to the establishment of the circuit models, the through-thickness conductivity of the CFRP can be explained more quantitative, a smaller R2 represents a more conductive material with a better interphase properties. Simultaneously, it also can supply a simple way to distinguish the insulating material and conductive material.So Establishing of a circuit model is a better way to compare the enhanced effect of conductive nanofillers.

AC conductivity

The through-thickness AC conductivity of the CF/DVB-PANI, CF/DVB-MWCNT(0.8%) -PANI and CF/DVB-GO(0.5%) -PANI were calculated by the equation 9 in the frequency range from 10^2 to 10^5 Hz. CFRP laminates are in the same fraction (50 wt%) of PANI-DBSA mixture. CF/Epoxy and CF/DVB were also measured as a control sample.

$$\sigma = \frac{1}{\rho} = \frac{l}{Z'S} \qquad (3-9)$$

Where: σ is the AC conductivity, ρ is the resistivity, S is the cross-sectional area, l is the thickness of the sample.

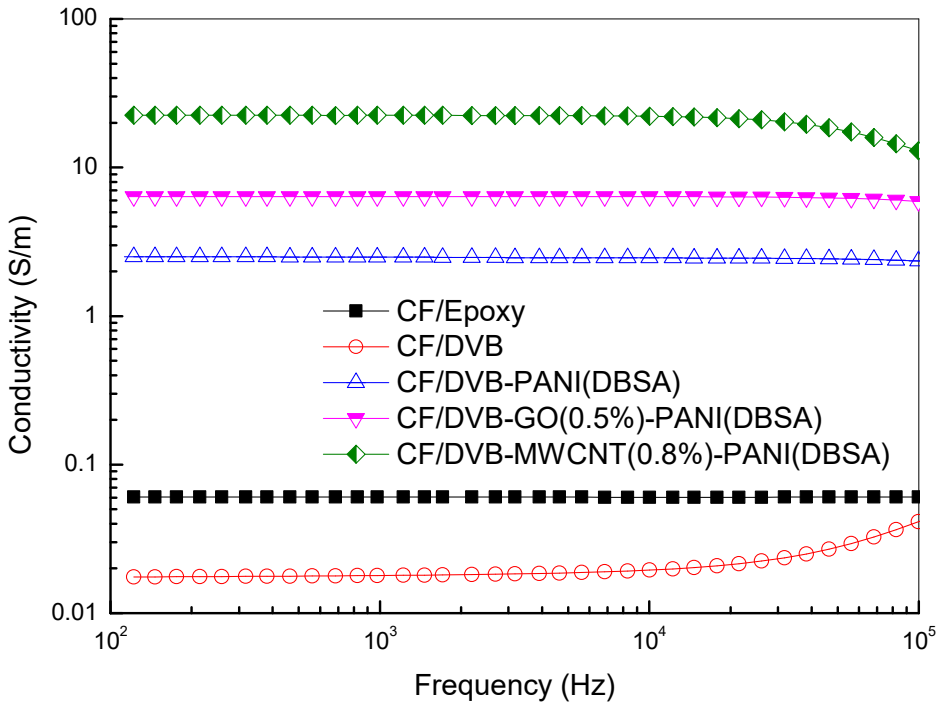

Fig. 3.4 Thethrough-thickness AC conductivity of CFRP with different matrix

As showed in Fig. 3.4, the through-thickness conductivity of CF/Epoxy and CF/DVB are only 6.04×10^{-2} and 1.75×10^{-2} S/m, respectively, while the conductivity of CF/DVB-PANI(DBSA) is much higher (2.5 S/m at the frequency of 10^2 Hz). The highest conductivity up to 22.4 S/m was measured in the MWCNT/PANI hybrids reinforced CF/DVB system, which is 3.52 times higher than the GO/PANI hybrids. It needs to be pointed out that, the conductivity of CF/DVB-MWCNT-PANI(DBSA) system has been improved by more than 3 orders of magnitude compared to CF/DVB, and more than 2 orders of magnitude compared to CF/epoxy. In>10 S/m of electrical conductivity, this new CFRP can potentially be employed as electromagnetic shielding material [14].

The conductivity enhancement mechanism of carbon/PANI hybrids can be explained in terms of “interfacial excess energy” [152] and quantum tunneling effect [153]. It is well known that with the increase of the conductive filler’s content, the interfacial excess energy caused by nanofillers into the polymer matrix will reach a critical point, then the fillers begin to coagulate so as to avoid any further increase of the energy and form networks which facilitate electrical conduction. When PANI

particles were introduced into DVB, the PANI surface became infiltrated with DVB and form polymer-filler interphase. Meanwhile, the extraordinary high surface area of MWCNT and GO [154, 155] are believed to contribute to much higher interfacial excess energy to facilitate the formation of conductive networks, which in turn lead to a higher quantum tunneling effect, therefore improving the electrical conductivity of the CFRP composites.

Mechanism of enhanced conductivity

In order to study the enhancement mechanism of MWCNT/PANI and GO/PANI hybrids, UV-Vis, XRD, SEM and interphase properties were also studied in this part. The CF/DVB-PANI, CF/DVB-MWCNT(0.8%) -PANI and CF/DVB-GO(0.5%) -PANI were measured, where the CFRP laminates are in the same fraction (50 wt%) of PANI-DBSA mixture. CF/DVB was also measured as a control sample.

UV-visible analysis

UV–Vis spectroscopy is considered as an important tool for the investigation of the electronic structure of PANI and more specifically the charge carrier delocalization in DVB composites. Fig. 3.5 shows the UV-Vis spectra of DVB-PANI, DVB-PANI(DBSA), DVB-MWCNT(0.8%) -PANI(DBSA) and DVB-GO(0.5%) -PANI(DBSA). It should be noted that the related peak values are marked in this diagram. Two absorption peaks in DVB-PANI at below 350 and 630nm are attributed to the characteristic peaks of undoped PANI [156]. For the doped PANI in the DVB-PANI(DBSA), DVB-MWCNT(0.8%) -PANI(DBSA) and DVB-GO(0.5%) -PANI(DBSA) samples in Fig. 3.5, peaks in 630nm disappeared. This indicates that PANI is in a fully protonated state. Two new peaks at 450 and 810nm occur, which can be attributed to the delocalized polarons, relating to the doping process and conductivity of PANI [121, 122].

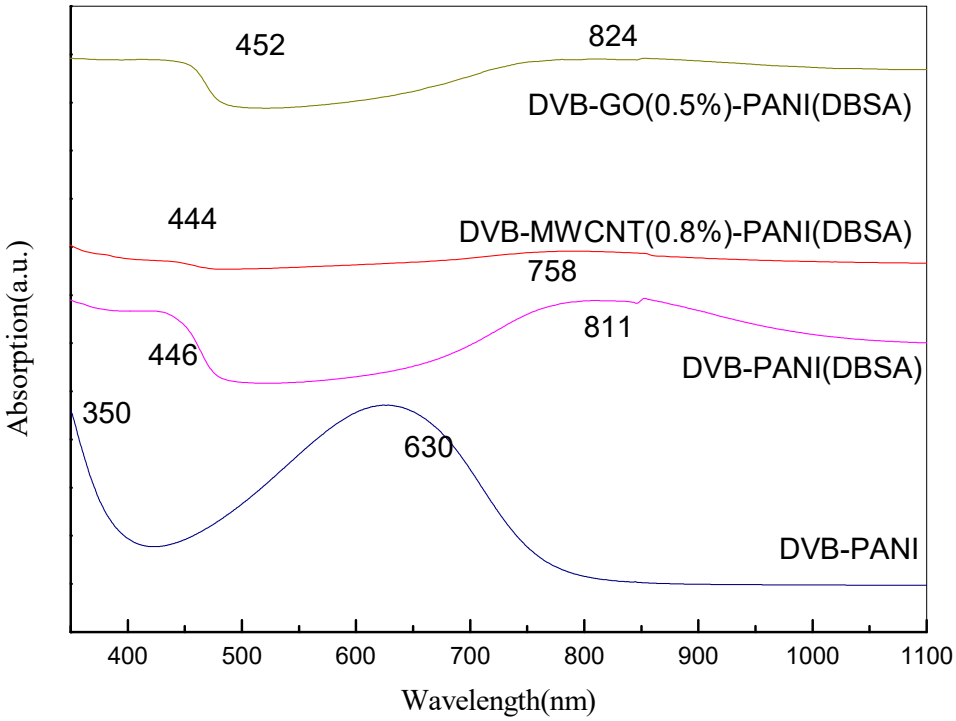

Fig. 3.5. UV-Vis spectra of DVB-PANI, DVB-PANI(DBSA), DVB-MWCNT(0.8%) -PANI(DBSA) and DVB-GO(0.5%) -PANI(DBSA) system

X-ray diffraction

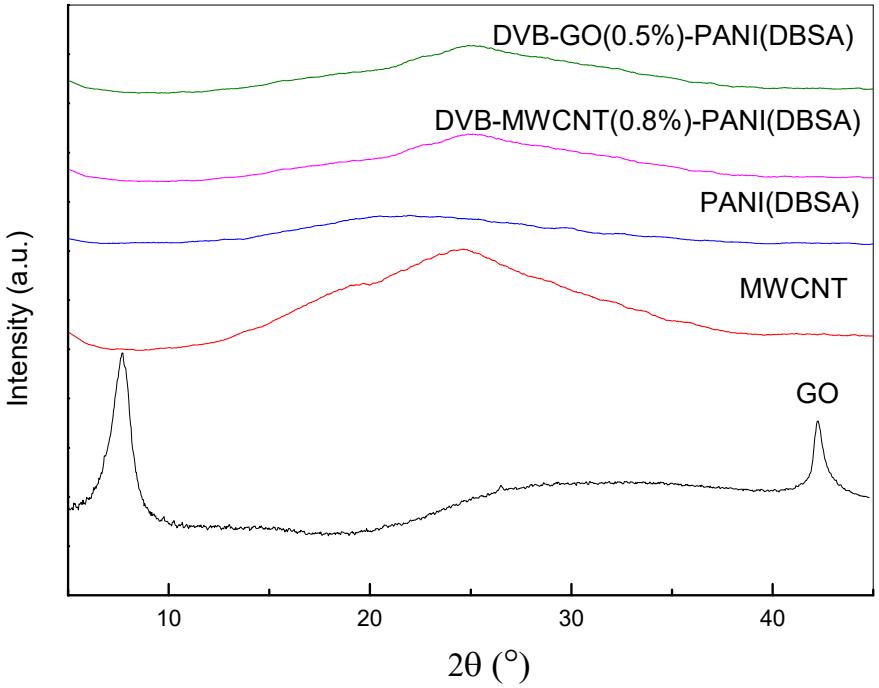

Fig. 3.6 XRD patterns for PANI, MWCNT, DVB-MWCNT(0.8%) -PANI(DBSA) and DVB-GO(0.5%) -PANI(DBSA)

Fig. 3.6 shows the XRD patterns of original PANI and MWCNT, and the composites with the best conductivity of DVB-PANI(DBSA) -MWCNT(0.8%) and DVB-PANI(DBSA) -GO(0.5%). We can see that pure PANI(DBSA) show a very broad reflection peak. After introducing MWCNT and GO, the reflection peaks become a little sharper and right shift, indicating an increase of orders that may be due to the increase of dispersion uniformity of conductive PANI. This means a better and more stabilized dispersion formed by introducing the MWCNT/PANI and GO/PANI hybrids, which would enhance the electron charge transfer in the CFRP composites, thereby leading to an increase in conductivity.

Dispersity

Cross-sections of DVB-PANI(DBSA), DVB-MWCNT(0.8%) -PANI(DBSA) and DVB-GO(0.5%) -PANI(DBSA) were characterized by SEM in order to observe the

dispersion change after the addition of carbon-based nanofillers. As showed in Fig. 3.7 (a), a lot of big PANI–DBSA particles are observed in DVB-PANI(DBSA) composites. In contrast, the DVB-MWCNT(0.8%) -PANI(DBSA) and DVB-GO(0.5%) -PANI(DBSA) composites appear as a uniform network structure as shown in Fig. 3.7(b-c), which clearly indicated that both MWCNT and GO can improve the dispersity of conductive PANI particles. This is consistent with the results of X-ray test. While the "quantum tunneling" effect usually happens at very small distances (below 10nm) between conductive fillers [157]. In the MWCNT/PANI and GO/PANI reinforced DVB system, the inlaid MWCNT or GO acted as bridges connecting the PANI particles throughout the DVB matrix, which helped to form a conductive path between both fillers by increasing the quantum tunneling effect. On the other hand, the dopant DBSA is the anionic surfactant simultaneously [158], which can benefit for the dispersion of MWCNT and GO in DVB/PANI system.

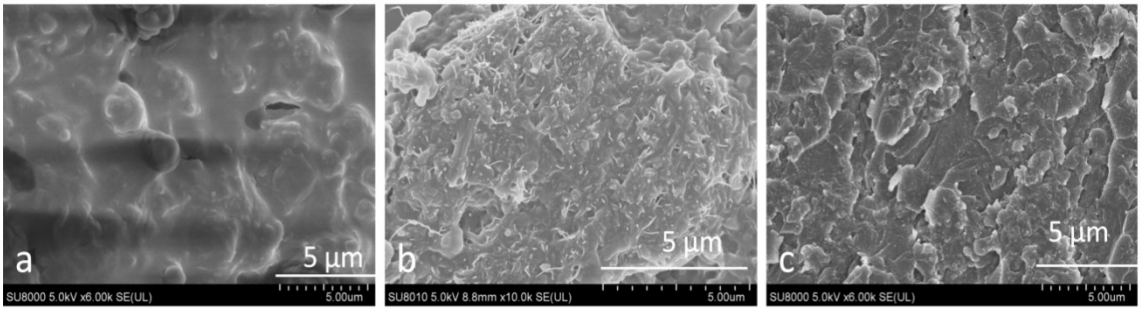

Fig. 3.7The SEM-images for (a) the DVB-PANI(DBSA) composites, (b) the DVB-MWCNT(0.8%) -PANI(DBSA) composites and (c) DVB-GO(0.5%) -PANI(DBSA)

Interphase properties

In order to prove that the hybrids move to the surface of the carbon fiber because of high "interfacial excess energy", the transition areas for the samples of DVB-PANI(DBSA), DVB-MWCNT(0.8%)-PANI(DBSA) and DVB-GO(0.5%)-PANI(DBSA) were tested by a nanoindenter.The results are shown

in Fig. 3.8.

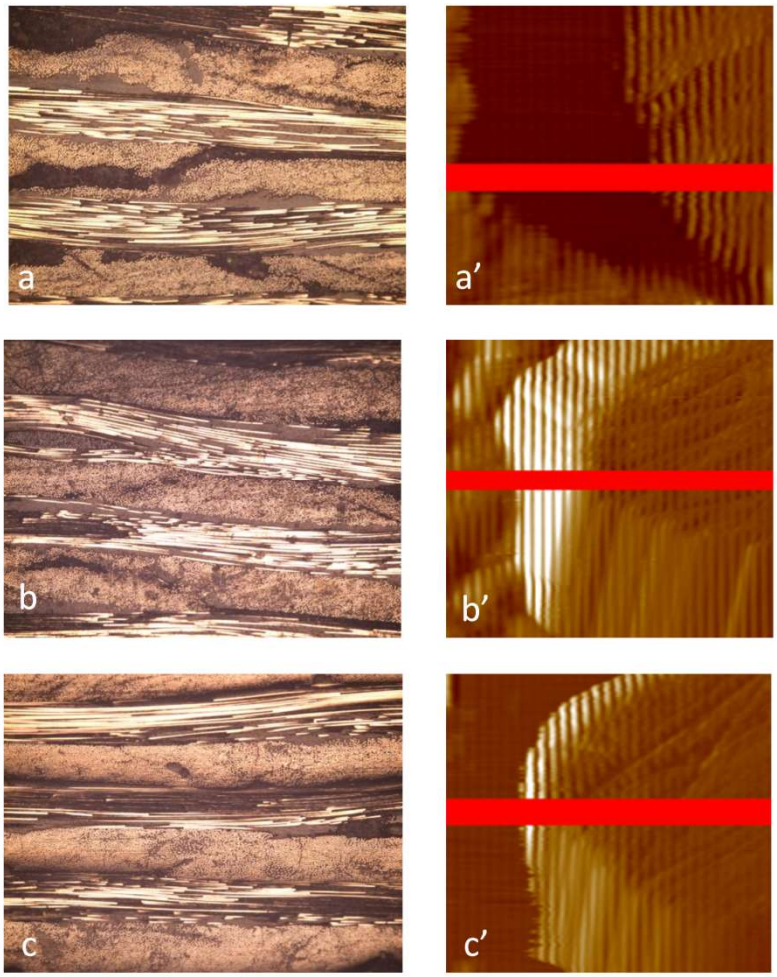

Fig. 3.8 Optic images and the image of an array of 0.15*667 grid nanoindentations on (a) CF/DVB-PANI(DBSA) (b) CF/DVB-MWCNT(0.8%) -PANI(DBSA), (c) DVB-GO(0.5%) -PANI(DBSA)

Fig. 3.8(a-c) shows the areas of interest considered on each test specimen. In Fig. 3.8(a'-c'), a line of 330 indentations were performed on each selected area, using a 15nm spacing between indents. Each indentation was programmed to apply a force of 1000 μN following the Fig. 3.9a. The representative load–displacement curves (Fig. 3.9b) was then analyzed according to the method described by Oliver and Pharr [159], from which the hardness and elastic modulus (Er) of the indented material can be calculated.

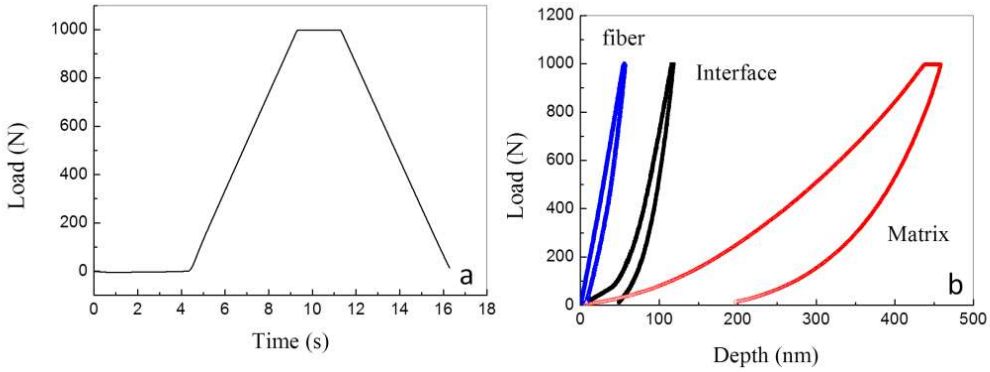

Fig. 3.9. The load curve of the indentation (a) and the example of load *vs.*displacement curve obtained from the indentation of CF/DVB-MWCNT(0.8%) -PANI (b).

The modulus profiles and hardness profiles calculated by individual line scans across the center of the fiber are shown in Fig. 3.10, including CF/DVB-PANI(DBSA) (Fig. 3.10a), CF/DVB-MWCNT(0.8%) -PANI(DBSA) (Fig. 3.10b) and DVB-GO(0.5%) -PANI(DBSA) (Fig. 3.10c). We can see that polymer matrix, carbon fibers, and their interphase can be easily distinguished in the modulus and hardness scan result. We can also see that the big particle of the PANI cannot affect the modulus of the matrix in Fig 3-9a. That may be because PANI and PDVB have similar low modulus compared to carbon fiber. The comparison clearly shows that the modulus and hardness of the DVB matrix are much lower than that of the carbon fiber and that intermediate regions exist in the interphase between fiber and matrix.

The transition region shows a gradual increase in modulus and hardness from the matrix to fiber. From the load-depth curve, hardness can be obtained at the max load in formula 3-10.

$$H = \frac{P_{max}}{A} \qquad (3\text{-}10)$$

Where A is the contact area, the indenter is with a three-sided pyramid Berkovich diamond indenter (radius of the indenter probe was (50 nm), the elastic modulus E can be expressed as follows according to formula 3[160]:

$$S = \frac{dP}{dH} = \frac{2E\sqrt{A_c}}{\sqrt{\pi}} \qquad (3\text{-}11)$$

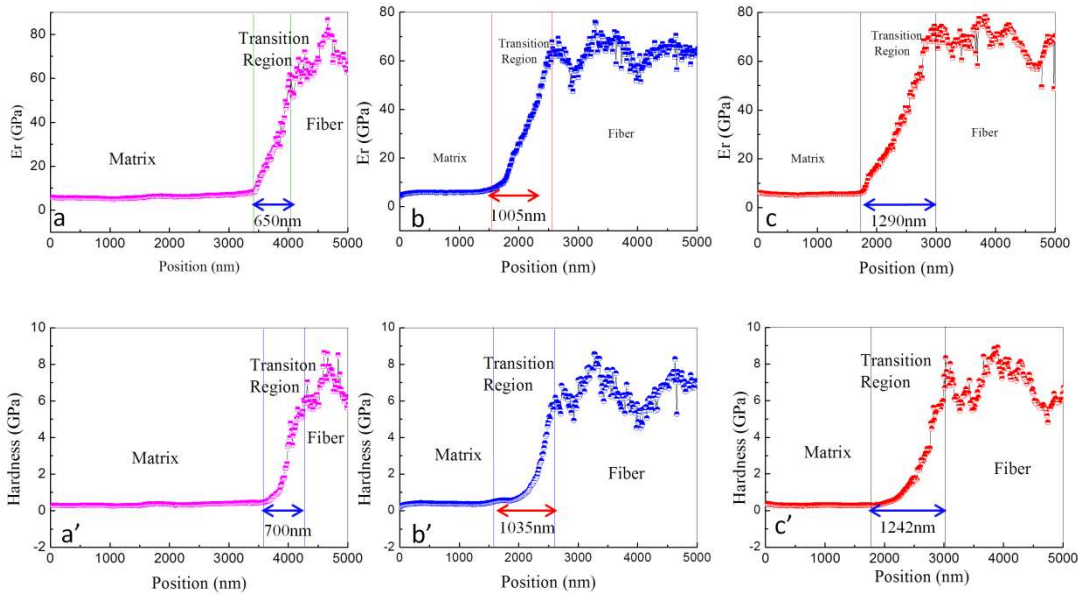

Fig. 3.10 Modulus and Hardness profiles obtained for composites (a) CF/DVB-PANI(DBSA) (b) CF/DVB-MWCNT(0.8%) -PANI(DBSA), (c) CF/DVB-GO(0.5%) -PANI(DBSA)

In the modulus profile in Fig. 3.10a, interphase thicknesses of CF/DVB-PANI(DBSA) is smaller. As a consequence, there is a sharp spatial gradient (steeper slope) between the fiber and the matrix that can easily cause the fiber to depend from the matrix under stress, which may result in poor overall conductive properties.

It is also apparent that the interface is between the carbon fiber-reinforcement (75 GPa) and the PDVB matrix (5 GPa). P.A.Smith[161] proposed that indentations on the edge of thecarbon fiber may lead to modulus values that are between that of the fiber and the matrix, giving the impression of an interphase. But the transition region within two to three times the indentation diameter is associated with restriction of the indentation. But in our system, the thickness of the smallest transition area is at least 650nm, which is more than 11 times to the indenter's diameters, which shows the effective results regarding the increase of the interphase region of the hybrid system.

While addition of MWCNT or GO as shown in Fig. 3.10(b-c) was found to significantly increase the interphase thickness, indicating that the high "interfacial excess energy" of the hybrids tend to gather around the surface of carbon fiber, which results in a more gradual gradient in modulus from fiber to the matrix. This is consistent with the presumption of conductivity enhancement mechanism.

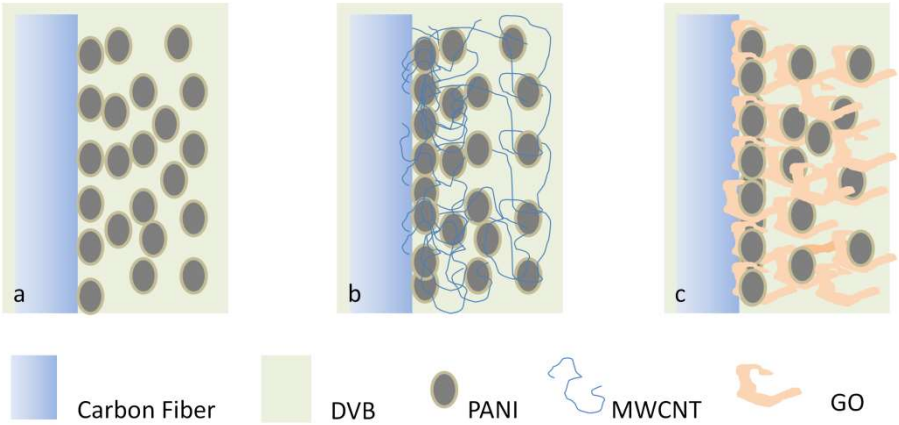

Fig. 3.11 Scheme of the morphology of the conductive composites: (a) CF/DVB-PANI(DBSA) (b) CF/DVB-MWCNT(0.8%) -PANI(DBSA), (c) CF/DVB-GO(0.5%) -PANI(DBSA)

Based on the above results, structural models for our CFRP composites were proposed. Fig. 3.11: (a-c) show a schematic representation of the CF/DVB-PANI(DBSA), CF/DVB-MWCNT(0.8%) -PANI(DBSA) and CF/DVB-GO(0.5%) -PANI(DBSA) systems respectively. As showed in Fig. 3.11(b-c), the system with binary MWCNT/PANI and GO/PANI hybrids form a gradient network from the carbon fiber surface due to their higher "interfacial excess energy", increasing the quantum tunneling effect, which helps to form a conductive path not only between fillers in the DVB matrix but also between carbon fiber and matrix interphase. Therefore, the electrical conductivity of the system is greatly improved by the addition of carbon-based nanofillers.

3.4 Conclusion

In this study, the enhancement effect and its mechanism of carbon-based nano-fillers/PANI hybrids on the electrical conductivity of CFRPs were systematically investigated. The experimental results demonstrated that both MWCNT/PANI and GO/PANI have a significantly positive influence on the AC conductivity properties of the composites. TheAC conductivity of the CF/DVB composites are 22.4 S/m by using MWCNT/PANI as fillers, which are 364 times higher than CF/Epoxy, 1280 higher than CF/DVB system, 3.52 times higher than the GO/PANI hydride system.Circuit models of CF/DVB, CF/DVB-MWCNT-PANI and CF/DVB-GO-PANI system were proposed for the first time. Meanwhile, TGA results prove that the stability of PDVB molecular chain is not reduced but reinforced by MWCNT and GO. Furthermore, the enhancement mechanism was explained by the "interfacial excess energy" and quantum tunneling effect. The significance of this paper is that the analysis here can be used to develop many other types of specific functional CFRP materials by taking advantage of the unique characteristics of carbon-based materials and conducting polymers.

Chapter 4

C_{60}/PANI hybrid reinforced polymer composites

Abstract:

Hybrid nanoparticles, fullerene (C_{60}) and polyaniline (PANI), were incorporated into the polydivinylbenzene (PDVB), and their decoupling effect of electrical and thermal conductivity was investigated. The hybrid particles were fabricated through a simple one-step process in the solution of divinylbenzene (DVB) monomer. The morphology and structure were characterized by TEM, SEM and FTIR. After the incorporation of C_{60}/PANI hybrids into DVB monomer, the electrical conductivity was improved significantly while the thermal conductivity was reduced simultaneously, resulting in effectively decoupling thermal/electrical conductivity. The AC electrical conductivity increased from 9×10^{-10} S/m to 63.7 S/m at the frequency of 1Hz, more than 10 orders of magnitude. On the contrary, the thermal conductivity was reduced to extremely low of only 0.164W/m. K from 0.579 W/m. K. Dissipative particle dynamics (DPD) simulations were also conducted to gain further understanding about the decoupling effect and mechanisms related to dispersibility of C_{60} in the polymer system. The DPD results exhibited better agreement with the experiment results of electrical and thermal conductivity. These results indicate that DPD can be a versatile method for designing functional polymer composites. Simultaneously, the decoupling of the electrical and thermal conductivity of polymer

bulk composites opens diverse opportunities for new materials and systems.

4.1 Introduction

Decoupling thermal and electrical conductivity is a very challenging work due to their strong correlations, but this work still attracts a lot of attention of scientists because of their broad application prospects. For instance, low thermal conductivity and high electrical conductivity and are necessary for thermoelectrics materials, which have huge potential applications for clean and renewable energy sources [162-165].

Some attempts have been done to add all kinds of conductive fillers into the matrix, but composites usually demonstrated inseparable electrical and thermal conductivity [166]. Fullerene(C_{60}) is a 60-atom carbon molecule. The strong phonon scattering of the C_{60}molecule can decrease the thermal conductivity by amplifying the oscillation amplitude of random C_{60} [167]. Therefore, C_{60} can decrease the thermal conductivity and thereby decouple the thermal and electrical performance [168]. On the other hand, C_{60} doped materials have also been reported to have the high possibility as excellent thermoelectric materials [169]. Also, C_{60} has been reported with low thermal conductivity of 10^{-3}~0.16 W/m. K[169, 170].

Conductive polyaniline (PANI), as one of the most excellent conductive polymers, has been widely used because of their lightweight, simple synthesis, low cost, and very low thermal conductivity [171-173]. Our lab has reported a new PANI polymer composites with high mechanical and electrical conductivity properties made by a simple single step method [6, 95, 105, 117, 129]. As far as we know, no study has been published on the decoupling effect of C_{60}/PANI reinforced polymer bulk material, only several reports reported the decoupling electrical and thermal conductivity of polymer composites [174, 175].

In this work, we innovatively filled the PANI/C_{60} hybrids into PDVB composites for decoupling electrical and thermal conductivity. Polyaniline (EB) acts as an electron donor due to the nitrogen's non-pair electron, C_{60} and dodecylbenzenesulfonic acid (DBSA) as an electron acceptor. The doping process and

polymerization were completed simultaneously. The C_{60}nanoparticles were employed to reduce the thermal conductivity. Cooperative effect of PANI and C_{60} is expected to decouple thermal and electrical transport. C_{60}/PANI hybrids were finally filled into the PDVB and their decoupling effect of electrical/thermal conductivity was studied.

4.2 Experimental details

Materials

C_{60} (purity >95%), 1.61 g/cm^3, was bought from Xiamen Funano New Material Technology Co. Ltd. PANI powder, 0.804 g/cm^3, supplied by Yuan Cheng Group., Wuhan, China. DBSA, Aladdin Industrial Corporation, Shanghai, China. DVB, provided by Aladdin Industrial Corporation, China.

Preparation of the polymer composites

Typically, C_{60} was added into DVB, and then dispersed by a sonicator. PANI (DBSA doped) paste with the weight ratio of 30:70 was prepared according to the procedure we reported before [6, 131]. The volume fraction of PANI is set at 20%. The volume fraction of C_{60} is controlled in 0.35vol%, 0.7vol%, 1.05vol%, 1.4vol%. Secondly, the suspension was poured into the mold and cured in a 120 ℃ hot-press machine for 2 h.

Characterizations

Fourier transform infrared (FTIR) spectra in the wave range from 400 cm^{-1} to 3700 cm^{-1} were collected on Perkin Elmer Spectrum One spectrometer (USA) with a resolution of 2 cm^{-1}.

Transmission Electron Microscopy (TEM) was conducted using a JEM-2010 (JEOL, Japan). The particles were dispersed in DVB with sonication and then deposited on a copper grid. Scanning Electron Microscope (SEM) was performed on a HITACHI SU8010/EDX electron microscope, coupled with an energy of 15 kV.

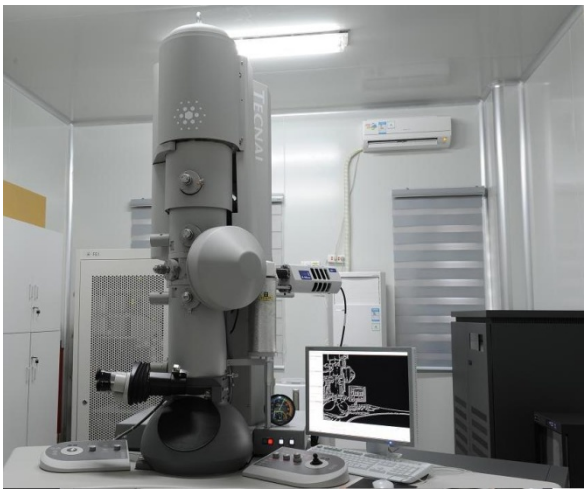

Fig. 4-1Transmission Electron Microscopy (TEM) used in the research

Thermogravimetric analysis (TGA) was carried out using a STA449C instrument from 100 to 800℃ under a N_2 flow of 100 mL min^{-1} at a heating rate of 10 ℃ min^{-1}.

Thermal conductivity was obtained by a DRL-II Xiangtan thermal conductivity tester. The top surface was set at 50 ℃. The alternating current (AC) electrical conductivity was performed on a Chenhua CHI660D electrochemical workstation under an AC voltage of 5 mV.

Simulation Details

MD and DPD simulation was adopted to investigate dispersibility of C_{60} in PANI(DBSA) -DVB composites. The dispersed state and aggregate state of PANI, DBSA, DVB, and C_{60} were calculated by MD simulation. Solubility parameters, χ parameters, and interaction parameters were calculated from energies of materials. The DPD simulation was conducted using the interaction parameter. Dispersibility of C_{60} was evaluated by the radial distribution function. The calculation process is performed according to Fig. 4-2. The models of the chemical component are shown in Fig. 4-3.

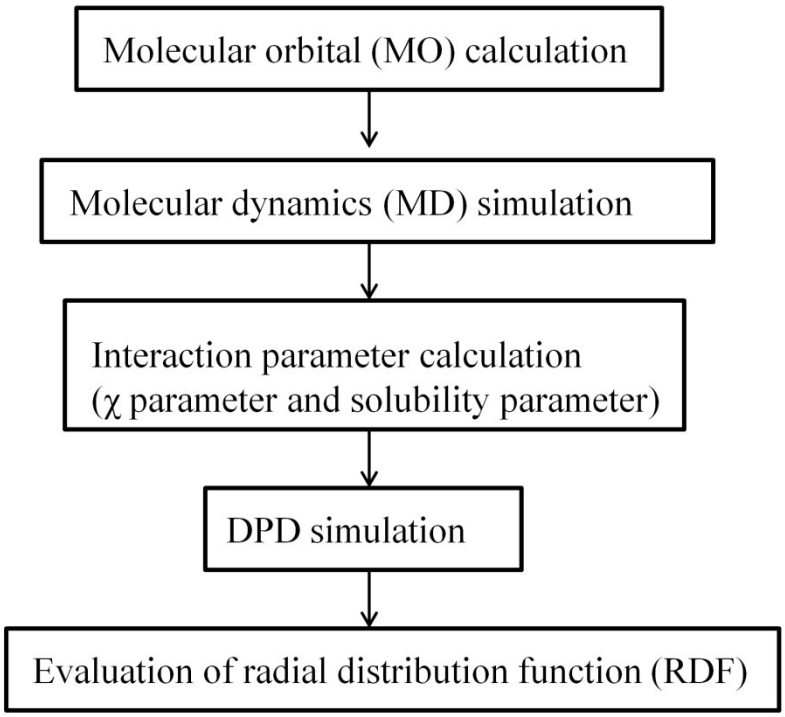

Fig. 4-2 The calculation process of DPD simulation [176].

In the molecular orbital calculation, the firefly quantum calculation package, which is one of the initial molecular orbital methods was used. As a force field parameter, the DREIDING force field was used. Unlike other force fields like AMBER, the DREIDING force field parameter is not defined by the combination of atoms. The force field parameter is determined by hybridized orbital of atoms. The detail of the force parameter is as follows [177]. The energy of materials was calculated by MD simulation to investigate solubility of PANI, DBSA, DVB and C_{60}. In the MD simulation, each 40 materials were included in 1000nm^3 (10nm×10nm×10nm) unit cell. Repeating units of PANI and DVB were inserted in each unit cell. The cell was pressured in NPT (300K, 10^8 Pa, 10 ps). After compressing, unit cell was relaxed in NPT under pressure of 10^5 Pa for 100 ps.

Particles in DPD are in accordance with Newton's equation of motion in formula 4-1.

$$\frac{dr_i}{dt} = v_i, \quad m_i \frac{dv_i}{dt} = f_i \qquad (4\text{-}1)$$

Forces of particles are conservative force, dissipative force, and random force as formula 4-2.

$$f_i = \sum_{i \neq j}\left(F_{ij}^{C} + F_{ij}^{D} + F_{ij}^{R}\right) \qquad (4\text{-}2)$$

Dissipative force, and random force is written as the formula4-3.

$$F_{ij}^{D} = -\gamma\omega^{D}\left(r_{ij}\right)\left(\hat{r}_{ij} \cdot v_{ij}\right)\left(\hat{r}_{ij}\right), \quad F_{ij}^{R} = \sigma\omega^{R}\left(r_{ij}\right)\zeta_{ij}\hat{r}_{ij} \qquad (4\text{-}3)$$

The r_{ij} is the distance between particle i and j. Parameters γ and σ are material factors. The ω is weight function to determine the cutoff distance and random variable. Dissipativeforce and random force are written in formula 4-4.

$$F_{ij}^{C} = \begin{cases} a_{ij}\left(1 - r_{ij}\right)\hat{r}_{ij} r_{ij} < 1 \\ 0 \qquad r_{ij} \geq 1 \end{cases} \qquad (4\text{-}4)$$

$\hat{r}$is the unit vector from particle i to j. Conservative force is proportional to interaction parameters a_{ij}. The more a_{ij} increase, the more aggregation occurs in DPD simulation. Interaction parameter a_{ij} is determined by solubility parameter δ of material in formula 4-5.

$$\delta = \sqrt{\frac{\Delta E}{V}} \qquad (4\text{-}5)$$

The ΔE is the energy gap between the vacuum state and the bulk state. The parameter V is molar volume of material. The χ parameter is determined by the gap of solubility parameter in formula 4-6.

$$\chi_{AB} = \frac{V_{seg}}{K_B}\left(\delta_A - \delta_B\right)^2 \qquad (4\text{-}6)$$

The v is molar volume per segment. The k_B is Boltzmann constant. The more a_{ij}increase, the more χ parameter increases.

$$a_{ij} = (16n - 1)/0.202/\rho + 3.268\chi_{ij} \qquad (4\text{-}7)$$

In formula 4-7, the ρ is density. PANI, DBSA, DVB and C_{60} are inserted in 64000 nm^3(40nm×40nm×40nm) unit cell.The unit cell was relaxed for 1.8ns. The ratio of PANI, DBSA and DVB is the same as the experiment.

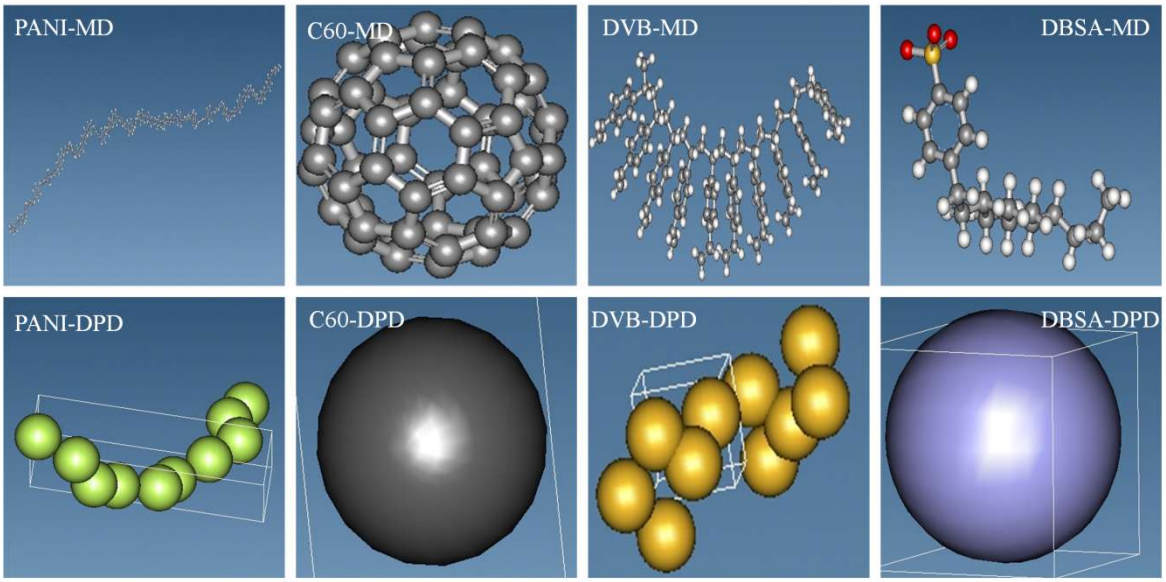

Fig. 4-3 Scheme of component from MD to DPD model [176].

4.3 Results and discussion

Morphologies and Structures of composites

In order to confirm the change of the structure after the adding of C_{60}, the morphology of PANI and PANI/C_{60} were observed by TEM. From the Fig. 4-4, it can be found that the PANI and PANI/C_{60} hybrids have a similar size, indicating that C_{60}cannot change the integral structure of PANI. While the PANI-C_{60} hybrids show a rougher surface than individual PANI due to the presence of C_{60}. This can be due to the possibility of doping interaction happened between the amine groups of PANI and C_{60} (reaction 1), leading to the injection of C_{60} on the surface PANI, so that formed Partial ground-state charge transfer inside this system. PANI+C_{60}→PANI $^{+}$+C_{60}^{-} [178]. Such doping behavior can increase the thickness of PANI and reduce the aggregation of PANI and thus improve the electric conductivity of the composites.

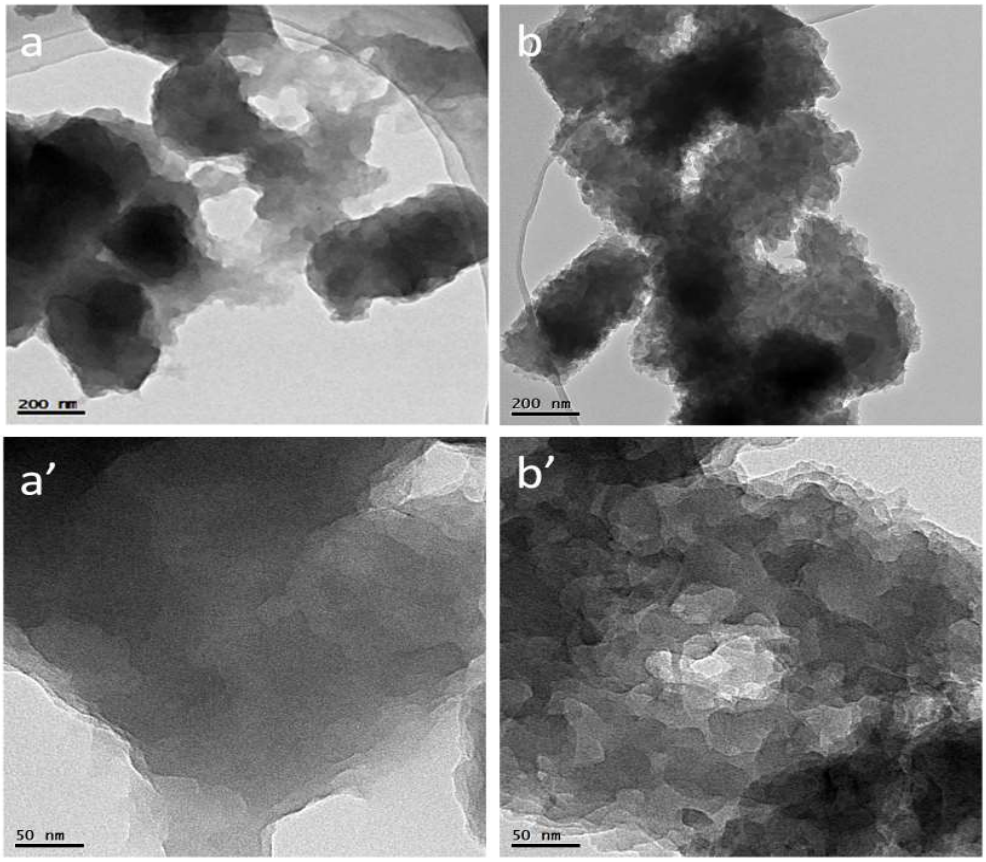

Fig. 4-4 TEM photographs of PANI (a) and PANI-C_{60} (b) [176].

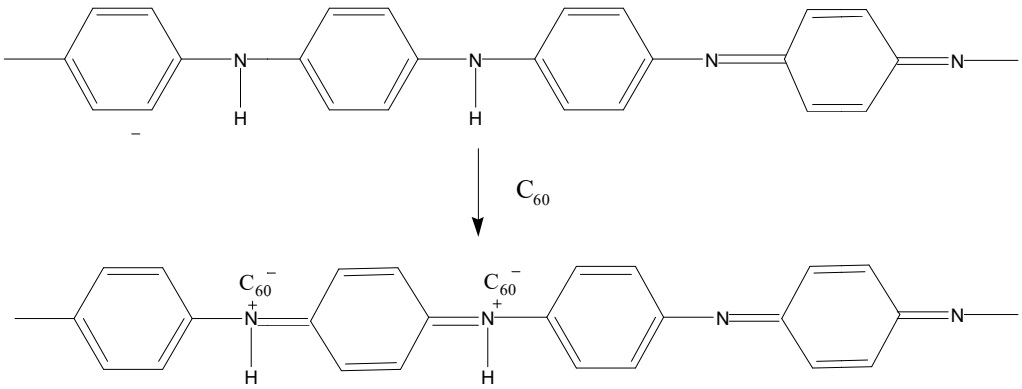

Reaction 4-1. The reaction between PANI and C60

Elemental mapping measurements were performed to investigate the existence and distribution of PANI and DBSA in the PANI-C_{60}/DVB composites. Fig. 4-5 shows the SEM image and EDX mapping of the PANI-C_{60}/DVB composite. It is clearly that those elementals of N (Fig. 4-5b) and S (Fig. 4-5d) are well dispersed on

the surface of composites, indicating that PANI and DBSA disperse well in the composites.

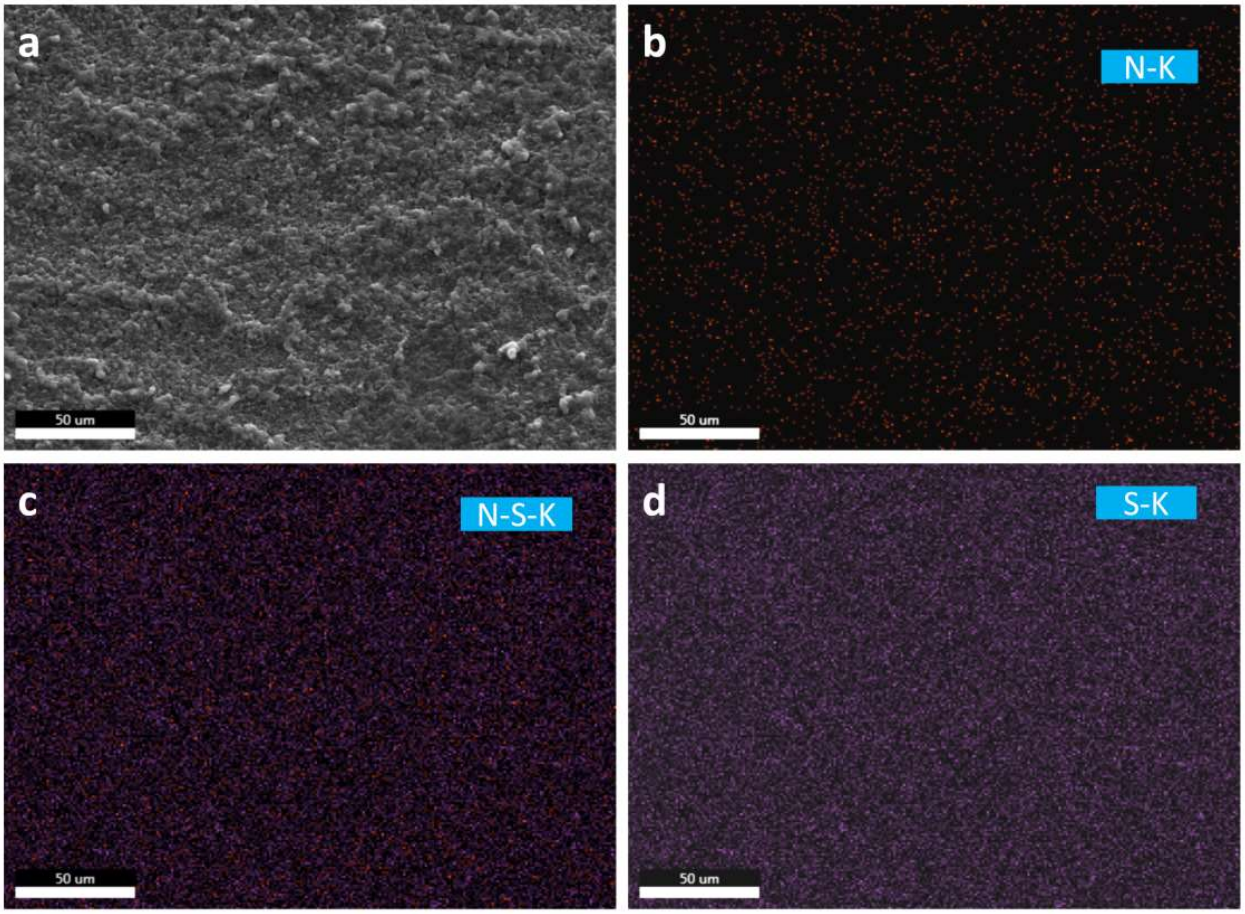

Fig. 4-5 SEM image of PANI-C_{60}/DVB (a) and corresponding elemental mapping of N (b), N-S (c) and S (d) [176]

As showed in Fig. 4-6, the characteristic peaks of PANI base form are detected at 1595 cm^{-1} ,1503 cm^{-1} and 1270 cm^{-1} homologous to quinine, benzene ring deformation and C-N stretching. C_{60} has four strong intermolecular modes at 525, 571, 1185, 1427 cm^{-1}. The characteristic peak for conducting PANI form is also observed at 1241 cm^{-1} in PANI-C_{60} samples. A blue shift (1287 cm^{-1}) is found in C_{60}-PANI hybrids reinforced composites, indicating that the doping reaction between PANI and C_{60} occurred by doping with N atom of PANI [178].

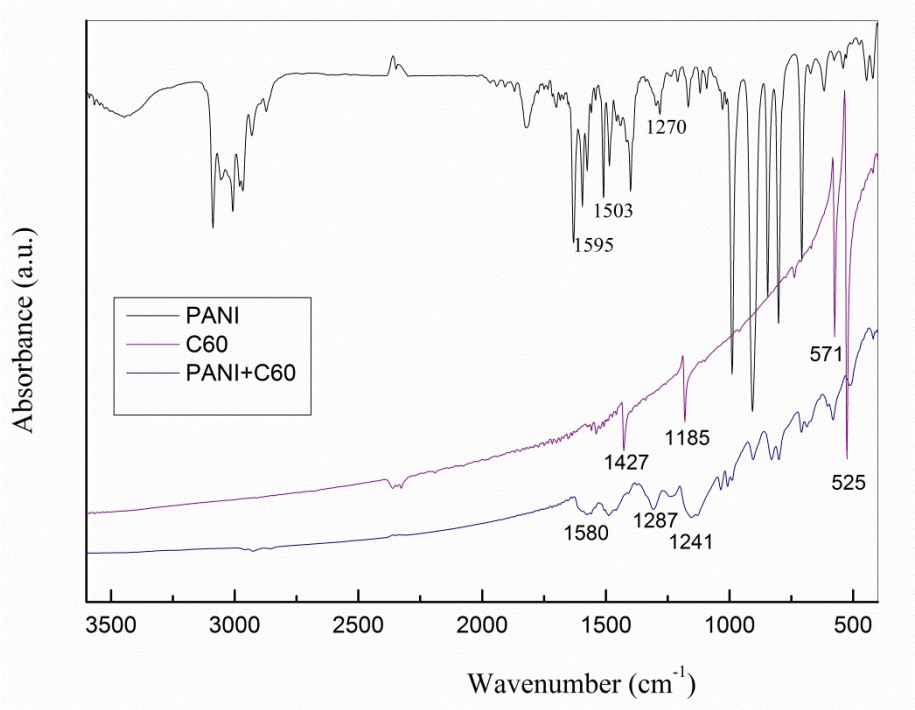

Fig. 4-6 FTIR spectra of PANI base, C_{60} and PANI-C_{60} hybrids in DVB solution [176].

Thermal performance

The thermal stability of C_{60}, PDVB-PANI nanocomposites with different C_{60} content was measured by TGA under a N_2 flow of 10℃/min. In Fig. 4-7, the C_{60} sample has no major mass loss until 800℃, the only 4% weight loss can due to the presence of impurities in C_{60} sample. In the case of PDVB nanocomposites, the C_{60} has a visible effect in delay the PDVB decomposition. According to the DTG curve, it is obvious that the composites have small exothermic peak after the addition of C60. At the same time, C60 tends to increase the decomposition temperature, especially in PDVB/C_{60}-1.05vol%, which has a 15 ℃ increase in the decomposition temperature. This can attribute to the physical block effect of C_{60} which mitigates the proliferation of thermal, same as other carbon materials like carbon nanotube and graphene [179-181]. Thus, the thermal stability is improved by the addition of C_{60}. In the case of the C_{60}-PANI/PDVB nanocomposites, the PANI/C_{60} hybrids are more stable, that can due to the fact that C_{60} has a low heat conductivity [182] and the highly effective free-radical-trapping effect of C_{60} [183], causing it hard to improve the thermal

deliver, therefore the thermal stability is improved only a little after the addition of C60.

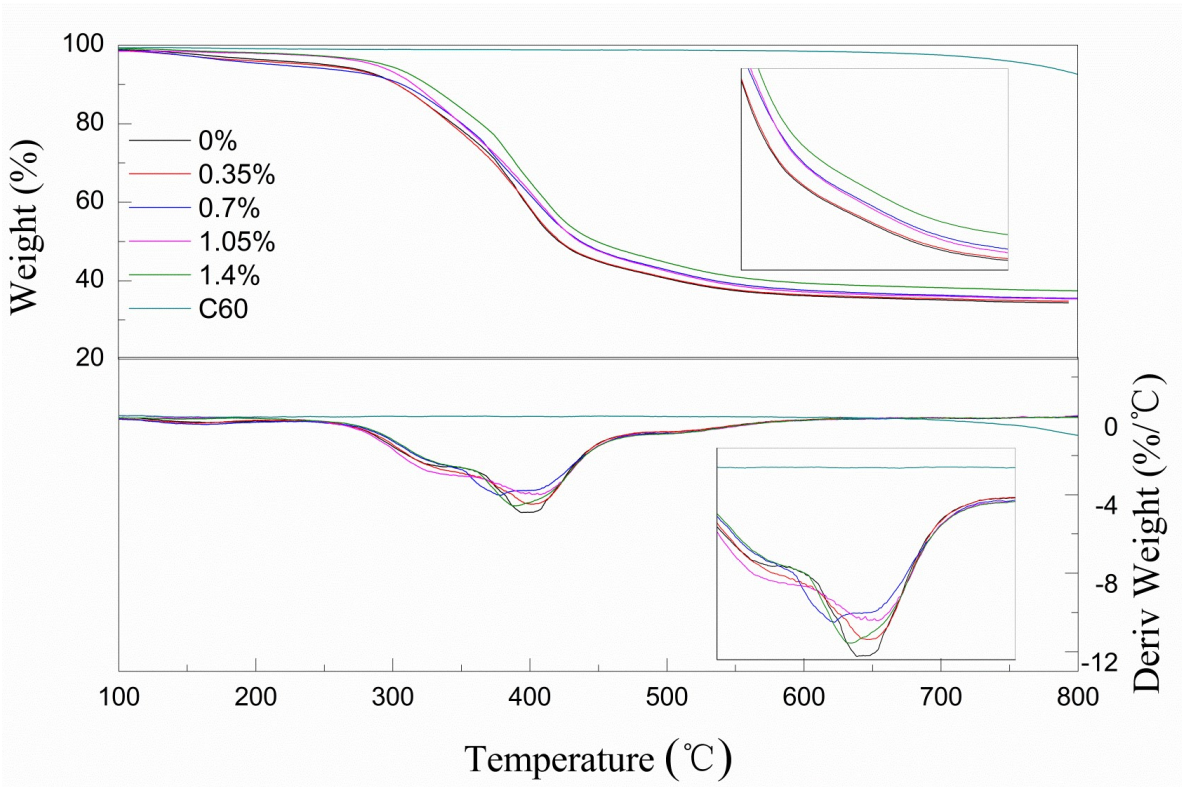

Fig. 4-7 TGA curves of C_{60} and PDVB-PANI nanocomposites with different C_{60} content [176].

Dissipative Particle Dynamics Simulation

The radial distribution function $G(r)$ of C_{60} in the PANI (DBSA) /DVB system was calculated and shown in Fig. 4-8. It exhibits the probability distribution of the distance between C_{60} and DVB centers; the content of C_{60} is 0.35vol%, 0.7vol%, 1.05vol%, and 1.4vol%. The blue lines and the yellow lines represent the dispersion state before and after the equilibrium, respectively.

Flory-Huggins parameter χ were calculated from atomistic simulations of mixing energies in Table 4- 1. Generally, the smaller the value of χ, the better mutual solubility between the polymer. The χ-parameter between PANI and other chemicals is smaller than the χ-parameter between C60 and the chemicals. DVB/PANI has the smallest χ, indicating the best mutual solubility between DVB and PANI. On the other hand, C60 has the smallest χ-parameter with PANI compare to with DBSA and DVB.

This indicates that C60 would have a relatively more contact with PANI compare to DBSA and DVB, resulting in better electrical network in the polymer. Thus, although the χ-parameter between C60 and other chemicals is much bigger than 0.5, which means insoluble [184]. While in our system, there are no significant precipitates of C60, this might be due to the doping reaction1 happened.

Table 4-1. Dissipative particle dynamics (DPD) used for χ parameters of components [176].

materials	χparameter
DVB/C60	3.648
DVB/DBSA	0.283
DVB/PANI	0.189
C60/DBSA	5.963
C60/PANI	2.177
DBSA/PANI	0.934

G(r) indicates that uniform distribution after equilibrium, which is almost same as the distribution before equilibrium, irrespectively of C60 contents. This means that no significant agglomerates of C60 in DVB-complex solutions. We can find that $G(r)$ indicates the obviously higher peaks after the equilibrium, but there are no large clusters of C_{60} found in the simulation process.The first peak is free C_{60} disperse in DVB. The small distance indicates the direct contact of C_{60} and DVB. After equilibrium, the first peak for the sample with 0.35vol% and 0.70vol%content of C_{60} is smaller, indicating that the free C_{60} is more. The second peak has the further distance when the content of C_{60} is 1.05vol%. This means that the C_{60} is doped with PANI, which can prevent the accumulation of C_{60} and enlarge the distance between C_{60} and DVB. But when we add more C_{60} to 1.40vol%, the first peak becomes higher and the second peak is not changed much. It means, when we add more C_{60}, the free C_{60} become more, but the C_{60} doped with PANI has already saturated. This result is in consistent with the experiment results of electrical and thermal conductivity.

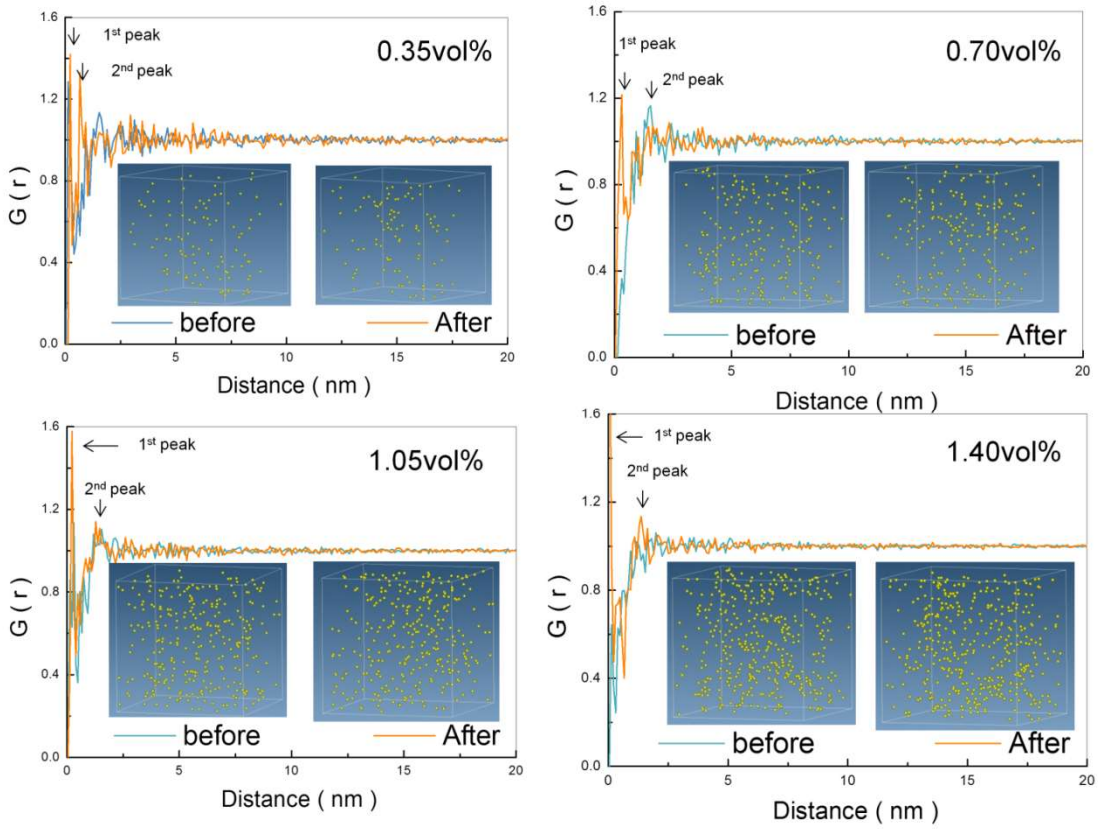

Fig. 4-8 Radial distribution functions between C_{60} and DVB [176]

Electrical conductivity

PANI, as a promising conduct polymer, was introduced into the PDVB polymer as conductive additives. Herein, the electrical conductivity of PDVB composites was measured and showed in Fig. 4-9. According to Fig. 4-9, the conductivity for the composites with additives can keep stable in all frequency. For pure PDVB and C_{60}/PDVB composites, σ_{AC} is monotonously increasing with frequency. This dependence is in accordance with the Eq4-8 [185].

$$\sigma_{AC} = \sigma_{DC} + 2\pi f\varepsilon'' \qquad (4\text{-}8)$$

In the formula, ε'' is the loss factor, f is the frequency, σ_{DC} is the DC conductivity. σ_{AC} is the AC conductivity.

While after addition of PANI and C_{60}, the AC conductivity of composites does not indicate any frequency reliance in the full frequency. This means that the dispersion of PANI is improved, resulting in better conducting 3-D networks. At the whole frequency, the AC conductivity increased with increasing C_{60} concentration

until 1.05vol% of C_{60}.

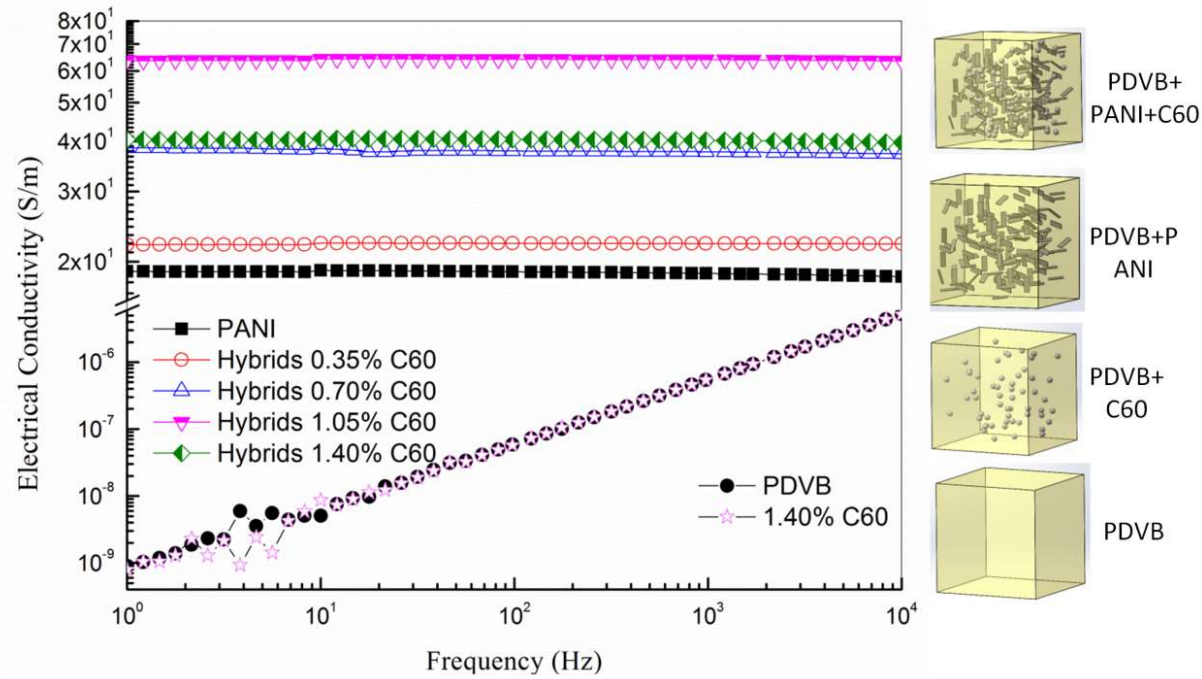

Fig. 4-9. Composites' electrical conductivity with different amount of C60 [176].

The electrical conductivity of pure PDVB is only 7.9×10^{-10} S/m and the electrical conductivity is not improved by the addition of C_{60} only. Both show the same increasing trend as the frequency increase. While after the addition of PANI, the conductivity was increased more than 10 orders of magnitude. This can attribute to the doping reaction (1 and 2) happened and the formation of PANI conductive network in PDVB composites. Because the PANI is with high conductivity, the introduction of PANI can increase the electrical conductivity of PDVB. After the PANI fraction in PDVB up to the percolation threshold for electronic movement, the continuous conductive path will form and lead to the substantial increase in electrical conductivity.

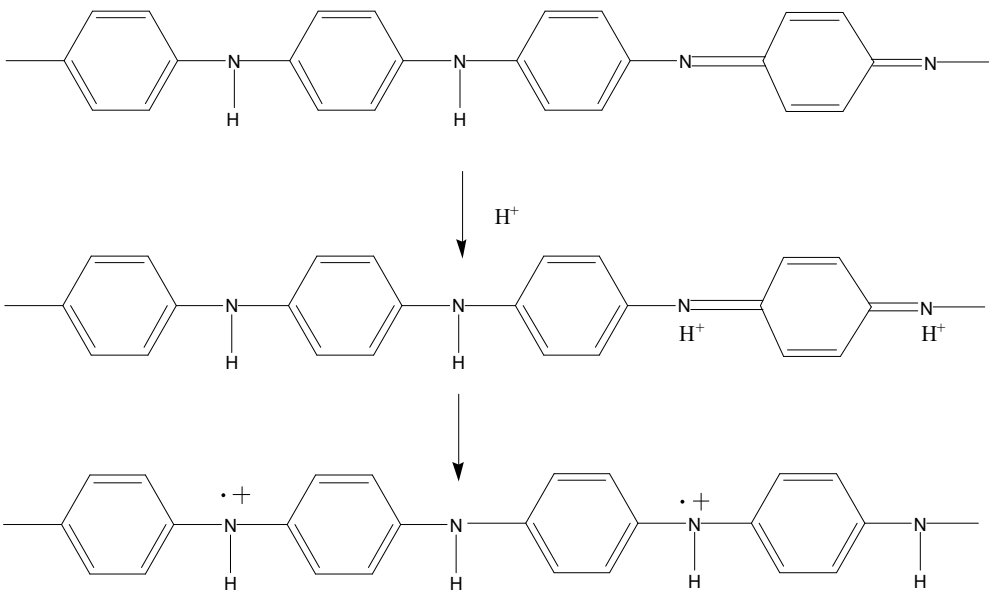

(2)

The conductivity of PDVB-PANI is 18.9 S/m, while the conductivity was improved by the addition of C_{60}, the highest conductivity of the composites with C60/PANI hybrids is up to 63.7 S/m, which is 3.37 times higher than the PDVB-PANI composites. This might be owing to the formation of C_{60} interpenetrating conductive passage in the PDVB composites, suggesting that the new conductive passages generated by C_{60}, which can effectively make up blank between the PANI. On the other hand, polyaniline (EB) can act as an electron donor and C_{60} as an electron acceptor, we can suppose that C_{60} changes the electronic distribution of PANI. This redox doping is illustrated by reaction 1.

The electrical conductivity also can be approximated by Eq 9 [186]:

$$\sigma = en\mu \qquad (4\text{-}9)$$

In the formula, e, n and μ represent the electron charged quantity, concentration and speed. Obviously, increasing of carrier concentration could help to improve the electrical conductivity. The increase of C_{60}'s content results in the increase of hole in p-type polymer and decrease of electron content in n-type polymer. As the filler load increases, an improvement of electrical conductivity comes from the growth of carrier concentration in the composites. While when C_{60} content increases up to 1.4vol%, the extra free C_{60} behaves like an electron barrier so that reduce the electrical

conductivity.

Thermal conductivity

The thermal conductivities of PDVB composites are shown in Fig. 4-10,the result shows 0.58 W/m K for the pure PDVB. The PANI and C_{60}nanoparticles were employed to obtain a low thermal conductivity. The doped PANI and C_{60} have been reported with low thermal conductivity of 0.08 W/m. K [187] and ~0.16 W/m.K [170].

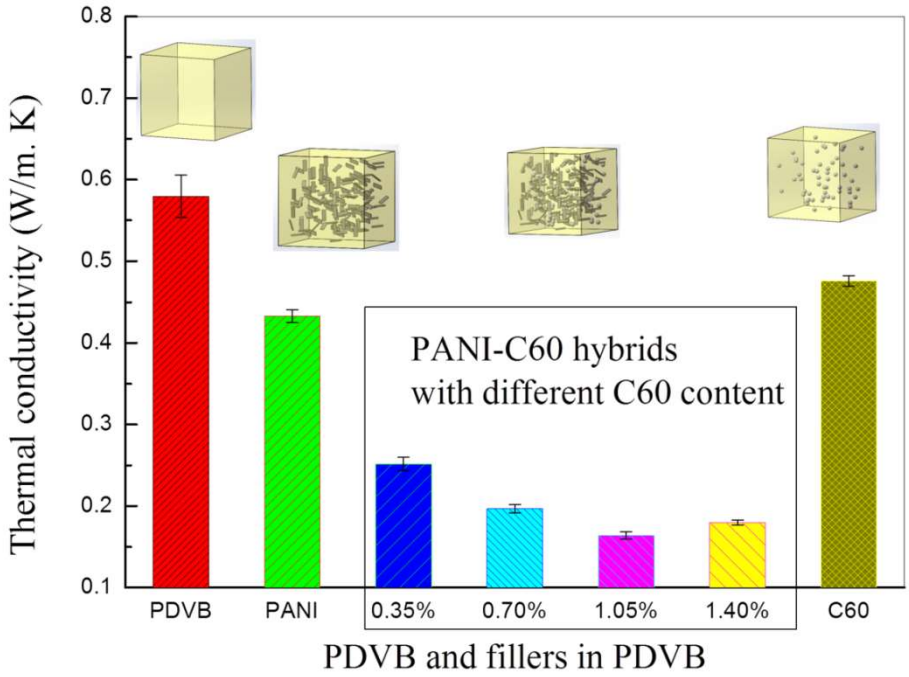

Fig. 4-10 The thermal conductivity of PANI/C_{60}-PDVB composites [176]

In Fig. 4-10, the introduction of the PANI and C_{60} decreases the thermal conductivity. In addition, the addition of hybrid PANI-C_{60} promotes a further reduction of the composite thermal conductivity. The minimum thermal conductivity is only 0.164 W/m K for PDVB composites with 1.05vol% of C_{60}, cutting down the thermal conductivity as high as 70%. And the thermal conductivity decreases as the C_{60} concentration increases in hybrids. Therefore, we conclude that the reduction of thermal conductivity in the presence of C_{60} is because C_{60} supply extra phonons scattering [188]. On the one hand, C_{60} may break direct PDVB–PDVB contact and

prevent the heat transfer from PDVB to PDVB. Therefore, C_{60}/PANI could significantly break the paths of thermal transport through increasing phonon scattering. On the other hand, the introduction of C_{60} would increase the content of the doped PANI which has very low thermal conductivity. We expect that these C_{60}/PANI grain barriers would affect carrier scattering when the amount of C_{60} reaches a certain level. Therefore, we conclude that C_{60} provide extra phonon scattering by large thermal defects.

4.4 Conclusion

In this work, the hybrid PANI/C_{60} was incorporated into PDVB composites in order to obtain the material with decoupling electrical and thermal conductivity. The hybrid particles were fabricated through a simple one-step process in the solution of DVB monomer. The doping process of PANI and polymerization of DVB was completed simultaneously. The morphology and structure were characterized by TEM SEM and FTIR. The results indicated that the doping interaction occurred between PANI and C_{60}, homogenous network of C_{60}/PANI was formed in the PDVB polymer. The thermal stability is obviously improved by the addition of C_{60}. The electrical and thermal conductivity were investigated. The results showed obvious decoupling effect. The AC electrical conductivity was improved significantly from 9×10^{-10} S/m to 63.7 S/m, more than 10 orders of magnitude. On the contrary, the thermal conductivity was reduced to extremely low of only 0.164W/m. K from 0.579 W/m. K. Dissipative particle dynamics (DPD) results exhibited better agreement with the experiment results of electrical and thermal conductivity. These results indicate that DPD method can be a new option for designing new functional polymer composite. Simultaneously, the decoupling of the electrical and thermal conductivity of polymer bulk composites may open potential routes for new functional composites.

Chapter 5

Comparative study of the carbon/PANI hybrid system

Abstract:

Doping actions in three systems are different and the system of PANI/Carbon hybrid system appears as a uniform network structure. GO has a smaller χ parameter than MWCNT and C_{60}. GO/PANI and C_{60}/PANI samples have higher decomposition temperatures and lower thermal losses, while the MWCNT/PANI hybrid reinforced composites have lower decomposition temperature and thermal loss, that is, MWCNT cannot improve the thermal stability of the composites. The electrical conductivity of MWCNT-PANI/PDVB follows the law of LANDAUER model. However, the electrical conductivities of GO-PANI/PDVB and C_{60}-PANI/PDVB systems do not follow the law at all. The calculated results of PANI/DVB are perfectly consistent with the experiment results. After addition of GO and MWCNT, the calculated results also have good agreement with the experimental results. Nevertheless,for the calculated result, there is a huge difference with the experimental results after the addition of C_{60}. Voigt-Reuss model was chosen to explain the modulus'change. For GO-PANI/PDVB, hardly differences are found between the Voigt-Reuss model and experimental values. However, in systems of MWCNT-PANI/PDVB and C60-PANI/PDVB, great divergence exists between the theoretical model and the experimental data.

5.1 General Introduction

Graphene oxide, Mutiwalled carbon nanotubes and fullerene, are different style of carbon. Graphene has a sheet-like structure consisting of one atom. Fullerene has a ball-like structure, and carbon nanotube has a cylindrical shape with graphene rounded. Both have a high specific surface area, mechanical properties, thermal conductivity as well as electric conductivity.

Researchers indicate that the Young's modulus of graphene oxide (GO) decreased, but it is still as high as 207.6 GPa [160]. Other carbon nanofillers with high modulus are MWCNT, whose modulus ranges from 270 to 950 GPa [161]. Another carbon nanofillers is C_{60} with the high modulus of 874 GPa [1]. Carbonnanofillers also have special electrical and thermal conductivities.

The comparative study of 3 different carbon/PANI hybrid systems will be discussed in this part.

5.2 Study of the hybrid system

Doping Action in 3 hybrid systems

The doping action in Reaction. 5-1 took place in all these systems, although among these 3, carbon nano fillers, only GO and C_{60} were reported to be capable of doping with polyaniline as showed in Reaction. 5-2. This is why the GO/PANI and C_{60}/PANI systems have better dispersion state which will be discussed in 5.2.2. Electrical enhancements of the GO/PANI and C_{60}/PANI systems are different with the MWCNT system. In the GO/PANI and C_{60}/PANI systems, the introduction of carbon nanofillers does not only lead to high conductivity of the systems, but also increases the content of PANI, so that improves the conductivity of PANI.

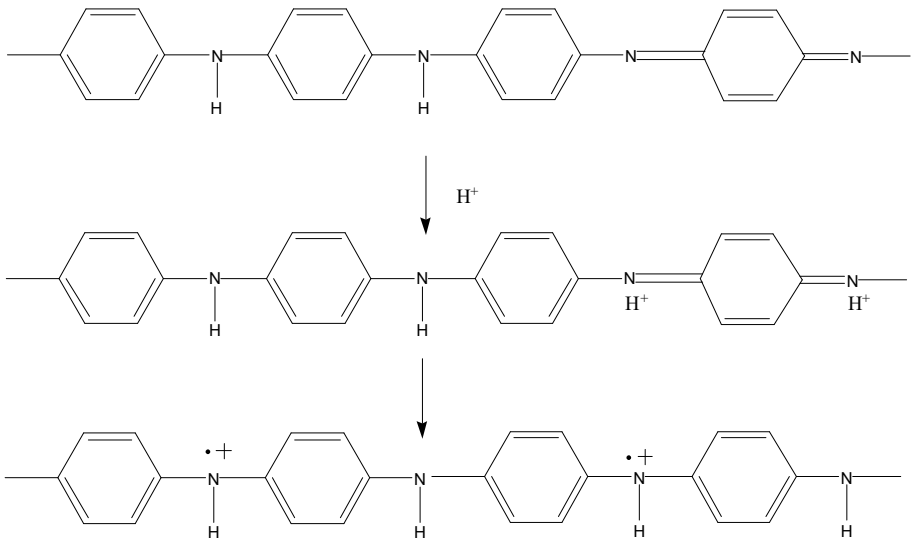

Reaction. 5-1 The doping action of PANI with acid

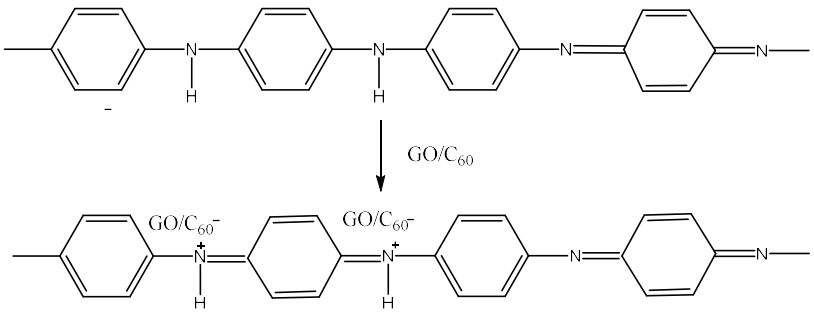

Reaction. 5-2The doping action of PANI with carbon nanofillers

Morphology comparison of 3 hybrid systems

In order to check the change of the microstructure after the addition of carbon nanofillers, morphology of PANI and PANI with different carbon nanofillers were observed by SEM.

As showed in Fig.5.1, many large PANI–DBSA particles are observed in PANI system. While the system of PANI/Carbon hybrid system appears as a uniform network structure as showed in Fig.5.1, which clearly indicated that both MWCNT, GO and C_{60} can improve the dispersity of conductive PANI particles.

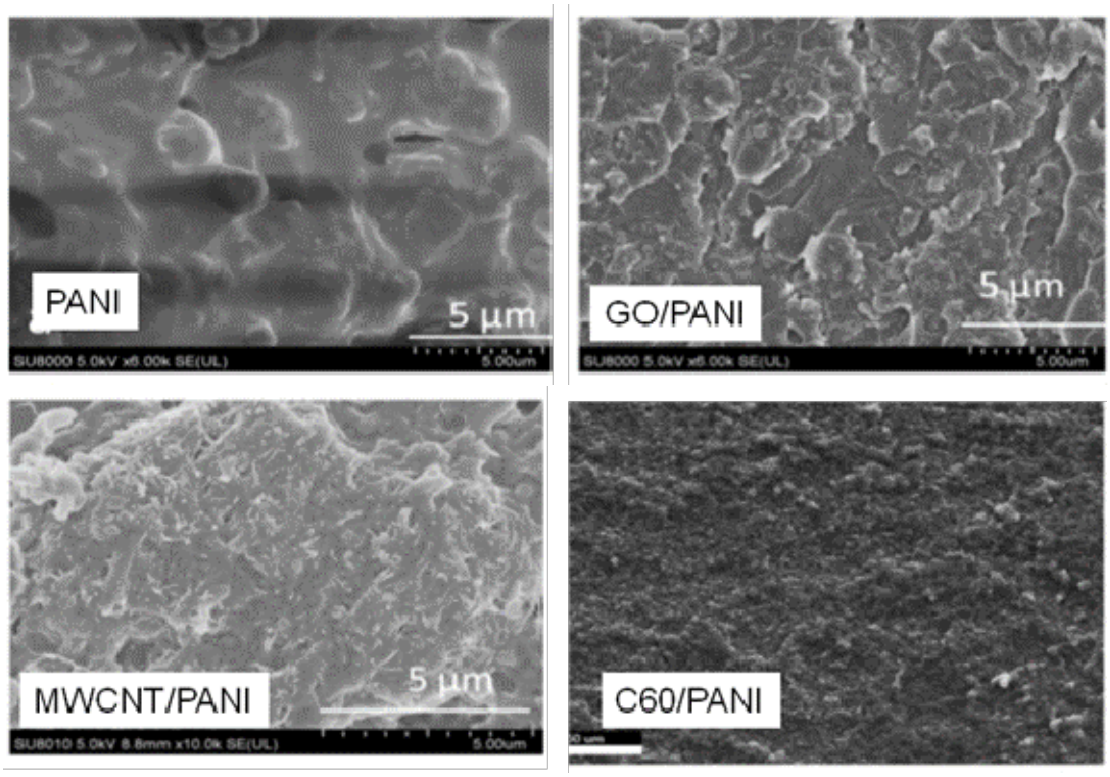

Fig.5.1 SEM image of PANI and PANI/Carbon hybrids.

Comparison of Flory-Huggins parameter

The Flory-Huggins parameter χ parameter and the binary interaction parameter a_{ij} was calculated and compared. GO has a smallest χ parameter comparing toMWCNT and C_{60}. Table 5.1shows the calculation results of binary interaction parameters. This is probably because GO has a sheet-like structure composed of hexagonal carbon. It attempts to take a structure in which hexagonal mesh structures are piled up by π-π interaction. Because MWCNT and C_{60} have a graphene rounded structure and the π-π interaction is also hard to work, the cohesive energy becomes larger than that of graphene. Therefore, theχ parameter becomes bigger than that of graphene.

Table 5.1The calculation results of binary interaction parameters.

Materials	χ parameter	a_{ij}
PANI/MWCNT	3.331	35.885
PANI/GO	0.739	27.416

PANI/C_{60}	3.648	36.922

Thermal Stability of 3 hybrid systems

The thermal stability of nanocomposites with nanofillers was calculated and compared. In Table 5.2, the GO/PANI and C_{60}/PANI samples have higher decomposition temperature and lower thermal loss while the MWCNT/PANI hybrids reinforced composites have lower decomposition temperature and thermal loss. That means MWCNT cannot improve the thermal stability of the composites. Because the addition of MWCNT is very low, if the MWCNT cannot affect the whole structure of the PANI or the polymer, it will not be able to improve the thermal stability. However, the introduction of GO and C_{60} can be dope with PANI. This behavior enables the formation of a more stable 3D PANI network inside the nanocomposites, which can improve the thermal stability.

Table 5.2The TGA results of composites with different nanofillers

Material	Decomposition Temperature(℃)	Thermal Loss(%)
PANI/PDVB	310	70
GO-PANI/PDVB	330	63
MWCNT-PANI/PDVB	315	68
C60-PANI/PDVB	325	65

Analysis of Electrical Conductivity

The conductivity comparisonof Carbon/PANI hybrids reinforced polymer was presented in Table 5.3. We can see that the pure DVB have low electrical conductivity in contrast to the doped PANI. The doped PANI can improve the electrical conductivity definitely. Furthermore, the dispersion state can also have an effect on the conductivity of the composites.

Several developments of this homogenization scheme to physical problems have been widely applied in the literature. This method was first employed by Landauer to study the effective conductivity of a composite with spherical fillers [189]. He developed the effective medium theory (EMT) [189] for a two-phase statethat provides another estimator. This theory considers each individual inclusion as surrounded by a homogeneous medium. It assumed that the total conductivity was induced by all elements. Thereby, in order to analyze our system, we then directly applied the Landauer's model to explain the conductivity happened in these 3 hybrid systems.

According to Landauer model [189]for the composites with different mixtures, none of a theory can explain all situation. Among this, the most frequently used theory in the literature is showed in formula 5-1,

$$\rho_c = \rho_1 V_1 + \rho_2 V_2 \quad (5\text{-}1)$$

where ρ_c is the resistivity of the composites, $\rho_1$is the resistivity of component 1, ρ_2 is the resistivity of component 2,$V_1$is the volume fraction of component 1, and $V_2$is the volume fraction of component 2. In this model, the components of composites are supposed as random dispersion. Therefore, this equation supplies an upper limit for the resistivity, indicating the lower limit of the conductivity in formula 5-2.

$$\frac{1}{\sigma_c} = \frac{V_1}{\sigma_1} + \frac{V_2}{\sigma_2} \quad (5\text{-}2)$$

where σ_c is the electrical conductivity of the composites. σ_1 is the electrical conductivity of component 1, and σ_2 is the electrical conductivity of component 2,

The alternate hypothesis,

$$\sigma_c = \sigma_1 V_1 + \sigma_2 V_2 \quad (5\text{-}3)$$

Formula 5-3gives the maximum upper limit of the plain mix of the composites which can be expressed as the formula 6.1.LANDAUER propoesed that these two expressions were the upper and lower limits of the conductivity of the mixed system.

In PANI/PDVB system, PDVB is consideredas component 1 and PDVB is considered as component 2; In GO-PANI/PDVB, MWCNT-PANI/PDVBand C_{60}-PANI/PDVB systems, PANI/PDVB system is supposed as component 1 and the carbon nanofillers

is supposed as component 2. According to the above formulations,the upper and the lower limit of the composite's conductivity are achieved in the Table 5.3.

Table 5.3The electrical conductivity of material and composites

Electric Conductivity	Lower limit by Calculated (S m^{-1})	Upper limit by Calculated (S m^{-1})	Experiment (S m^{-1})
DVB	—	—	10^{-9}
GO	—	—	0.14
MWCNT	—	—	10^{6}
C60	—	—	10^{-3}
PANI(DBSA)	—	—	10^{3}
PANI/PDVB	$1.25*10^{-9}$	220	22
GO-PANI/PDVB	8.58	21.78	40
MWCNT-PANI/PDVB	22	8021	78
C60-PANI/PDVB	0.099	21.78	63.7

Depending on the calculation results, we can find that only PANI/PDVB and MWCNT-PANI/PDVB systems can fit the law of LANDAUER model. The electrical conductivity of PANI/DVB system is 22 S m^{-1} which is between the lower limit ($1.25x10^{-9}$ S m^{-1})and the upper limit(220 S m^{-1}). The electrical conductivity of MWCNT-PANI/PDVB is 78 S m^{-1} which is between the lower limit (22 S m^{-1})and the upper limit(8021 S m^{-1}). However, the electrical conductivities of GO-PANI/PDVB and C60-PANI/PDVB systems cannot fit the law at all. The electrical conductivities of both systems are much higher than the upper limit calculated by the LANDAUER law. This also confirms that the doping action happened inside the system and the introduction of GO or C_{60} can improve the dispersion of PANI. It cannot be assumed as a simple mix in these two systems.

6.2.6 Comparison of Thermal Conductivity

A number of theoretical models have been proposed to predict the effective thermal conductivity of filled composites. Thermal conductivity and diffusion in a solid are governed by Fick's law. Hatta [138] calculatedthe thermal conductivity of short fiber reinforced composites using Eshelby theory. The MTM has proven that this approach is an effective way to predict the thermal conductivity for composites[137]. Therefore, in this study, Hatta and Taya's theory is applied for the discussion.

Because the thermal conductivities of graphene and carbon nanotube have been reported to possess similar values (3000 W/mK) [190], the doped PANI and C_{60} have been reported with low thermal conductivity of 0.08 W/mK[187] and 0.16 W/mK [170]. Therefore,the thermal conductivity may be enhanced by GO and MWCNT, by reducing with PANI and C_{60}. In this part, the thermal conductivity of composites were calculated according to Hatta and Taya's theory [138] and compared with the experimental results.

In the case of completely random distribution, the thermal conductivity can be expressed as a formula. MWCNTcan be considered as short fiber,and GOcan be supposed as short fiber with wired cross-section.Hence,the system for MWCNT and GO reinforced polymer composites and the thermal conductivity can be expressed as the formula 5.4.

$$K_{11} = K_{33} = K^m\left(1 - \frac{V_f(K^m - K^f)[(K^f - K^m)(2S_{33} + S_{11}) + 3K^m}{3(K^f - K^m)^2(1 - V_f)S_{11}S_{33} + K^m(K^f - K^m)R + 3(K^m)^2}\right) \quad (5.4)$$

where K_{11}, K_{33} is the thermal conductivity of the composites in different direction, K^m is the thermal conductivity of the matrix, K^f is the thermal conductivity of the fillers, V_f is the volume fraction of the fillers and$S_{ij}$is tensor and depends on the shape of the filler.

For the sphere of PANI and C60, the thermal conductivity can be expressed as follows:

$$S_{11} = S_{33} = \frac{1}{3} \quad (5.5)$$

$$K_{11} = K_{33} = K^m\left\{1 + \frac{V_f}{\frac{(1 - V_f)}{3} + \frac{K^m}{K^f - K^m}}\right\} \quad (5.6)$$

Calculation of S

GO, penny shape can be given in follows.

$$S_{11} = S_{22} = \frac{\pi a_3}{4a_1} \tag{5.7}$$

$$S_{33} = 1 - \frac{\pi a_3}{2a_1} \tag{5.8}$$

where a is the length in three directions.

MWCNT

Aspect ratio

$$\alpha = \frac{a_3}{a_1} \tag{5.9}$$

$$S_{11} = S_{22} = \frac{a_1^2 a_3}{2(a_3^2 - a_1^2)^{\frac{3}{2}}}\left\{\frac{a_3}{a_1}\left(\frac{a_3^2}{a_3^2} - 1\right)^{\frac{1}{2}} - \cosh^{-1}\frac{a_3}{a_1}\right\}$$

$$= \frac{\alpha}{2(\alpha^2-1)^{\frac{3}{2}}}\left\{\alpha(\alpha^2 - 1)^{\frac{1}{2}} - \cosh^{-1}\alpha\right\} \tag{5.10}$$

$$S_{33} = 1 - 2S_{22} \tag{5.11}$$

According to formula 5.3-5.11, the calculated results of the composite's conductivity were set in Table 5.4.

Table 5.4 Thermal conductivities by experiment and theoretical calculated modulus

Thermal conductivity	Experiment(W/mK)	Calculated(W/mK)
PDVB	0.58	_
Doped PANI	0.08	_
PANI/PDVB	0.43	0.45
GO	3000	_
MWCNT	3000	_
C60	0.16	_
GO-PANI/PDVB	0.42	0.427
MWCNT-PANI/PDVB	0.43	0.427
C_{60}-PANI/PDVB	0.16	0.426

According to the calculated results, the calculated results of PANI/DVB are perfectly consistent with the experimental results. After addition of GO and MWCNT, the calculated results also have good agreement with the experimental results. However, the calculated results after adding C_{60} cause a huge difference with the experimental results. That means the introduction of C_{60} results in some change, which could be due to the change of dispersion state of doped PANI or the doping action between C_{60} and PANI.

Comparison of Mechanical Properties

In this work, the geometry and orientation of the particles in the matrix are the maximum disparity during the 3 different nanofillers: GO, MWCNT and C60. Thus, we only considered the geometry and orientation of the particles. The inclusions are summed straight and full load transfer between particles and matrix and the system is restricted as a two-phase composite. The included materials for each phase are assumed as linearly elastic and isotropic.

Micromechanical modeling comes from the properties of various components of the composite. Their arrangement is a very convenient method for understanding and predicting the composite behavior. The well-knew Weng's model is used to calculate the theoretical Young's modulus of the composites. MWCNT is considered as the micro fibers, while the GO can be assumed as discs andC_{60} is assumed as a sphere. Under this hypothesis, the results were presented in Fig.5.2.

Before applying the models, the mechanical properties of the matrix and the nanofillers are checked and showed in Table 5.5. Graphene is one of the strongest materials with the Young's modulus of E = 1.0 TPa. Researchers indicate that the Young's modulus of graphene oxide (GO) decreased, but it ranges from 130 to 1000GPa [160]. Other carbon nanofillers with high modulus are MWCNT, with the modulus range from 270 to 1000GPa [161]. Another carbon nanofillers is C_{60} with the high modulus of 874 GPa [1].

Table 5.5 The original property of MWCNT/PANI hybrid systems

Material parameter	Value
E_0 (GPa)	5.2
υ_0	0.35
E_1(GPa)	1000
υ_1	0.25

$$\frac{E_{comp}}{E_0} = \frac{\kappa_{comp}\mu_{comp}(3\kappa_0+\mu_0)}{\kappa_0\mu_0(3\kappa_{comp}+\mu_{comp})} \quad (5.12)$$

where, E_{comp} is the modulus of the composites, E_0 is the modulus of the fillers, κ_{comp} is the bulk modulus of the composites,μ_{comp} is the shear modulus of the composites, $\kappa_0$is the bulk modulus of the composites, and μ_0 is the shear modulus of the composites.

$$\frac{\kappa_{comp}}{\kappa_0} = \frac{1}{1+cp} \quad (5.13)$$

$$\frac{\mu_{comp}}{\mu_0} = \frac{1}{1+cq} \quad (5.14)$$

$$p = \frac{p_2}{p_1} \quad (5.15)$$

$$p_1 = 1 + c[2(S_{1122} + S_{2222} + S_{2233} - 1)(a_3 + a_4) + (S_{1111} + 2S_{2211} - 1)(a_1 - 2a_2)]/3a$$

(5.16)

$$p_2 = [a_1 - 2(a_2 - a_3 - a_4)]/3a \quad (5.17)$$

Moreover, the fiber-like inclusions can be expressed as follows.

$$S_{1111} = \frac{1}{2(1-\nu_0)}\left\{1 - 2\nu_0 + \frac{3\alpha^2-1}{\alpha^2-1} - \left[1 - 2\nu_0 + \frac{3\alpha^2}{\alpha^2-1}\right]g\right\} \quad (5.18)$$

$$S_{2222} = S_{3333} = \frac{3}{8(1-\nu_0)}\frac{\alpha^2}{\alpha^2-1} + \frac{1}{4(1-\nu_0)}\left[1 - 2\nu_0 + \frac{9}{4(\alpha^2-1)}\right]g \quad (5.19)$$

$$S_{2233} = S_{3322} = \frac{1}{4(1-\nu_0)}\left\{\frac{\alpha^2}{2(\alpha^2-1)} - \left[1 - 2\nu_0 + \frac{3}{4(\alpha^2-1)}\right]g\right\} \quad (5.20)$$

$$S_{2211} = S_{3311} = -\frac{1}{2(1-\nu_0)}\frac{\alpha^2}{\alpha^2-1} + \frac{1}{4(1-\nu_0)}\left\{\frac{3\alpha^2}{\alpha^2-1)}\left[1 - 2\nu_0 + \frac{3}{2(\alpha^2-1)}\right]\right\}g \quad (5.21)$$

$$S_{1122} = S_{1133} = \frac{1}{4(1-\nu_0)}\left[1 - 2\nu_0 + \frac{1}{\alpha^2-1)}\right] + \frac{1}{2(1-\nu_0)}\left[1 - 2\nu_0 + \frac{3}{2(\alpha^2-1)}\right] \quad (5.22)$$

$$S_{2323} = S_{3232} = \frac{1}{4(1-\nu_0)}\left\{\frac{\alpha^2}{2(\alpha^2-1)} + \left[1 - 2\nu_0 - \frac{3}{4(\alpha^2-1)}\right]g\right\} \quad (5.23)$$

$$S_{1212} = S_{1313} = \frac{1}{4(1-\nu_0)}\left\{1 - 2\nu_0 - \frac{\alpha^2+1}{\alpha^2-1} - \frac{1}{2}\left[1 - 2\nu_0 - \frac{3(\alpha^2+1)}{\alpha^2-1}\right]g\right\} \quad (5.24)$$

Where,

$$g = \frac{\alpha}{(\alpha^2-1)^{3/2}}\{\alpha(\alpha^2-1)^{1/2} - cosh^{-1}\alpha\} \tag{5.25}$$

$$\alpha = l/d \tag{5.26}$$

For MWCNT l =20μm, d =15nm. $\alpha = 1333$,g can be obtained as 1 by the formula.

Combing the formula 5.13 and the formula 5.15 to 5.26, a series of $\frac{\kappa_{comp}}{\kappa_0}$ will be obtained.

$$q_1 = 1 - c\left\{\frac{2}{5}\frac{2S_{1212}-1}{2S_{1212}+\mu_0/(\mu_1-\mu_0)} + \frac{1}{3}\frac{2S_{2323}-1}{2S_{2323}+\mu_0/(\mu_1-\mu_0)} - \frac{1}{15a} * [(S_{1122} - S_{2233})(2a_3 - a_4 + a_5 a) + 2(S_{1111} - S_{2211} - 1)(a_1 + a_2) + (S_{1122} - S_{2222} + 1)(2a_3 - a_4 - a_5 a)\right\} \tag{5.27}$$

$$q_2 = -\frac{2}{5}\frac{1}{2S_{1212}+\mu_0/(\mu_1-\mu_0)} - \frac{1}{3}\frac{1}{2S_{2323}+\mu_0/(\mu_1-\mu_0)} + \frac{1}{15a} * [2(a_1 + a_2 - a_3) + a_4 + a_5 a] \tag{5.28}$$

$$q = q_2/q_1 \tag{5.29}$$

$$a_1 = 6(\kappa_1 - \kappa_0)(\mu_1 - \mu_0)(S_{2222} + S_{2233} - 1) - 2(\kappa_0\mu_1 - \kappa_1\mu_0) + 6\kappa_1 \tag{5.30}$$

$$a_2 = 6(\kappa_1 - \kappa_0)(\mu_1 - \mu_0)S_{1133} + 2(\kappa_0\mu_1 - \kappa_1\mu_0) \tag{5.31}$$

$$a_3 = -6(\kappa_1 - \kappa_0)(\mu_1 - \mu_0)S_{3311} - 2(\kappa_0\mu_1 - \kappa_1\mu_0) \tag{5.32}$$

$$a_4 = 6(\kappa_1 - \kappa_0)(\mu_1 - \mu_0)(S_{1111} - 1) + 2(\kappa_0\mu_1 - \kappa_1\mu_0) + 6\mu_1(\kappa_1 - \kappa_0) \tag{5.33}$$

$$a_5 = 1/[S_{3322} - S_{3333} + 1 - \frac{\mu_1}{(\mu_1-\mu_0)}] \tag{5.34}$$

$$a = 6(\kappa_1 - \kappa_0)(\mu_1 - \mu_0)[2S_{1133}S_{3311} - (S_{1111} - 1)(S_{3322} + S_{3333} - 1)] + 2(\kappa_0\mu_1 - \kappa_1\mu_0)[2(S_{1133} + S_{3311}) + (S_{1111} - S_{3322} - S_{3333})] - 6\kappa_1(\mu_1 - \mu_0)(S_{1111} - 1) - 6\mu_1(\kappa_1 - \kappa_0)(S_{2222} + S_{2233} - 1) - 6\kappa_1\mu_0 \tag{5.35}$$

Combining the formula 5.14 and the formula 5.27 to 5.35, a series of $\frac{\mu_{comp}}{\mu_0}$ can also be obtained. Substitute $\frac{\kappa_{comp}}{\kappa_0}$ and $\frac{\mu_{comp}}{\mu_0}$ into the formula 5.12, $\frac{E_{comp}}{E_0}$ can be obtained in Fig.5.2.

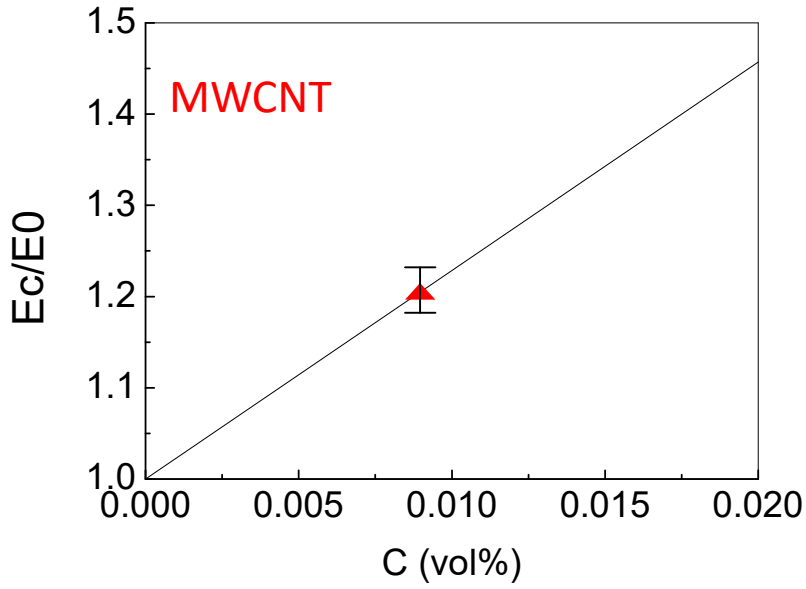

Fig.5.2 $\frac{E_{comp}}{E_0}$ of MWCNT/PANI hybrids reinforced polymer composites

In the GO/PANI hybrid reinforced polymer system, GO can be assumed as randomly oriented discs.

Table 5.6 The original property of GO/PANI hybrid systems

Material parameter	Value
E_0 (GPa)	5.2
υ_0	0.35
E_1(GPa)	300
υ_1	0.3

$$\kappa_{comp} = \kappa_V - c_1[1 - c_1 \frac{2k_1+l_1-3\kappa_0}{3(k_1+\mu_0)}]^{-1}[\frac{(2k_1+l_1-3\kappa_0)(2k_1+l_1-3\kappa_V)}{9(k_1+\mu_0)} \quad (5.36)$$

$$\mu_{comp} = \mu_V - \frac{c_1}{5}[1 - c_1 \frac{k_1-l_1-\mu_0}{15(k_1+\mu_0)} - \frac{2}{5}c_1 \frac{m_1-\mu_0}{m_1+\gamma_0} - \frac{2}{5}c_1 \frac{p_1-\mu_0}{p_1+\mu_0}]^{-1}[\frac{(k_1-l_1-\mu_0)(k_1-l_1-\mu_V)}{3(k_1+\mu_0)} + \frac{2(m_1-\mu_0)(m_1-\mu_V)}{m_1+\gamma_0} + \frac{2(p_1-\mu_0)((p_1-\mu_V)}{p_1+\mu_0} \quad (5.37)$$

where the Voigt bounds κ_V and μ_V are given in formula 5.38 and 5.39.

$$\kappa_V = c_0\kappa_0 + c_1\kappa_1 \tag{5.38}$$

$$\mu_V = c_0\mu_0 + \frac{c_1}{5}(\mu_1 + 2m_1 + 2p_1) \tag{5.39}$$

Bulk modulus of κ and shear modulus of μ can be obtained in 5.40 and 5.41.

$$\kappa_0 = \frac{E_0}{3(1-2\nu_0)} \tag{5.40}$$

$$\mu_0 = \frac{E_0}{2(1+\nu_0)} \tag{5.41}$$

$$k_1 = \kappa_1 + 1/3\mu_1 \tag{5.42}$$

$$l_1 = \kappa_1 - 2/3\mu_1 \tag{5.43}$$

For isotropic material, $m_1=p_1=\mu_1$

Combining the formula 5.36 to the formula 5.43, a series of $\frac{E_{comp}}{E_0}$ can be obtained in Fig.5.3.

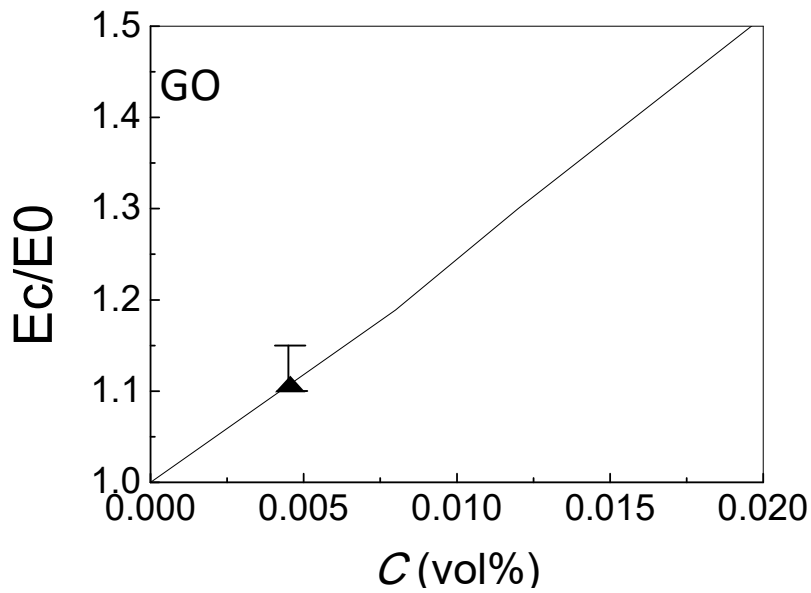

Fig.5.3 $\frac{E_{comp}}{E_0}$ of GO/PANI hybrids reinforced polymer composites

In the C_{60}/PANI hybrid reinforced polymer composites systems, the composite's bulk modulus of κ_{comp} and the shear modulus of μ_{comp} are given in the formula 5.44 and 5.45.

Table 5.7 The original property of C60/PANI hybrid systems

Material parameter	Value
E_0 (GPa)	5.2
υ_0	0.35
E_1(GPa)	870
υ_1	0.3

$$\frac{\kappa_{comp}}{\kappa_0} = 1 + \frac{c_1}{\frac{3c_0\kappa_0}{3\kappa_0+4\mu_0} + \frac{\kappa_0}{\kappa_1-\kappa_0}} \tag{5.44}$$

$$\frac{\mu_{comp}}{\mu_0} = 1 + \frac{c_1}{\frac{6c_0(\kappa_0+2\mu_0)}{5\ \ 3\kappa_0+4\mu_0} + \frac{\mu_0}{\mu_1-\mu_0}} \tag{5.45}$$

where c_0 and c_1 are the volume fractions of the matrix and inclusion phase. Combining the formula 5.12, formula 5.40, 5.41, 5.44 and 5.45, a series of $\frac{E_{comp}}{E_0}$ can be obtained in Fig.5.4.

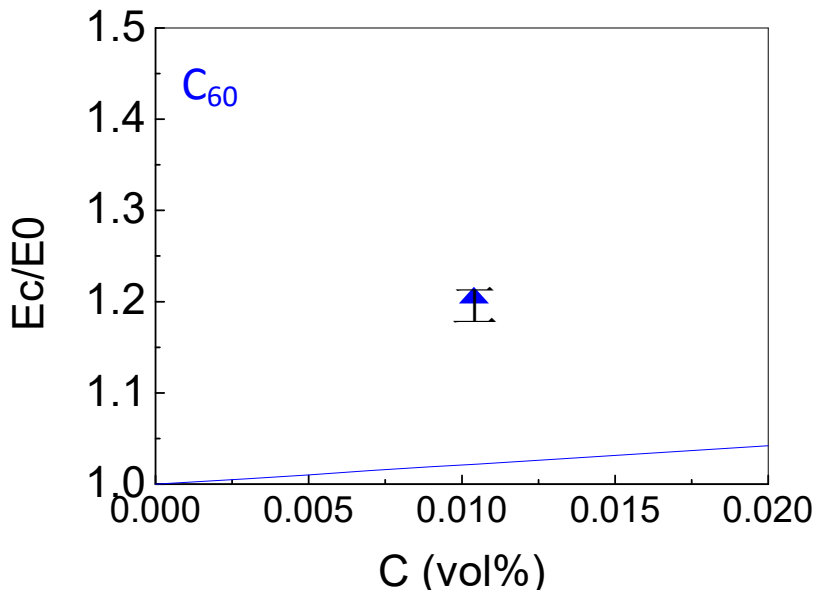

Fig.5.4 $\frac{E_{comp}}{E_0}$ of C60/PANI hybrids reinforced polymer composites

Table 5.7 The comparable results of E_1 in three systems

Modulus	MWCNT	GO	C_{60}
E1(GPa)	1000	300	-
Reference(GPa)	300-1000	130-1000	600-900

Then we applied the GO/PANI system models into the 3-pointbending results in Fig.5.5. In Fig.5.5, we can find that the 3-point bending modulus obtained by theoretical models established in formula 5.12 have a good consistent with the experiment. Therefore, Weng's models can be applied in our systems.

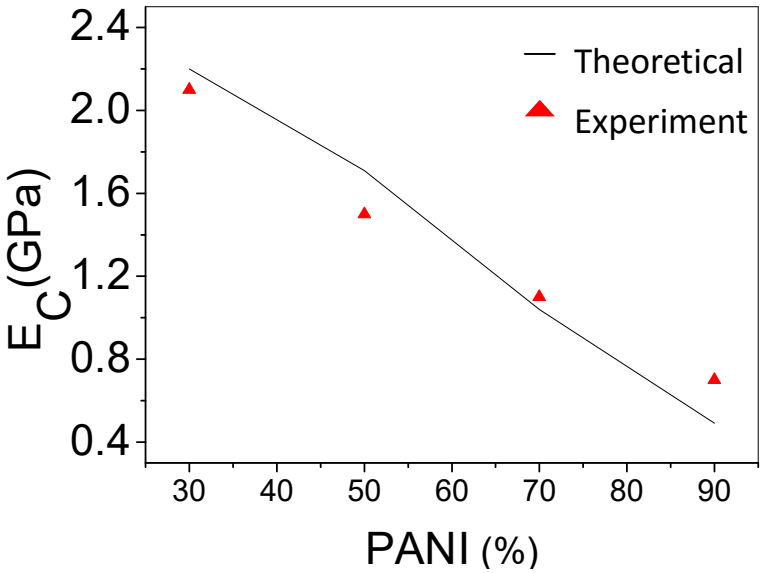

Fig.5.53-point bending modulus for GO/PANI hybrids reinforced polymer composites

5.3 Conclusion

Doping actions in three systems are different and the system of PANI/Carbon hybrid system appears as a uniform network structure. GO gets a smaller χ parameter than MWCNT and C_{60}. GO/PANI and C_{60}/PANI samples have higher decomposition temperature and lower thermal loss, while the MWCNT/PANI hybrid reinforced composites have lower decomposition temperature and thermal loss, which mean MWCNTs cannot improve the thermal stability of the composites. The electrical conductivity of MWCNT-PANI/PDVB can fit the law of LANDAUER model. However, the electrical conductivities of GO-PANI/PDVB and C_{60}-PANI/PDVB

systems cannot fit the law at all. The calculated results of PANI/DVB are perfectly consistent with the experimental results. After addition of GO and MWCNT, the calculated results also have perfect consistence with the experimental results. However, the calculated result after the addition of C_{60} introduces a huge difference with the experimental results. Voigt-Reuss model was chosen to explain the modulus change. For GO-PANI/PDVB, hardly differences are found between the Voigt-Reuss model and experimental values. However, in systems of MWCNT-PANI/PDVB and C_{60}-PANI/PDVB, great divergence exists between the theoretical model and the experimental data.

Chapter 6

Summary and Perspective

The present thesis focuses on the enhancement effect of carbon-based nano-fillers/polyaniline hybrids on the conductivity of the polymers. The objectives of this thesis are (1) to develop conductive polymer system; (2) to gain a better understanding of the conductive mechanism of the polymer composites; (3) to provide a feasible and economical method for the design of polymer nanocomposites.

There are in total 4 main chapters in this thesis not including the introduction and summary. Chapter 2 targets graphene oxide (GO) added to a polymer composites system consisting of surfactant-wrapped/doped polyaniline (PANI) and divinylbenzene (DVB). The nanocomposites were fabricated by a simple blending, ultrasonic dispersion and curing process. The new composites show higher conductivity (0.02–9.8 S/cm) than the other reported polymer system filled with PANI (10-9–10-1S/cm).

Chapter 3 focuses on the conductivity enhancement effect and its mechanism for different types of carbon-based nano-fillers/conduct polymer hybrids in carbon fiber reinforced polymer (CFRP). Multi-walled carbon nanotubes (MWCNT) /polyaniline (PANI) and graphene oxide (GO) /PANI hybrids were separately dispersed into divinylbenzene (DVB) to make the CFRP composites. The alternating current (AC) electrical conductivity results show that both the binary MWCNT/PANI and GO/PANI hybrids have significant enhancement on AC conductivity of the CFRP composites. The maximum AC conductivity of CFRP made of MWCNT/PANI was measured to be 22.4 S/m, which has improved by more than 3 orders of magnitude compared to CF/DVB, and more than 2 orders of magnitude compared to CF/epoxy. Thus,

CF/MWCNT-PANI composites can be considered as promising candidates for multifunctional material where high conductivity is demanded.

Chapter 4 aims at hybrid nanoparticles, fullerene (C_{60}) and polyaniline (PANI), were incorporated into the polydivinylbenzene (PDVB), and their decoupling effect of electrical and thermal conductivity was investigated. The hybrid particles were fabricated through a simple one-step process in the solution of divinylbenzene (DVB) monomer. Dissipative particle dynamics (DPD) simulations were also conducted to gain further understanding about the decoupling effect and mechanisms related to dispersibility of C_{60} in the polymer system. The DPD consequences exhibited better agreement with the experimental results of electrical and thermal conductivity.

Chapter 5 targets the comparative study of 3 different carbon/PANI hybrid systems. The doping actions in three systems are different and the system of PANI/Carbon hybrid system appears as a uniform network structure. GO has a smallest χ parameter than MWCNT and C_{60}. GO/PANI and C_{60}/PANI samples have higher decomposition temperatures and lower thermal losses, while the MWCNT/PANI hybrids reinforced composites have lower decomposition temperature and thermal loss,that means MWCNT cannot improve the thermal stability of the composites. The electrical conductivity of MWCNT-PANI/PDVB can fit the law of LANDAUER model. However, the electrical conductivities of GO-PANI/PDVB and C60-PANI/PDVB systems cannot fit the law at all. The calculated results of PANI/DVB are perfectly consistent with the experiment results. After addition of GO and MWCNT, the calculated results also have perfect consistence with the experimental results. Nevertheless, the calculated result after the addition of C_{60} introduces a huge difference with the experimental results. Voigt-Reuss model was chosen to explain the modulus change. For GO-PANI/PDVB, there are hardly differences between Voigt-Reuss model and experimental values. However, in systems of MWCNT-PANI/PDVB and C60-PANI/PDVB, great divergence exists between the theoretical model and the experimental data

"How far can we push the design of multifunctional polymer composites? " This was the question we consider from now on. It highlighted the quest for hybrid strategies

toward multifunctional materials. I believe that by transplanting new features learnt from conducting polymer systems into the design of carbon/conduct polymer hybrid system. Significant progress has already been, and will continuously be made in the creation and manipulation of complex multifunctional polymer composites.

Attachment: DPD Simulation

Computer simulation method is based on reasonable molecular structure model and physical principles to calculate the change in the process. That is, the use of molecular mechanics, molecular dynamics and quantum mechanics theory and other theoretical mechanisms directly calculated or by means of experimental data to determine the molecular conformation or related molecules and molecules, molecules and systems, molecular and atomic interaction or dynamic behavior and through computer graphics. The visualization model shows this spatial model or interaction. It is distinct from the experimental and theoretical method of the third scientific research. The classical molecular dynamics (MD) is a study of the atomic details of the system from the microscopic scale. It is necessary to obtain a positive solution by the classical Newton's motion equation of each particle in the system, which is limited by the current computer computing ability, which leads to not only the time scale and limits the possibility of research on a spatial scale. It is not possible to use the MD method to simulate a slightly more complex point of the system, which makes it necessary to introduce the dynamic simulation method on the scale. In the microscopic simulation method, the system is subjected to a certain degree of coarse granulation, ignoring the information on the atomic scale, which can be used to reflect the physical properties of the reaction system on larger time scales and larger spatial scales. In 1992, Hoogerbrugge and Koelman proposed a new mesoscopic simulation technique, which is called dissipation particle dynamics (DPD), based on molecular dynamics (Mn) and lattice gas automata; a spring model was used to study the hydrodynamic behavior. In 1995, Espan1 and warren introduced the fluctuation-dissipation theorem into the DPD method, introducing a new dissipation particle dynamics formula. In their model, the interaction between all the particles is divided into three parts: the conservative force, the dissipation force, and the random force. The dissipation force and the random force must satisfy the certain relation so that the system satisfies the regular rule of the regular ensemble. These two forces together, play the role of a hot bath. Compared with the atomistic simulation method,

DPD simulation can study the larger spatial scale and time range, so that at present, DPD has been successfully applied to block copolymer, surfactant, colloid and other systems.

In the DPD method, beads or particles represent the real system of atomic clusters. Each particle is evolved under the action of Newton's motion under three pairs of forces, as showed in the formula. 1 and formula. 2.

$$\frac{dr_i}{dt} = v_i \tag{1}$$

$$m_i \frac{dv_i}{dt} = \sum_{i \neq j} (F_{ij}^C + F_{ij}^D + F_{ij}^R) \tag{2}$$

where m_i is the particle mass, r_i and v_i are the particle position vector and the velocity vector.

$$F_{ij}^C = a_{ij}\omega(r_{ij})\widehat{r_{ij}} \tag{3}$$

$$F_{ij}^D = -\gamma\omega^2(r_{ij})(\widehat{r_{ij}} \cdot \overrightarrow{v_{ij}})\widehat{r_{ij}} \tag{4}$$

$$F_{ij}^R = \sigma\omega(r_{ij})\theta_{ij}\widehat{r_{ij}} \tag{5}$$

$$\omega(r) = \begin{cases} 1 - r/r_c & r_{ij} < r_c \\ 0 & r_{ij} \geq r_c \end{cases} \tag{6}$$

In the three pairs of forces: (1) the conservative force F_{ij}^C (Formula.3), a_{ij} represents the exclusion between the particles i and j, we can use it to distinguish the type of particles; (2) Dissipation force F_{ij}^D(Formula.4), representing the consumption of mesoscale scale energy: (3) The random force F_{ij}^R(Formula.5), represents the energy flow from the microscopic, $\sigma$is the intensity of the random force, andθ_{ij} is the stochastic variable satisfying the Gaussian statistics:

$$\langle\theta_{ij}(t)\rangle = 0 \tag{7}$$

$$\langle\theta_{ij}(t)\rangle\langle\theta_{kl}(t')\rangle = (\delta_{ij}\delta_{kl} + \delta_{il}\delta_{jk})\delta(t - t') \tag{8}$$

Weight function $\omega(r)$ shows that the interaction between the system particles is a soft interaction and can overlap each other, where r_c is the truncated radius. Through the relationship $\sigma^2 = 2\gamma k_B T$, dissipative force F_{ij}^D and random force

F_{ij}^{R}together to play a hot bath thermostat effect, where k_B is the Boltzmann constant. For simplicity, all physical quantities in the DPD simulation are dimensionless, r_c is the length unit, and the particle mass m for the mass unit, the $k_B T$ is the energy unit. At the same time, using the energy equalization theorem to normalize the temperature of all particles, time unit is,

$$\sqrt{mr^2/k_B T} \tag{9}$$

In the mesoscopic simulation, researchers focused on several different integration algorithm to explore.Verlocity-Verlet algorithm are a relatively simple and effective one, which is based on the classic Verletalgorithm, does not introduce any adjustment parameters.

Chenet al. studied the phase behavior and microstructure formation of cetyltrimethylammonium bromide (CTAB) /octane/butanol/water mixed system, and obtained the phase diagram consistent with the experimental results [191]. The unique properties of nanomaterial carbon nanotubes composites make them aware of the focus of the material industry. Liba et al. proposed a dissipative particle dynamics model. The dissipative particle dynamics can be used to characterize and optimize the experimental conditions, and also to study the thermodynamic equilibrium properties of the system and the dynamics of the non-equilibrium process. In recent years, its application in the polymer system has developed rapidly, also shows a certain application potential in the nano-scale fluid movement at the same time. The morphology and kinetics of the polymer system are in the mesoscopic scale, using a simple bead-spring model, the polymer segments can be represented by DPD particles, in addition to the actual polymer rheology and other properties of the study [192]. Block copolymers and their mesoscopic phase separation, biofilm morphology and transformation and polymer brush are the front of the current research [193]. Dissipative particle dynamics are the first to be applied to the study of small molecule hydrodynamics [194]. The current work is mainly on the study of the flow characteristics of complex systems such as amphoteric molecules in an external force field or special boundary condition. Chen for simulating monolayer carbon nanotubes

and discussed the applicability of this model at the level of suitability for simulating carbon nanotube mechanical devices [195]; Wang et al. reported the volume fraction, degree of functionalization and length of polyethylene segments on the phase separation and properties of polyethylene / carbon nanotube systems; his group studied the self-organization behavior of polymer chain-linked nanorods [196]. The morphology and transformation of the polymer nanotubes can be controlled by the topological structure, segment structure and solvent selectivity [196]. Angelikopoulos studied the adsorption of surfactants on a pair of cross-carbon nanotubes and found that at the appropriate concentration and nanotube spacing, the surfactant will form a central aggregation at the intersection of carbon nanotubes and stabilize the whole structure [197].

List of Publications

Original Papers:

1. **X. Cheng**, T. Yokozeki, L. Wu, H. Wang, J. Koyanagi, H. Wang Q. Sun. The enhancement effect of carbon-based nano-fillers/polyaniline hybrids on the through-thickness electric conductivity of carbon fiber reinforced polymer.Composites Part A, (submitted)
2. **X. Cheng,** T. Yokozeki, M. Yamamoto, H. Wang, L. Wu, J. Koyanagi, Q. Sun, The decoupling electrical and thermal conductivity of fullerene/polyaniline hybrids reinforced polymer composites, Composites Science and Technology 144 (2017) 160-168.
3. **X. Cheng,** T. Yokozeki, L. Wu, H. Wang, J. Zhang, J. Koyanagi, Z. Weng,Q. Sun, Electrical conductivity and interlaminar shear strength enhancement ofcarbon fiber reinforced polymers through synergetic effect between graphene oxide and polyaniline, Composites Part A: Applied Science and Manufacturing 90 (2016) 243-249
4. **X. Cheng,** V. Kumar, T. Yokozeki, T. Goto, T. Takahashi, J. Koyanagi, L. Wu, R. Wang, Highly conductive graphene oxide/polyaniline hybrid polymer Nanocomposites with simultaneously improved mechanical properties, Compos. Pt. A-Appl. Sci. Manuf. 82 (2016) 100-107

Other Publicaions:

5. Rui Wang, DongxianZhuo, ZixiangWeng, Lixin Wu,* **X. Cheng,**, Yu Zhou, Jianlei Wang and Bowen Xuan. A novel nanosilica/graphene oxide hybrid and its flame retarding epoxy resin with simultaneously improved mechanical, thermal conductivity, and dielectric properties Journal of Materials Chemistry A. (2015)
6. lin ma; lixin Wu* **X. Cheng,**; dongxianzhuo; zixiangweng; ruiwang Improving the interlaminar properties of the laminate composites using a situ accumulation method to construct the multi-Scale reinforcement of carbon nanofibers/carbon fibers .. Composites Part A, (2014)
7. **X. Cheng,**, Zhang Datong, Liu Dongyuan,The Specific Lighting Protection for the 1.5MW Wind Turbine Blade. Patent Number: 200920171142.9, (2009).
8. Zhang Jun, He Ming, **X. Cheng,**, Patent Number: 2008201399767, (2008).The Pumping Aided Device of Composite Resin Infusion Process.
9. **X. Cheng,**,Chenchun, Zhang Zuoguang*, Li Min. Investigation of epoxy resin film formula for moderate-temperature hot-melt prepreg. Fiber Reinforced Plastics/Composite, (2007).

Acknowledgements

The main research presented in this thesis was carried out under the supervision of Professor Tomohiro Yokozeki in the Department of Aeronautics and Astronautics, School of Engineering of the University of Tokyo between Oct. 2011 and Mar. 2012, Apr. 2015 and Oct. 2017. First and foremost, I would like to express my gratitude to my supervisor, Professor Tomohiro Yokozeki, for his constructive guidance, precise suggestions, and constant encouragement throughout this thesis work. As a foreign student, I have continuously received unparalleled support from Professor Tomohiro Yokozeki both academically and personally. Without him, my experience in Japan would have been nonexistent from the very beginning.

Big thanks should be given to Prof. J.Koyanagi and Dr. Michihiro Yamamoto from the Department of Materials Science and Technology, Tokyo University of Sciencefor their collaboration work described in chapter 4. I also would like to convey deepgratefulness toDr. Vipin Kumar Singh for his firsthand investigations on the conduct polymer in chapter 2. I also sincerely thank Prof. Takahira Aoki for his professional discussions on the mechanic properties.

Research results described in chemistry part were under the supervision of Professor Prof Lixin Wu and Prof Qingfu Sun in Fujian Insititute of Research on the Structure of Matter, Chinese Academy of Sciences. Here, I sincerely enjoy the continuous encouragement and support from them. Dr. Zixiangwong and Dr. Rui Wang at Fujian Insititute of Research on the Structure of Matter, Chinese Academy of Sciences for their professional discussions on the material characterization.

Special thanks to the secretaries of the Aoki-Yokozeki group, I would like to further thank Ms Yayoi Kobayashi for her nice arrangement and support in the laboratory. She has also helped me so much in my daily life. Although I caused a number of troubles, she has always been patient and helpful to me.

Finally, I dedicate this thesis to my family and friends. I like them more than I can express in words. Their support has been precious encouragement for me.

Xiuyan Cheng

July, 2017

Reference

[1] Soutis C. Fibre Reinforced Composites In Aircraft Construction. Progress In Aerospace Sciences. 2005;41(2):143-51.

[2] Meier U. Composite Materials In Bridge Repair. Applied Composite Materials. 2000;7(2-3):75-94.

[3] Garden HN, Hollaway LC. An Experimental Study Of The Influence Of Plate End Anchorage Of Carbon Fibre Composite Plates Used To Strengthen Reinforced Concrete Beams. Composite Structures. 1998;42(2):175-88.

[4] Hirano Y, Yamane T, Todoroki A. Through-Thickness Electric Conductivity Of Toughened Carbon-Fibre-Reinforced Polymer Laminates With Resin-Rich Layers. Composites Science And Technology. 2016;122:67-72.

[5] Yu H, Heider D, Advani S. A 3D Microstructure Based Resistor Network Model For The Electrical Resistivity Of Unidirectional Carbon Composites. Composite Structures. 2015;134:740-9.

[6] Yokozeki T, Goto T, Takahashi T, Qian D, Itou S, Hirano Y, Et Al. Development And Characterization Of CFRP Using A Polyaniline-Based Conductive Thermoset Matrix. Composites Science And Technology. 2015;117:277-81.

[7] Park J-M, Kwon D-J, Wang Z-J, Roh J-U, Lee W-I, Park J-K, Et Al. Effects Of Carbon Nanotubes And Carbon Fiber Reinforcements On Thermal Conductivity And Ablation Properties Of Carbon/Phenolic Composites. Composites Part B-Engineering. 2014;67:22-9.

[8] Salinier A, DagrÉOu S, LÉOnardi F, Derail C, NavascuÉS N. Electrical, Rheological And Mechanical Characterization Of Multiscale Composite Materials Based On Poly(Etherimide)/Short Glass Fibers/Multiwalled Carbon Nanotubes. Composite Structures. 2013;102:81-9.

[9] Wilder JWG, Venema LC, Rinzler AG, Smalley RE, Dekker C. Electronic Structure Of Atomically Resolved Carbon Nanotubes. Nature. 1998;391(6662):59-62.

[10] De Vivo B, Lamberti P, Spinelli G, Tucci V, Guadagno L, Raimondo M, Et Al. Improvement Of The Electrical Conductivity in Multiphase Epoxy-Based MWCNT Nanocomposites By Means Of An Optimized Clay Content. Composites Science And Technology. 2013;89:69-76.

[11] Li W, He D, Dang Z, Bai J. In Situ Damage Sensing In The Glass Fabric Reinforced Epoxy Composites Containing CNT-Al2O3 Hybrids. Composites Science And Technology. 2014;99:8-14.

[12] Du X, Xu F, Liu H-Y, Miao Y, Guo W-G, Mai Y-W. Improving The Electrical Conductivity And Interface Properties Of Carbon Fiber/Epoxy Composites By Low Temperature Flame Growth Of Carbon Nanotubes. RSC Advances. 2016;6(54):48896-904.

[13] Lin Y, Gigliotti M, Lafarie-Frenot MC, Bai J, Marchand D, Mellier D. Experimental Study To Assess The Effect Of Carbon Nanotube Addition On The Through-Thickness Electrical Conductivity Of CFRP Laminates For Aircraft Applications. Composites Part B: Engineering. 2015;76:31-7.

[14] Moniruzzaman M, Winey KI. Polymer Nanocomposites Containing Carbon Nanotubes. Macromolecules. 2006;39(16):5194-205.

[15] Liu L, Grunlan JC. Clay Assisted Dispersion Of Carbon Nanotubes In Conductive Epoxy Nanocomposites. Advanced Functional Materials. 2007;17(14):2343-8.

[16] Sandler J, Shaffer MSP, Prasse T, Bauhofer W, Schulte K, Windle AH. Development Of A Dispersion Process for Carbon Nanotubes In an Epoxy Matrix and The Resulting Electrical Properties. Polymer. 1999;40(21):5967-71.

[17] Gojny FH, Wichmann MHG, Fiedler B, Kinloch IA, Bauhofer W, Windle AH, Et Al. Evaluation and Identification Of Electrical and Thermal Conduction Mechanisms In Carbon Nanotube/Epoxy Composites. Polymer. 2006;47(6):2036-45.

[18] Arjmand M, Mahmoodi M, Gelves GA, Park S, Sundararaj U. Electrical And Electromagnetic Interference Shielding Properties Of Flow-Induced Oriented Carbon Nanotubes In Polycarbonate. Carbon. 2011;49(11):3430-40.

[19] Gou J, Tang Y, Liang F, Zhao Z, Firsich D, Fielding J. Carbon Nanofiber Paper

For Lightning Strike Protection Of Composite Materials. Composites Part B-Engineering. 2010;41(2):192-8.

[20] NovÁK I, Krupa I. Electro-Conductive Resins Filled With Graphite For Casting Applications. European Polymer Journal. 2004;40(7):1417-22.

[21] Yousefi N, Sun XY, Lin XY, Shen X, Jia JJ, Zhang B, Et Al. Highly Aligned Graphene/Polymer Nanocomposites With Excellent Dielectric Properties For High-Performance Electromagnetic Interference Shielding. Adv Mater. 2014;26(31):5480-7.

[22] Kim H, Miura Y, Macosko CW. Graphene/Polyurethane Nanocomposites For Improved Gas Barrier And Electrical Conductivity. Chemistry Of Materials. 2010;22(11):3441-50.

[23] Luan VH, Tien HN, Cuong TV, Kong B-S, Chung JS, Kim EJ, Et Al. Novel Conductive Epoxy Composites Composed Of 2-D Chemically Reduced Graphene And 1-D Silver Nanowire Hybrid Fillers. J Mater Chem. 2012;22(17):8649-53.

[24] Chandrasekaran S, Seidel C, Schulte K. Preparation And Characterization Of Graphite Nano-Platelet (GNP)/Epoxy Nano-Composite: Mechanical, Electrical And Thermal Properties. European Polymer Journal. 2013;49(12):3878-88.

[25] Kumar D, Sharma RC. Advances In Conductive Polymers. European Polymer Journal. 1998;34(8):1053-60.

[26] Shirakawa H, Louis EJ, Macdiarmid AG, Chiang CK, Heeger AJ. Synthesis Of Electrically Conducting Organic Polymers - Halogen Derivatives Of Polyacetylene, (Ch)X. Journal Of The Chemical Society-Chemical Communications. 1977(16):578-80.

[27] Miller JS. The 2000 Nobel Prize In Chemistry - A Personal Accolade. Chemphyschem. 2000;1(4):229-30.

[28] Pang H, Xu L, Yan D-X, Li Z-M. Conductive Polymer Composites With Segregated Structures. Progress In Polymer Science. 2014;39(11):1908-33.

[29] Flandin L, Brechet Y, Cavaille JY. Electrically Conductive Polymer Nanocomposites As Deformation Sensors. Composites Science And Technology. 2001;61(6):895-901.

[30] Das NC, Chaki TK, Khastgir D. Effect Of Processing Parameters, Applied Pressure And Temperature On The Electrical Resistivity Of Rubber-Based Conductive Composites. Carbon. 2002;40(6):807-16.

[31] Hara T, Horii E, An KN, Cooney WP, Linscheid RL, Chao EYS. Force Distribution Across Wrist Joint - Application Of Pressure-Sensitive Conductive Rubber. Journal Of Hand Surgery-American Volume. 1992;17A(2):339-47.

[32] Shimojo M, Namiki A, Ishikawa M, Makino R, Mabuchi K. A Tactile Sensor Sheet Using Pressure Conductive Rubber With Electrical-Wires Stitched Method. Ieee Sensors Journal. 2004;4(5):589-96.

[33] Depaoli MA, Waltman RJ, Diaz AF, Bargon J. AN Electrically Conductive Plastic Composite Derived From Polypyrrole And Polyvinyl-Chloride. Journal Of Polymer Science Part A-Polymer Chemistry. 1985;23(6):1687-98.

[34] Macfarlane DR, Meakin P, Sun J, Amini N, Forsyth M. PyrrolidiniumImides: A New Family Of Molten Salts And Conductive Plastic Crystal Phases. Journal Of Physical Chemistry B. 1999;103(20):4164-70.

[35] Bowman D, Mattes BR. Conductive Fibre Prepared From Ultra-High Molecular Weight Polyaniline For Smart Fabric And Interactive Textile Applications. Synth Met. 2005;154(1-3):29-32.

[36] Ma R, Lee J, Choi D, Moon H, Baik S. Knitted Fabrics Made From Highly Conductive Stretchable Fibers. Nano Letters. 2014;14(4):1944-51.

[37] Tchmutin IA, Ponomarenko AT, Krinichnaya EP, Kozub GI, Efimov ON. Electrical Properties Of Composites Based On Conjugated Polymers And Conductive Fillers. Carbon. 2003;41(7):1391-5.

[38] Yang C, Wong CP, Yuen MMF. Printed Electrically Conductive Composites: Conductive Filler Designs And Surface Engineering. Journal Of Materials Chemistry C. 2013;1(26):4052-69.

[39] Tanaka K, Okada M, Koike T, Yamabe T. Theoretical-Studies On The Structural-Changes Of Conjugated Conductive Polymers In The Heavily-Doped Regime. Synth Met. 1989;31(2):181-90.

[40] Szuwarzynski M, Wolski K, Zapotoczny S. Enhanced Stability Of Conductive

Polyacetylene In Ladder-Like Surface-Grafted Brushes. Polymer Chemistry. 2016;7(36):5664-70.

[41] Ghasemi-Mobarakeh L, Prabhakaran MP, Morshed M, Nasr-Esfahani MH, Baharvand H, Kiani S, Et Al. Application Of Conductive Polymers, Scaffolds And Electrical Stimulation For Nerve Tissue Engineering. Journal Of Tissue Engineering And Regenerative Medicine. 2011;5(4):E17-E35.

[42] Balint R, Cassidy NJ, Cartmell SH. Conductive Polymers: Towards A Smart Biomaterial For Tissue Engineering. Acta Biomaterialia. 2014;10(6):2341-53.

[43] Jagur-Grodzinski J. Electronically Conductive Polymers. Polymers For Advanced Technologies. 2002;13(9):615-25.

[44] Lee SE, Jeong Y, Lee T, Han MJ, Han IT. Electrically Conductive Composite For Electronic Device Comprises Polymer Matrix Comprising Cellulose, And Electrically Conductive Carbon Nanoparticles Dispersed In Matrix, In Which Nanoparticles Have Multiple Hydrogen Bonding Moiety. Samsung Electronics Co Ltd; Korea Res Inst Chem Technology; Univ Ind &Academic Coop In Chungnam Nat.

[45] Kim GB, Lee HS, Kim BW, Chu IC, Song KH, Kwak JW. Method For Manufacturing Electro-Conductive Plastic Of E.G. Electronic Device, Involves Reforming Mesoporous Polymer Bead, And Processing Surface Of Filler Before Coating With Chemical Combination Inducing Process. Hyundai Motor Co Ltd.

[46] Bocchini S, Accardo D, Ariano P, Lombardi M, Biso M, Ansaldo A, Et Al. Actuators Based On Intrinsic Conductive Polymers/Carbon Nanoparticles Nanocomposites. In: Barcohen Y, Editor. Electroactive Polymer Actuators And Devices2013.

[47] Kito A, Nomura R, Kaneno K, Kobayashi S, Uodome K. Coating Composition For E.G. Transparent Conductive Film, Comprises Binder, Solvent Containing Alcohol, Water And High-Boiling Point Solvent, And Intrinsic Conductive Polymer Containing Polythiophene Compound And Polystyrene Sulfonate. Hitachi Maxell Kk.

[48] Labee R, Mercx F, Van Der Mee M, Karlik D, Guo M, Zou D, Et Al. Composition Useful For Forming Article Such As Molded Article Comprises Thermoplastic Polymer, Thermally Insulative Filler, And Thermally Conductive Filler

With Specific Intrinsic Thermal Conductivity. Labee R; Mercx F; Van Der Mee M; Karlik D; Guo M; Zou D; Sabic Innovative Plastics Ip Bv.

[49] Huang W, Wu X, Xu X. Intrinsic Conductive Shape Memory Polymer Has Polymer Structure Containing Epoxy Polymer Component Containing Epoxy Resin, Curing Agent And/Or Accelerant, And Conductive Polyaniline Ingredient Containing Aniline Monomer And Oxidant. Univ Jiangsu.

[50] Cheng W, Ren C, Xu X, Yan T, Zhang W. PTFE Product Comprises PTFE Powder And Antistatic Agent Comprising Intrinsic Conductive Polymer Material Or Carbon Black, Graphite, And Conductive Metal Powder. Beili Chem Zhangjiagang Co Ltd.

[51] Grote JG, Zetts JS, Nelson RL, Hopkins FK, Huddleston JB, Yaney PP, Et Al. Advancements In Conductive Cladding Materials For Nonlinear Optic Polymer Based Optoelectronic Devices. In: Iftekharuddin KM, Awwal AAS, Editors. Photonic Devices And Algorithms For Computing Iii2001. P. 10-8.

[52] Yang L, Cheng T, Zeng W, Lai W, Huang W. Inkjet-Printed Conductive Polymer Films For Optoelectronic Devices. Progress In Chemistry. 2015;27(11):1615-27.

[53] Grote JG, Drummond JP. Nonlinear Optic Polymer Core - Conductive Polymer Clad Optoelectronic Device. In: Feldman MR, Grote JG, Hibbsbrenner MK, Editors. Optoeletronic Integrated Circuits And Packaging Iii1999. P. 86-95.

[54] Nambiar S, Yeow JTW. Conductive Polymer-Based Sensors For Biomedical Applications. Biosensors &Bioelectronics. 2011;26(5):1825-32.

[55] Cochrane C, Koncar V, Lewandowski M, Dufour C. Design And Development Of A Flexible Strain Sensor For Textile Structures Based On A Conductive Polymer Composite. Sensors. 2007;7(4):473-92.

[56] Toshima N. Conductive Polymers As A New Type Of Thermoelectric Material. Macromol Symp. 2002;186:81-6.

[57] Aoai T, Nishio R, Hayashi N, Nomura K. Photo Doping Process Of Conductive Polymer With PAG And Application For Organic Thermoelectric Materials. Journal Of Photopolymer Science And Technology. 2016;29(2):335-41.

[58] Wu J, Chung DDL. Combined Use Of Magnetic And Electrically Conductive

Fillers In A Polymer Matrix For Electromagnetic Interference Shielding. Journal Of Electronic Materials. 2008;37(8):1088-94.

[59] Fox RT, Wani V, Howard KE, Bogle A, Kempel L. Conductive Polymer Composite Materials And Their Utility In Electromagnetic Shielding Applications. Journal Of Applied Polymer Science. 2008;107(4):2558-66.

[60] Das NC, Khastgir D, Chaki TK, Chakraborty A. Electromagnetic Interference Shielding Effectiveness Of Hybrid Conductive Polymer Composite. Journal Of Elastomers And Plastics. 2002;34(3):199-223.

[61] Chen M, Zhang L, Duan S, Jing S, Jiang H, Luo M, Et Al. Highly Conductive And Flexible Polymer Composites With Improved Mechanical And Electromagnetic Interference Shielding Performances. Nanoscale. 2014;6(7):3796-803.

[62] Kim YS. Anisotropic Conductive Film Of Printed Circuit Board Has Multiple Conductive Cylinders Formed In A Direction From An Upper Surface To A Lower Surface Contain A Conductive Polymer. Samsung Electro-Mechanics Co.

[63] Liu H, Kuo K, Liu HT, Kuo KM. Conductive Type Microwave Absorbing Material By Adjusting Surface Resistance Of Conductive Polymer Film Having Conjugated Bonding Of Alternating Single Bond And Double Bond To Achieve Effect Of Attenuating Microwave Of Specific Frequency. Nat Chung-Shan Inst Sci &Technology.

[64] Liu J, Zhang M, Zhang P, Zhang J, Pan D. Preparing Ferrite-Conductive Polymer Wave-Absorbing Material, Involves Dispersing Ferrite, Conductive Monomer And Hydrochloric Acid, Adding Ammonium Persulfate, Drying To Form Ferrite-Polymer Material, And Irradiating Microwave. Univ Yangzhou.

[65] Han P, Zhang X, Qiao J, Cai C, Lai J, Song Z, Et Al. Conductive Polymer Fiber Used In Fabric For Manufacturing E.G. Antistatic Article And Electromagnetic Shielding Material, Comprises Conductive Layer Integrated On At Least Portion Of Surface, Preferably Integrated On Whole Surface Of Fiber. China Petroleum &Chem Corp; Beijing Res Inst Chem Ind China Petro; Sinopec Corp; Sinopec Beijing Res Inst Chem Ind.

[66] Cai X, Liu X. Anticorrosive Earth Electrode For Common Carbon Steel Earth

Network, Has Conductive Polymer Material Anticorrosive Layer Covered On Metal Conductor, Where Section Of Conductive Polymer Material Anticorrosive Layer Is Quincuncial Shape. Wuhan Ailao High Tech Co Ltd.

[67] Kim H. Ink Composition Employing Ink, Anticorrosive Material And Conductive Polymer, And Window Name Plate Employing The Composition. Geum Young Co Ltd.

[68] Ogata K, Takei K, Lee K, Lee B, Lee J, Lim M, Et Al. Active Material Used In Electrode For Secondary Battery, Comprises Secondary Particles Comprising Primary Particles Of Silicon-Containing Material, Electrically Conductive Material, And Chemically Cross-Linked Water-Insoluble Polymer. Samsung Electronics Co Ltd; Samsung Sdi Co Ltd.

[69] Nishio K, Fujimoto M, Yoshinaga N, Furukawa N, Ando O, Ono H, Et Al. Characteristics Of A Lithium Secondary Battery Using Chemically-Synthesized Conductive Polymers. Journal Of Power Sources. 1991;34(2):153-60.

[70] Yoshio M, Yoshitake H. Positive Electrode Used In Non-Aqueous Electrolyte Secondary Battery, Comprises Conductive Binder And Active Material Comprising Phosphate/Silicate-Based Lithium Complex Compound And Substance Which Is Non-Doped P-Type Semiconductor Polymer. Univ Yamaguchi.

[71] Gustafsson JC, Inganas O, Andersson AM. Conductive Polymers As Electrochromic Material In Solid-State Electrochromic Devices1992.

[72] Shim GH, Foulger SH. Coupling Of Crystalline Colloidal Arrays With Intrinsically Conductive Polymers: Reflection-Type Electrochromic Devices. Photonics And Nanostructures-Fundamentals And Applications. 2012;10(4):440-6.

[73] Saikia D, Pan Y-C, Wu C-G, Fang J, Tsai L-D, Kao H-M. Synthesis And Characterization Of A Highly Conductive Organic-Inorganic Hybrid Polymer Electrolyte Based On Amine Terminated Triblock Polyethers And Its Application In Electrochromic Devices. Journal Of Materials Chemistry C. 2014;2(2):331-43.

[74] Chua L, Ho PK, Png R, Ang MC, Choo K, Tang CG. Material Useful In Layer I.E. Electron-Injection Layer Or Electron-Extraction Layer, A Device And Organic Semiconductors, Comprises N-Doped Electrically Conductive Polymer Comprising

Electron-Deficient Aromatic Moiety, And Counter-Cation. Univ Singapore Nat.

[75] Hwang S, Adachi C, Hwang SB. Semiconductor Material Used In Element E.G. Thermoelectric Conversion Element, Contains Conductive Polymer And Dopant, And Can Be Converted Into Its Types Based On Dopant Concentration In Material. Univ Kyushu Nat Corp.

[76] Maxian O, Pedrazzoli D, Manas-Zloczower I. Conductive Polymer Foams With Carbon Nanofillers - Modeling Percolation Behavior. Express Polymer Letters. 2017;11(5):406-18.

[77] Trivedi AH, Garcia J, Burhan AB, Schruben DL. Extension Of Effective-Medium Theory To 3-Component System - 2 Conductive Particle Types In The Polymer Matrix. Polymer Engineering And Science. 1994;34(14):1115-20.

[78] Mutlay I, Tudoran LB. Percolation Behavior Of Electrically Conductive Graphene Nanoplatelets/Polymer Nanocomposites: Theory And Experiment. Fullerenes Nanotubes And Carbon Nanostructures. 2014;22(5):413-33.

[79] Aoki K. Simulated Fractal Formation In Electrochemical Switching Of Conducting Polymer Film Into An Insulating Form On The Basis Of The Propagation Theory Of The Conductive Zone. Journal Of Electroanalytical Chemistry. 1991;300(1-2):13-22.

[80] Xu HP, Wu YH, Yang DD, Wang JR, Xie HQ. Study On Theories And Influence Factors Of Ptc Property In Polymer-Based Conductive Composites. Reviews On Advanced Materials Science. 2011;27(2):173-83.

[81] Mollaamin F, Monajjemi M. Fractal Dimension On Carbon Nanotube-Polymer Composite Materials Using Percolation Theory. Journal Of Computational And Theoretical Nanoscience. 2012;9(4):597-601.

[82] Mikitaev AK, Kozlov GV. DescriptionOf The Degree Of Reinforcement Of Polymer/Carbon Nanotube Nanocomposites In The Framework Of Percolation Models. Physics Of The Solid State. 2015;57(5):974-7.

[83] Xia J, Pan Y, Shen L, Yi XS. A Model-Based Approach To Electrical Percolation Behavior Of CB-HDPE Composites. J Mater Sci. 2000;35(24):6145-50.

[84] Carmona F, Ravier J. To What Extent Is The Structure Of A Random Composite

Compatible With A Percolation Model? Physica B-Condensed Matter. 2003;338(1-4):247-51.

[85] Zumbusch A, Fleury L, Brown R, Bernard J, Orrit M. Probing Individual 2-Level Systems In A Polymer By Correlation Of Single Molecular Fluorescence. Physical Review Letters. 1993;70(23):3584-7.

[86] Medalia AI. Electrical-Conduction In Carbon-Black Composites. Rubber Chemistry And Technology. 1986;59(3):432-54.

[87] Wang J, Carson JK, North MF, Cleland DJ. A New Structural Model Of Effective Thermal Conductivity For Heterogeneous Materials With Co-Continuous Phases. International Journal Of Heat And Mass Transfer. 2008;51(9–10):2389-97.

[88] Kim J, Kang YT, Choi CK. Analysis Of Convective Instability And Heat Transfer Characteristics Of Nanofluids. Physics Of Fluids. 2004;16(7):2395-401.

[89] Takagi H, Kako S, Kusano K, Ousaka A. Thermal Conductivity Of PLA-Bamboo Fiber Composites. Advanced Composite Materials. 2007;16(4):377-84.

[90] Velmurugan V, Ramachandran R, Raina JP. Thermal Property Analysis Of Epoxy Based Silver Nanocomposites. Journal Of The Indian Chemical Society. 2015;92(5):822-4.

[91] Badran B, Gerner FM, Ramadas P, Henderson T, Baker KW. Experimental Results For Low-Temperature Silicon Micromachined Micro Heat Pipe Arrays Using Water And Methanol As Working Fluids. Experimental Heat Transfer. 1997;10(4):253-72.

[92] Agari Y, Ueda A, Nagai S. Electrical And Thermal-Conductivities Of Polyethylene Composites Filled With Biaxial Oriented Short-Cut Carbon-Fibers. Journal Of Applied Polymer Science. 1994;52(9):1223-31.

[93] Krushnamurty K, Rini M, Srikanth I, Ghosal P, Das AP, Deepa M, Et Al. Conducting Polymer Coated Graphene Oxide Reinforced C–Epoxy Composites For Enhanced Electrical Conduction. Composites Part A: Applied Science And Manufacturing. 2016;80:237-43.

[94] Cheng X, Kumar V, Yokozeki T, Goto T, Takahashi T, Koyanagi J, Et Al. Highly Conductive Graphene Oxide/Polyaniline Hybrid Polymer Nanocomposites With

Simultaneously Improved Mechanical Properties. Compos Pt A-Appl Sci Manuf. 2016;82:100-7.

[95] Hirano Y, Yokozeki T, Ishida Y, Goto T, Takahashi T, Qian D, Et Al. Lightning Damage Suppression In A Carbon Fiber-Reinforced Polymer With A Polyaniline-Based Conductive Thermoset Matrix. Composites Science And Technology. 2016;127:1-7.

[96] Gibson RF. A Review Of Recent Research On Mechanics Of Multifunctional Composite Materials And Structures. Composite Structures. 2010;92(12):2793-810.

[97] Mohanty AK, Misra M, Hinrichsen G. Biofibres, Biodegradable Polymers And Biocomposites: An Overview. Macromolecular Materials And Engineering. 2000;276-277(1):1-24.

[98] Najafi SK, Tajvidi M, Chaharmahli M. Long-Term Water Uptake Behavior Of Lignocellulosic-High Density Polyethylene Composites. Journal Of Applied Polymer Science. 2006;102(4):3907-11.

[99] Coulon C, Clerac R. Electron Spin Resonance: A Major Probe For Molecular Conductors. Chem Rev. 2004;104(11):5655-87.

[100] De Albuquerque JE, Mattoso LHC, Faria RM, Masters JG, Macdiarmid AG. StudyOf The Interconversion Of Polyaniline Oxidation States By Optical Absorption Spectroscopy. Synth Met. 2004;146(1):1-10.

[101] Del Castillo-Castro T, Castillo-Ortega MM, Villarreal I, Brown F, Grijalva H, Perez-Tello M, Et Al. Synthesis And Characterization Of Composites Of DBSA-Doped Polyaniline And Polystyrene-Based Ionomers. Compos Pt A-Appl Sci Manuf. 2007;38(2):639-45.

[102] Goto T, Awano H, Takahashi T, Yonetake K, Sukumaran SK. Effect Of Processing Temperature On Thermal Doping Of Polyaniline Without Shear. Polymers For Advanced Technologies. 2011;22(8):1286-91.

[103] Da Silva MJ, Sanches AO, Malmonge LF, Malmonge JA. Electrical, Mechanical, And Thermal Analysis Of Natural Rubber/Polyaniline-Dbsa Composite. Mater Res-Ibero-Am J Mater. 2014;17:59-63.

[104] Jia W, Tchoudakov R, Segal E, Joseph R, Narkis M, Siegmann A. Electrically

Conductive Composites Based On Epoxy Resin With Polyaniline-DBSA Fillers. Synth Met. 2003;132(3):269-78.

[105] Kumar V, Yokozeki T, Goto T, Takahashi T. Mechanical And Electrical Properties Of PANI-Based Conductive Thermosetting Composites. Journal Of Reinforced Plastics And Composites. 2015;34(16):1298-305.

[106] Tsotra P, Friedrich K. Thermal, Mechanical, And Electrical Properties Of Epoxy Resin/Polyaniline-Dodecylbenzenesulfonic Acid Blends. Synth Met. 2004;143(2):237-42.

[107] Jia QM, Li JB, Wang LF, Zhu JW, Zheng M. Electrically Conductive Epoxy Resin Composites Containing Polyaniline With Different Morphologies. Mater Sci Eng A-Struct Mater Prop Microstruct Process. 2007;448(1-2):356-60.

[108] Massoumi B, Farjadbeh F, Mohammadi R, Entezami AA. Synthesis Of Conductive Adhesives Based On Epoxy Resin/Nanopolyaniline And Chloroprene Rubber/Nanopolyaniline: Characterization Of Thermal, Mechanical And Electrical Properties. J Compos Mater. 2013;47(9):1185-95.

[109] Afzal AB, Akhtar MJ, Ahmad M. Morphological Studies Of DBSA-Doped Polyaniline/PVC Blends. J Electron Microsc. 2010;59(5):339-44.

[110] Wang H, Hao Q, Yang X, Lu L, Wang X. Effect Of Graphene Oxide On The Properties Of Its Composite With Polyaniline. ACS Appl Mater Interfaces. 2010;2(3):821-8.

[111] Zhang K, Zhang LL, Zhao XS, Wu J. Graphene/Polyaniline Nanofiber Composites As Supercapacitor Electrodes. Chemistry Of Materials. 2010;22(4):1392-401.

[112] Chen JK, Gui XC, Wang ZW, Li Z, Xiang R, Wang KL, Et Al. Superlow Thermal Conductivity 3D Carbon Nanotube Network For Thermoelectric Applications. ACS Appl Mater Interfaces. 2012;4(1):81-6.

[113] Yue L, Pircheraghi G, Monemian SA, Manas-Zloczower I. Epoxy Composites With Carbon Nanotubes And Graphene Nanoplatelets - Dispersion And Synergy Effects. Carbon. 2014;78:268-78.

[114] King JA, Barton RL, Hauser RA, Keith JM. Synergistic Effects Of Carbon

Fillers In Electrically And Thermally Conductive Liquid Crystal Polymer Based Resins. Polym Compos. 2008;29(4):421-8.

[115] SzabÓ T, Berkesi O, DÉKÁNy I. DRIFT Study Of Deuterium-Exchanged Graphite Oxide. Carbon. 2005;43(15):3186-9.

[116] Hussain S, Yorucu C, Ahmed I, Hussain R, Chen B, Bilal Khan M, Et Al. Surface Modification Of Aramid Fibres By Graphene Oxide Nano-Sheets For Multiscale Polymer Composites. Surface And Coatings Technology. 2014;258:458-66.

[117] Cheng X, Kumar V, Yokozeki T, Goto T, Takahashi T, Koyanagi J, Et Al. Highly Conductive Graphene Oxide/Polyaniline Hybrid Polymer Nanocomposites With Simultaneously Improved Mechanical Properties. Composites Part A: Applied Science And Manufacturing. 2016;82:100-7.

[118] Grossiord N, Regev O, Loos J, Meuldijk J, Koning CE. Time-Dependent Study Of The Exfoliation Process Of Carbon Nanotubes In Aqueous Dispersions By Using UV−Visible Spectroscopy. Analytical Chemistry. 2005;77(16):5135-9.

[119] Ghislandi M, Tkalya E, Schillinger S, Koning CE, De With G. High Performance Graphene- And Mwcnts-Based PS/PPO Composites Obtained Via Organic Solvent Dispersion. Composites Science And Technology. 2013;80:16-22.

[120] Rao PS, Anand J, Palaniappan S, Sathyanarayana DN. Effect Of Sulphuric Acid On The Properties Of Polyaniline–Hcl Salt And Its Base. European Polymer Journal. 2000;36(5):915-21.

[121] Silva MJ, Sanches AO, Malmonge LF, Medeiros ES, Rosa MF, Mcmahan CM, Et Al. Conductive Nanocomposites Based On Cellulose Nanofibrils Coated With Polyaniline-DBSA Via In Situ Polymerization. Macromol Symp. 2012;319(1):196-202.

[122] Han MG, Cho SK, Oh SG, Im SS. Preparation And Characterization Of Polyaniline Nanoparticles Synthesized FromDBSA Micellar Solution. Synth Met. 2002;126(1):53-60.

[123] Yao Q, Wang Q, Wang LM, Wang Y, Sun J, Zeng HR, Et Al. The Synergic Regulation Of Conductivity And Seebeck Coefficient In Pure Polyaniline By

Chemically Changing The Ordered Degree Of Molecular Chains. J Mater Chem A. 2014;2(8):2634-40.

[124] Li M, Huang XY, Wu C, Xu HP, Jiang PK, Tanaka T. Fabrication Of Two-Dimensional Hybrid Sheets By Decorating Insulating PANI On Reduced Graphene Oxide For Polymer Nanocomposites With Low Dielectric Loss And High Dielectric Constant. J Mater Chem. 2012;22(44):23477-84.

[125] Wu CS, Liao HT. Preparation And Characterization Of Functionalized Graphite/Poly(Butylene Terephthalate) Composites. Polym Bull. 2015;72(7):1799-816.

[126] Yuan NY, Ma FF, Fan Y, Liu YB, Ding JN. High Conductive Ethylene Vinyl Acetate Composites Filled With Reduced Graphene Oxide And Polyaniline. Compos Pt A-Appl Sci Manuf. 2012;43(12):2183-8.

[127] Jeevananda T, Palaniappan S, Siddaramaiah. Spectral And Thermal Studies On Polyaniline–Epoxy Novolac Resin Composite Materials. Journal Of Applied Polymer Science. 1999;74(14):3507-12.

[128] Yang XJ, Tong Z, Yu YZ, Yen W. Synthesis Of Conductive Polyaniline/Epoxy Resin Composites: Doping Of The Interpenetrating Network. Synth Met. 2004;142(1-3):57-61.

[129] Kumar V, Yokozeki T, Goto T, Takahashi T. Synthesis And Characterization Of PANI-DBSA/DVB Composite Using Roll-Milled PANI-DBSA Complex. Polymer. 2016;86:129-37.

[130] Dikin DA, Stankovich S, Zimney EJ, Piner RD, Dommett GHB, Evmenenko G, Et Al. Preparation And Characterization Of Graphene Oxide Paper. Nature. 2007;448(7152):457-60.

[131] Cheng X, Yokozeki T, Wu L, Wang H, Zhang J, Koyanagi J, Et Al. Electrical Conductivity And Interlaminar Shear Strength Enhancement Of Carbon Fiber Reinforced Polymers Through Synergetic Effect Between Graphene Oxide And Polyaniline. Composites Part A: Applied Science And Manufacturing. 2016;90:243-9.

[132] Zhang X, Fan X, Yan C, Li H, Zhu Y, Li X, Et Al. Interfacial Microstructure And Properties Of Carbon Fiber Composites Modified With Graphene Oxide. ACS

Appl Mater Interfaces. 2012;4(3):1543-52.

[133] Sadasivuni KK, Ponnamma D, Kumar B, Strankowski M, Cardinaels R, Moldenaers P, Et Al. Dielectric Properties Of Modified Graphene Oxide Filled Polyurethane Nanocomposites And Its Correlation With Rheology. Composites Science And Technology. 2014;104:18-25.

[134] Yang H, Gong J, Wen X, Xue J, Chen Q, Jiang Z, Et Al. Effect Of Carbon Black On Improving Thermal Stability, Flame Retardancy And Electrical Conductivity Of Polypropylene/Carbon Fiber Composites. Composites Science And Technology. 2015;113:31-7.

[135] Du F, Scogna RC, Zhou W, Brand S, Fischer JE, Winey KI. Nanotube Networks InPolymer Nanocomposites: Rheology And Electrical Conductivity. Macromolecules. 2004;37(24):9048-55.

[136] Huang WC, Wu YZ, Qiu L, Dong CK, Ding J, Li D. Tuning Rheological Performance Of Silica Concentrated Shear Thickening Fluid By Using Graphene Oxide. Adv Condens Matter Phys. 2015:5.

[137] Jimenez-Suarez A, Campo M, Sanchez M, Romon C, Urena A. InfluenceOf The Functionalization Of Carbon Nanotubes On Calendering Dispersion Effectiveness In A Low Viscosity Resin For VARIM Processes. Composites Part B-Engineering. 2012;43(8):3482-90.

[138] Shan FL, Gu YZ, Li M, Liu YN, Zhang ZG. Effect Of Deposited Carbon Nanotubes On Interlaminar Properties Of Carbon Fiber-Reinforced Epoxy Composites Using A Developed Spraying Processing. Polym Compos. 2013;34(1):41-50.

[139] Tibbetts GG, Lake ML, Strong KL, Rice BP. A Review Of The Fabrication And Properties Of Vapor-Grown Carbon Nanofiber/Polymer Composites. Composites Science And Technology. 2007;67(7-8):1709-18.

[140] Shioya M, Inoue H, Sugimoto Y. Reduction In Tensile Strength Of Polyacrylonitrile-Based Carbon Fibers In Liquids And Its Application To Defect Analysis. Carbon. 2013;65:63-70.

[141] Zhu S, Chung DDL. Analytical Model Of Piezoresistivity For Strain Sensing In

Carbon Fiber Polymer-Matrix Structural Composite Under Flexure. Carbon. 2007;45(8):1606-13.

[142] Abry JC, Choi YK, Chateauminois A,Dalloz B, Giraud G, Salvia M. In-Situ Monitoring Of Damage In CFRP Laminates By Means Of AC And DC Measurements. Composites Science And Technology. 2001;61(6):855-64.

[143] Wang S, Chung DDL. Self-Sensing Of Flexural Strain And Damage In Carbon Fiber Polymer-Matrix Composite By Electrical Resistance Measurement. Carbon. 2006;44(13):2739-51.

[144] Schueler R, Joshi SP, Schulte K. Damage Detection In CFRP By Electrical Conductivity Mapping. Composites Science And Technology. 2001;61(6):921-30.

[145] Hatui G, Bhattacharya P, Sahoo S, Dhibar S, Das CK. CombinedEffect Of Expanded Graphite And Multiwall Carbon Nanotubes On The Thermo Mechanical, Morphological As Well As Electrical Conductivity Of In Situ Bulk Polymerized Polystyrene Composites. Compos Pt A-Appl Sci Manuf. 2014;56:181-91.

[146] Hummers WS, Offeman RE. Preparation Of Graphitic Oxide. J Am Chem Soc. 1958;80(6):1339-.

[147] Shindo H KW, Koyanagi J, Moon SK, Ogasawara T, Sugimoto S. . Synthesis Of Graphene Composite Material And Their Mechanical Properties. Proceedings Of 6th Japanese Conference On Composite Materials 2015, 3D-13. 2015.

[148] Bubnova O, Khan ZU, Wang H, Braun S, Evans DR, Fabretto M, Et Al. Semi-Metallic Polymers. Nat Mater. 2014;13(2):190-4.

[149] Long D, Lequeux F. Heterogeneous Dynamics At The Glass Transition In Van Der Waals Liquids, In The Bulk And In Thin Films. Eur Phys J E. 2001;4(3):371-87.

[150] Lee JK, An KW, Ju JB, Cho BW, Cho WI, Park D, Et Al. Electrochemical Properties Of PAN-Based Carbon Fibers As Anodes For Rechargeable Lithium Ion Batteries. Carbon. 2001;39(9):1299-305.

[151] Chen W-C, Wen T-C, Hu C-C, Gopalan A. Identification Of Inductive Behavior For Polyaniline Via Electrochemical Impedance Spectroscopy. Electrochimica Acta. 2002;47(8):1305-15.

[152] Miyasaka K, Watanabe K, Jojima E, Aida H, Sumita M, Ishikawa k.

electrical-conductivity of carbon polymer composites as a function of carbon content. J Mater Sci. 1982;17(6):1610-6.

[153] Goldhaber-Gordon D, Montemerlo MS, Love JC, Opiteck GJ, Ellenbogen JC. Overview Of Nanoelectronic Devices. Proceedings Of The Ieee. 1997;85(4):521-40.

[154] Lehman JH, Terrones M, Mansfield E, Hurst KE, Meunier V. Evaluating The Characteristics Of Multiwall Carbon Nanotubes. Carbon. 2011;49(8):2581-602.

[155] SzabÓ T, TombÁCz E, IllÉS E, DÉKÁNy I. Enhanced Acidity And Ph-Dependent Surface Charge Characterization Of Successively Oxidized Graphite Oxides. Carbon. 2006;44(3):537-45.

[156] Abad B, Alda I, Diaz-Chao P, Kawakami H, Almarza A,Amantia D, Et Al. Improved Power Factor Of Polyaniline Nanocomposites With Exfoliated Graphene Nanoplatelets (Gnps). J Mater Chem A. 2013;1(35):10450-7.

[157] Al-Saleh MH, Sundararaj U. A Review Of Vapor Grown Carbon Nanofiber/Polymer Conductive Composites. Carbon. 2009;47(1):2-22.

[158] VilčÁKovÁ J, Moučka R, Svoboda P, IlčÍKovÁ M, Kazantseva N, HřibovÁ M, Et Al. Effect Of Surfactants And Manufacturing Methods On The Electrical And Thermal Conductivity Of Carbon Nanotube/Silicone Composites. Molecules. 2012;17(11):13157.

[159] Oliver WC, Pharr GM. An ImprovedTechnique For Determining Hardness And Elastic-Modulus Using Load And Displacement Sensing Indentation Experiments. J Mater Res. 1992;7(6):1564-83.

[160] Oliver WC, Pharr GM. An ImprovedTechnique For Determining Hardness And Elastic Modulus Using Load And Displacement Sensing Indentation Experiments. J Mater Res. 2011;7(6):1564-83.

[161] Young TJ, Crocker LE, Broughton WR, Ogin SL, Smith PA. Observations On Interphase Characterisation In Polymer Composites By Nano-Scale Indentation Using AFM And FEA. Composites Part A: Applied Science And Manufacturing. 2013;50:39-43.

[162] Biswas K, He J, Blum ID, Wu C-I, Hogan TP, Seidman DN, Et Al. High-Performance Bulk Thermoelectrics With All-Scale Hierarchical Architectures.

Nature. 2012;489(7416):414-8.

[163] Bell LE. Cooling, Heating, Generating Power, AndRecovering Waste Heat With Thermoelectric Systems. Science. 2008;321(5895):1457-61.

[164] Snyder GJ, Toberer ES. Complex Thermoelectric Materials. Nature Materials. 2008;7(2):105-14.

[165] Dresselhaus MS, Chen G, Tang MY, Yang R, Lee H, Wang D, Et Al. New Directions For Low-Dimensional Thermoelectric Materials. Adv Mater. 2007;19(8):1043-53.

[166] Smith MK, Singh V, Kalaitzidou K, Cola BA. High Thermal And Electrical Conductivity Of Template Fabricated P3HT/MWCNT Composite Nanofibers. ACS Appl Mater Interfaces. 2016;8(23):14788-94.

[167] Itoh T, Ishikawa K, Okada A. Effect Of Fullerene Addition On Thermoelectric Properties Of N-Type Skutterudite Compound. J Mater Res. 2007;22(1):249-53.

[168] Shi X, Chen LD, Bai SQ, Huang XY, Zhao XY, Yao Q, Et Al. Influence Of Fullerene Dispersion On High Temperature Thermoelectric Properties Of Bayco4sb12-Based Composites. Journal Of Applied Physics. 2007;102(10):103709.

[169] Wang Z, Vemishetti A, Ejembi JI, Wei G, Zhang B, Wang L, Et Al. High Thermoelectric Performance Of Fullerene Doped Bi0.5Sb1.5Te3 Alloys. Materials Science And Engineering: B. 2016;205:36-9.

[170] Sumino M, Harada K, Ikeda M, Tanaka S, Miyazaki K, Adachi C. Thermoelectric Properties Of N-Type C60 Thin Films And Their Application In Organic Thermovoltaic Devices. Applied Physics Letters. 2011;99(9):093308.

[171] Salvatierra RV, Cava CE, Roman LS, Zarbin AJG. ITO-Free And Flexible Organic Photovoltaic Device Based On High Transparent And Conductive Polyaniline/Carbon Nanotube Thin Films. Advanced Functional Materials. 2013;23(12):1490-9.

[172] Niu ZW, Yang ZH, Hu ZB, Lu YF, Han CC. Polyaniline-Silica Composite Conductive Capsules And Hollow Spheres. Advanced Functional Materials. 2003;13(12):949-54.

[173] Zhu Y, Zhang JC, Zheng YM, Huang ZB, Feng L, Jiang L. Stable,

Superhydrophobic, And Conductive Polyaniline/Polystyrene Films For Corrosive Enviromnents. Advanced Functional Materials. 2006;16(4):568-74.

[174] Zhang K, Zhang Y, Wang S. Effectively Decoupling Electrical And Thermal Conductivity Of Polymer Composites. Carbon. 2013;65:105-11.

[175] Kim D, Kim Y, Choi K, Grunlan JC, Yu C. Improved Thermoelectric Behavior Of Nanotube-Filled Polymer Composites With Poly(3,4-Ethylenedioxythiophene) Poly(Styrenesulfonate). Acs Nano. 2010;4(1):513-23.

[176] Cheng X, Yokozeki T, Yamamoto M, Wang H, Wu L, Koyanagi J, Et Al. The Decoupling Electrical And Thermal Conductivity Of Fullerene/Polyaniline Hybrids Reinforced Polymer Composites. Composites Science And Technology.

[177] Mayo SL, Olafson BD, Goddard WA. Dreiding - A Generic Force-Field For Molecular Simulations. Journal Of Physical Chemistry. 1990;94(26):8897-909.

[178] Sapurina IY, Gribanov AV, Mokeev MV, Zgonnik VN, TrchovÁ M, Stejskal J. Polyaniline Composites With Fullerene C60. Physics Of The Solid State. 2002;44(3):574-5.

[179] Hodlur RM, Rabinal MK. Self Assembled Graphene Layers On Polyurethane Foam As A Highly Pressure Sensitive Conducting Composite. Composites Science And Technology. 2014;90:160-5.

[180] Smart SK, Cassady AI, Lu GQ, Martin DJ. The Biocompatibility Of Carbon Nanotubes. Carbon. 2006;44(6):1034-47.

[181] Bom D, Andrews R, Jacques D, Anthony J, Chen BL, Meier MS, Et Al. Thermogravimetric Analysis Of The Oxidation Of Multiwalled Carbon Nanotubes: Evidence For The Role Of Defect Sites In Carbon Nanotube Chemistry. Nano Letters. 2002;2(6):615-9.

[182] Olson JR, Topp KA, Pohl RO. Specific-Heat And Thermal-Conductivity Of Solid Fullerenes. Science. 1993;259(5098):1145-8.

[183] Song P, Shen Y, Du B, Guo Z, Fang Z. Fabrication Of Fullerene-Decorated Carbon Nanotubes And Their Application In Flame-Retarding Polypropylene. Nanoscale. 2009;1(1):118-21.

[184] Ovejero G, PÉRez P, Romero MD, GuzmÁN I, Dı´Ez E. Solubility And Flory

Huggins Parameters Of SBES, Poly(Styrene-B-Butene/Ethylene-B-Styrene) Triblock Copolymer, Determined By Intrinsic Viscosity. European Polymer Journal. 2007;43(4):1444-9.

[185] Sohi NJS, Bhadra S, Khastgir D. The Effect Of Different Carbon Fillers On The Electrical Conductivity Of Ethylene Vinyl Acetate Copolymer-Based Composites And The Applicability Of Different Conductivity Models. Carbon. 2011;49(4):1349-61.

[186] Tsai T-C, Chang H-C, Chen C-H, Whang W-T. Widely Variable Seebeck Coefficient And Enhanced Thermoelectric Power Of PEDOT:PSS Films By Blending Thermal Decomposable Ammonium Formate. Organic Electronics. 2011;12(12):2159-64.

[187] De Albuquerque JE, Melo WLB, Faria RM. Photopyroelectric Spectroscopy Of Polyaniline Films. Journal Of Polymer Science Part B-Polymer Physics. 2000;38(10):1294-300.

[188] Kulbachinskii VA, Kytin VG, Popov MY, Buga SG, Stepanov PB, Blank VD. Composites Of Bi2–Xsbxte3 Nanocrystals And Fullerene Molecules For Thermoelectricity. Journal Of Solid State Chemistry. 2012;193:64-70.

[189] Senthil T, Weng ZX, Wu LX. Interlaminar Microstructure And Mechanical Response Of 3D Robust Glass Fabric-Polyester Composites Modified With Carbon Nanofibers. Carbon. 2017;112:17-26.

[190] Wan J, Jiang JW, Park HS. Negative Poisson's Ratio In Graphene Oxide. Nanoscale. 2017;9(11):4007-12.

[191] Chen Z, Cheng X, Cui H, Cheng P, Wang H. Dissipative Particle Dynamics Simulation Of The Phase Behavior And Microstructure Of CTAB/Octane/1-Butanol/Water Microemulsion. Colloids And Surfaces A-Physicochemical And Engineering Aspects. 2007;301(1-3):437-43.

[192] Anand DV, Patnaik BSV, Vedantam S. A Dissipative Particle Dynamics Study Of A Flexible Filament In Confined Shear Flow. Soft Matter. 2017;13(7):1472-80.

[193] Liu X, Yang K, Guo H. Dissipative Particle Dynamics Simulation Of The Phase Behavior Of T-Shaped Ternary Amphiphiles Possessing Rodlike Mesogens. Journal Of Physical Chemistry B. 2013;117(30):9106-20.

[194] Duong-Hong D, Wang J-S, Liu GR, Chen YZ, Han J, Hadjiconstantinou NG. Dissipative Particle Dynamics Simulations Of Electroosmotic Flow In Nano-Fluidic Devices. Microfluidics And Nanofluidics. 2008;4(3):219-25.

[195] Liba O, Kauzlaric D, Abrams ZR, Hanein Y, Greiner A, Korvink JG. A Dissipative Particle Dynamics Model Of Carbon Nanotubes. Molecular Simulation. 2008;34(8):737-48.

[196] Wang Y-C, Ju S-P, Cheng H-Z, Lu J-M, Wang H-H. Modeling Of Polyethylene And Functionalized CNT Composites: A Dissipative Particle Dynamics Study. J Phys Chem C. 2010;114(8):3376-84.

[197] Angelikopoulos P, Bock H. Directed Self-Assembly Of Surfactants In Carbon Nanotube Materials. Journal Of Physical Chemistry B. 2008;112(44):13793-801.